Functional characterisation of glutaredoxin S15 from *Arabidopsis thaliana*

Dissertation

zur Erlangung des
Doktorgrades der Naturwissenschaften (Dr. rer. nat.)
der
Mathematisch-Naturwissenschaftlichen Fakultät der
Rheinischen Friedrich-Wilhelms-Universität Bonn

vorgelegt von

M. Sc. Anna Maria Moseler
Wittlich, Deutschland

Bonn, Juli 2017

Erstgutachter: Prof. Dr. Andreas Meyer
Chemical Signalling
Institut für Nutzpflanzenwissenschaften und Ressourcenschutz
Universität Bonn
Friedrich-Ebert-Allee 144
D-53113 Bonn

Zweitgutachter: Prof. Dr. Volker Knoop
Molekulare Evolution
Institut für Zelluläre & Molekulare Botanik
Universität Bonn
Kirschallee 1
D-53115 Bonn

Prüfungsdatum: 24.10.2017
Erscheinungsjahr: 2017

Table of contents

Summary

Iron-sulfur clusters (ISCs) are essential cofactors that are composed of iron and inorganic sulfur. A complex assembly pathway conveys their initial synthesis and subsequent binding to the respective apoproteins. With the exception of plastids, that are equipped to synthesise ISCs for their own set of FeS-proteins, all other cellular FeS-proteins depend on the mitochondrial ISC machinery and the ATP-binding cassette transporter ATM3 in the inner membrane of mitochondria that transports a yet unidentified sulfur-component from the mitochondrial matrix into the cytosol. FeS-protein maturation can be divided into three steps: the assembly of the ISC on a scaffold protein, the transfer of the nascent ISC via carrier proteins and the insertion of the ISC into specific apoproteins.

This work focusses on the role of the monothiol glutaredoxin S15 (GRXS15) as a carrier protein as well as the impact of the glutathione pool on maturation of mitochondrial and cytosolic FeS-proteins. Here, the identification of previously unrecognised embryonic lethal Arabidopsis mutants deficient in mitochondrial GRXS15 is shown. Recombinant GRXS15 coordinates an ISC in the presence of reduced glutathione as a cofactor. Genetic interference with ISC coordination through targeted mutagenesis diminished the ability of the protein to complement a yeast mutant lacking the homologous mitochondrial Grx5p. Similarly, the mutated GRXS15 variant K_{83}/A was not able to fully complement the lethal Arabidopsis mutants. Partial complementation results in a dwarf phenotype and severely diminished aconitase activity. Furthermore, the complemented mutants displayed disturbances in metabolic pathways that are connected with lipoylated proteins. Taken together, genetic evidence and metabolic characterisation uncovered the role of mitochondrial GRXS15 in FeS-protein maturation, particularly that of aconitase and lipoic acid synthase. Lack of “classical” oxidoreductase activity *in vitro* additionally supports the function of GRXS15 as an ISC carrier protein. Unexpectedly, the K_{83}/A variant showed an enhanced GSSG-dependent oxidation of redox-sensitive GFP (roGFP2). This increased catalytic activity, however, is not based on an improved interaction with roGFP2 but rather points to an essential role of the amino acid substitution on GRX function itself.

Furthermore, it is shown that neither a reduced glutathione amount nor an increase in mitochondrial matrix GSSG influences the maturation of mitochondrial as well as cytosolic FeS-proteins. GSH-depletion does not affect the downstream targets of GRXS15. Still, ISC coordination of GRXS15 is stabilised by GSH addition *in vitro*, while the GRXS15 holoprotein is just slightly destabilised by GSSG. The negligible impact of GSSG on GRXS15 function was also confirmed *in vivo* using an *atm3-4gr2epc2* double mutant. Although high mitochondrial

GSSG aggravates the *atm3* phenotype the *atm3-4gr2epc2* shows no decreased activity of cytosolic FeS-proteins.

Zusammenfassung

Eisen-Schwefel (FeS) Cluster sind lebenswichtige Cofaktoren, die aus Eisen und anorganischem Schwefel bestehen. Eine komplexe Assemblierungsmaschinerie ist die Grundlage für die Synthese des Clusters und dessen Einbau in entsprechende Zielproteine. Während Plastiden ein eigenes System für die Biogenese von plastidären FeS-Proteinen besitzen, sind alle anderen zellulären FeS-Proteine von der mitochondrialen Assemblierungsmaschinerie sowie dem ABC-Transporter ATM3 der inneren mitochondrialen Membran abhängig, welcher eine noch unbekannte, schwefelhaltige Verbindung in das Zytosol exportiert. Die Biogenese der FeS-Proteine kann in drei Schritte unterteilt werden: der Cluster wird auf einem Gerüstprotein zusammengesetzt, anschließend durch ein Trägerprotein abgelöst und schließlich in das entsprechende Zielprotein eingebaut.

Der Fokus dieser Arbeit richtet sich auf das Monothiol-Glutaredoxin S15 als Trägerprotein und auf den Einfluss des Glutathionpools auf die Biogenese mitochondrialer und zytosolischer FeS-Proteine. In dieser Arbeit wurde gezeigt, dass die Deletion des GRXS15 zu einem embryo-letalen Phänotyp führt. Des Weiteren kann rekombinantes GRXS15 mit Hilfe von reduziertem Glutathion als Cofaktor einen FeS-Cluster koordinieren. Beeinträchtigung dieser Koordinierung durch gezielte Mutagenese führt zu einer verminderten Komplementation einer Hefemutante, welcher das entsprechend homologe mitochondriale Grx5p fehlt. Dementsprechend konnte eine mutierte K_{83}/A Variante des GRXS15 auch nicht vollständig die Arabidopsis Null-Mutante komplementieren. Die unvollständige Komplementierung führt zu einem Zwergenwachstum der Pflanzen sowie einer stark verringerten Aconitaseaktivität. Außerdem zeigt die Mutante Störungen in Stoffwechselwegen, welche in Verbindung mit lipoylierten Proteinen stehen. Basierend auf genetischen Nachweisen als auch metabolischer Charakterisierung wurde die Rolle des GRXS15 in der Biogenese von FeS-Proteinen, insbesondere Aconitase und Liponsäure-Synthase, gezeigt. Weitere Unterstützung findet diese Aussage dadurch, dass GRXS15 *in vitro* nicht die Oxidoreduktaseaktivität eines „klassischen" Glutaredoxins besitzt. Interessanterweise weist die K_{83}/A Variante eine erhöhte Aktivität in der Oxidation von roGFP2 auf. Diese ist allerdings nicht auf eine verbesserte Interaktion mit roGFP2 zurückzuführen, sondern deutet auf eine andere wichtige Rolle der Amniosäurensubsitution für die Funktion von Glutaredoxinen hin.

Zusätzlich wird in dieser Arbeit gezeigt, dass weder eine geringere Quantität an Glutathion noch ein Anstieg an GSSG Einfluss auf die Biogenese mitochondrialer und zytosolischer FeS-Proteine hat. Arabidopsismutanten mit einer geringeren Menge an Glutathion zeigen nicht den gleichen Phänotyp wie *grxs15* Mutanten. Nichtsdestotrotz stabilisiert die Zugabe von GSH das

GRXS15 Holoprotein *in vitro*. Allerdings führt die Addition von GSSG nur zu einer sehr leichten Destabilisierung des Komplexes. Der geringe Einfluss an übermäßigem GSSG konnte auch in einer *atm3-4gr2epc2* Doppelmutante gezeigt werden. Auch wenn der erhöhte Gehalt an GSSG den *atm3* Phänotyp verstärkt, konnte keine verminderte Aktivität an zytosolischen FeS-Proteinen nachgewiesen werden.

1. Introduction

1.1 Reactive oxygen species and S-glutathionylation

The Great Oxidation Event 2.4 billion years ago has profoundly shaped the history of life. Although it took another 1.8 billion years until atmospheric concentrations of molecular oxygen (O_2) rose to modern levels (Lyons et al., 2014), anaerobic organisms were required to adapt to the rise of O_2 relatively quickly at evolutionary timescales leading probably to the first major mass extinction of most species. This is because from a biochemical point of view, oxygen and its derivatives were anything but beneficial: they were highly reactive and toxic as a result. Nevertheless, cells evolved strategies not just how to deal with oxygen but also how to benefit from its reactivity by harnessing aerobic respiration. The reduction of O_2 provides the largest free energy release per electron transfer, with the exception of fluorine. Unlike fluorine, O_2 has a greater stability and can consequently accumulate in Earth's atmosphere (Thannickal, 2009). An unavoidable consequence of aerobic metabolism is the production of reactive oxygen species (ROS), mainly produced by oxygen-dependent reactions in energy transduction at the inner mitochondrial membrane and thylakoid membrane of plastids (Huang et al., 2016; Mittler et al., 2004). ROS commonly occurring in biological systems are the superoxide anion ($O_2^{\bullet -}$) and hydrogen peroxide (H_2O_2). Furthermore, H_2O_2 is able, in combination with ferrous iron, to form $O_2^{\bullet -}$ and a hydroxyl radical ($^{\bullet}OH$) in the so-called Fenton reaction (Fenton, 1894). Hydroxyl radicals can cause severe cell damage through uncontrolled oxidation of various cellular macromolecules such as proteins, unsaturated fatty acids or nucleic acids (Møller et al., 2007). In modern organisms ROS are, however, not just by-products of "breathing oxygen" but additionally have specific roles in signal transduction through selective oxidation of target molecules (Huang et al., 2016). Here, each ROS has its individual effects due to differences in their chemistry, determining diffusion range, half-life, membrane permeability or reactivity (Schwarzländer and Finkemeier, 2013).

The proteinogenic amino acid cysteine is particularly susceptible to ROS-mediated modifications but is at the same time important for protein folding, enzyme activity and metal coordination. The cysteine thiol group (-SH) can be found in several oxidation states such as disulfide bond (-S-S-), sulfenic (-SOH), sulfinic ($-SO_2H$) or sulfonic acid ($-SO_3H$) (Giles et al., 2003). Alterations in the oxidation state can influence protein activity as well as metal-binding properties and especially in proteins where a reduced thiol is an absolute requirement for activity, spontaneous changes in the oxidation state must be avoided (Gupta and Luan, 2003; Meinhard and Grill, 2001). Cells have developed mechanisms to strictly control ROS production or removal and to maintain the appropriate redox state of cellular compounds which

is essential for life (Møller, 2001). A temporary posttranslational modification to prevent the irreversible oxidation of a thiol (e.g., sulfinic and sulfonic acid formation) or to regulate the activity of a catalytic residue is the formation of a mixed disulfide between the protein thiol and the tripeptide glutathione (GSH) called S-glutathionylation.

Because of their sessile lifestyle plants are particularly interesting in terms of redox regulation as they are facing light-dark cycles as well as irregular environmental conditions. Furthermore, plants possess two organelles with an electron transport chain, plastids and mitochondria that are potential sources of ROS. Additionally, plants are very oxygen-rich due to endogenous O_2 production as during photosynthesis or detoxification of H_2O_2 (Schwarzländer and Finkemeier, 2013). Glutathione is the most abundant low-molecular-weight thiol (γ-L-glutamyl-L-cysteinyl-glycine) in most prokaryotes and eukaryotes and is commonly synthesised in two sequential reactions catalysed by glutamate-cysteine ligase (GSH1) and glutathione synthase (GSH2). In Arabidopsis, disruption of one of these genes and thus, loss of total glutathione leads to embryo or early seedling lethal phenotypes demonstrating the importance of glutathione for plant growth and development (Cairns et al., 2006; Pasternak et al., 2008). Significant depletion of total glutathione based on point mutations in GSH1 already results in severely diminished growth in *zir1* (ZINCTOLERANCE INDUCED BY IRON 1) or even growth arrest in *rml1*[1] (ROOT MERISTEMLESS 1) Arabidopsis mutants (Shanmugam et al., 2012; Vernoux et al., 2000). Glutathione exists in a reduced (GSH) or oxidised form (GSSG) where two glutathione molecules are linked by a disulfide bond. GSSG is converted back to GSH at the expense of NADPH by glutathione reductases (GR). In bacteria, yeasts, and animals, one GR gene is found; whereas in Arabidopsis, two GR genes are encoded. GR1 is present in the cytosol and the peroxisomes, whereas GR2 is dual-targeted to plastids and mitochondria (Chew et al., 2003a; Kataya and Reumann, 2010; Marty et al., 2009). Similar to the loss of glutathione, insufficient reduction of the GSSG pool in Arabidopsis leads to embryo lethality. Interestingly, the embryo lethality of the *gr2* mutant is due to inactivation of the chloroplastic isoform of GR2, because plants complemented with just mitochondrial targeted GR2 are not viable in contrast to plants with only plastid-targeted GR2. Cytosolic GR1 is unable to compensate for the absence of organellar glutathione reduction (Marty et al, unpublished).

The cellular significance of glutathione is not restricted to glutathionylation of proteins. In plants, it additionally participates in the glutathione/ascorbate cycle. Here, GSH acts as an

[1] The nomenclature rules applied in this thesis generally follows the Arabidopsis convention when dealing with plant abbreviations. Later on yeast proteins are referred to by the relevant gene symbol, initial letter uppercase and with the suffix ‘p’ , Alleles created by recombinant DNA technology are named by use of a symbol indicating deletion (Δ) and the symbol for the gene that is altered

electron donor allowing the regeneration of reduced ascorbate, another major antioxidant in the plant cell (Noctor and Foyer, 1998). Furthermore, GSH can also provide electrons to several enzymes contributing to the redox-regulation of thiols like glutaredoxins (GRXs) which are involved in the catalysis of glutathionylation, de-glutathionylation as well as reduction of disulfide bridges. Furthermore, GSH is required in several reactions as cofactor as in detoxification of methylglyoxal or nitric oxide forming S-nitrosoglutathione (GSNO) (Noctor et al., 2011).

1.1.1 The glutaredoxin system

Glutaredoxin was originally discovered in a mutant of *Escherichia coli* lacking thioredoxin (TRX) and described as a GSH-dependent hydrogen donor for ribonucleotide reductase (Holmgren, 1976; Holmgren, 1979). Furthermore, the GRX was able to reduce low molecular weight substrates such as S-sulfocysteine and bis(2-hydroxyethyl)disulfide (HED) (Bushweller et al., 1992; Holmgren, 1989). In the following years more and more GRXs were characterised from yeast (Gan et al., 1990), mammals (Hopper et al., 1989; Padilla et al., 1995), and plants (Sha et al., 1997) resulting in a generalisation of GRXs as ubiquitously expressed small oxidoreductases present in most prokaryotes and eukaryotes.

As members of the TRX superfamily, all GRXs share a similar three-dimensional structure, the so-called TRX fold. This consists of a central four-stranded β-sheet with three flanking α-helices and the active site motif. The active site contains either a CxxC[2] or CxxS motif, classifying the GRX family roughly in dithiol and monothiol GRXs (Eklund et al., 1992; Xia et al., 1992). Proteins evolved on the TRX fold are often involved in detoxification or redox reactions mediating dithiol-disulfide exchange reactions. In contrast to TRXs, which are reduced by NAD(P)H-dependent TRX reductases (NTRs) or ferredoxin-dependent TRX reductases (FTRs), GRXs are generally reduced by GSH although some exceptions have been proposed (Fernandes et al., 2005; Tamarit et al., 2003) (Figure 1A). Subsequently, the generated GSSG is reduced by the NTR-related FAD-dependent GRs. Similar to NTRs, GRs obtain their reducing power from the pool of NADPH (Meyer et al., 2012) and thus connect the cell's energy metabolism with the maintenance of its redox balance or thiol/disulfide-metabolism (Giles et al., 2003).

[2] abbreviations for amino acids are listed in Supplementary Table 2

GRX-catalysed reactions are divided into two distinct classes depending on the involved cysteines of the active site motif: the dithiol and monothiol mechanism. The dithiol reaction mechanism (Figure 1B) is used to reduce intra- or intermolecular disulfide bridges between two cysteines present in peptides. Here, the reduction process starts with the N-terminal active site cysteine of the GRX in its deprotonated thiolate form. This thiol, which is called the catalytic cysteine, has a low pK_a value allowing the initiation of a nucleophilic attack on the target disulfide and the formation of a transient covalently bound mixed disulfide between the catalytic cysteine of the GRX and a cysteine of the target peptide. In the second step, the second cysteine (resolving cysteine) of the GRX reduces the mixed disulfide, yielding the reduced target and an oxidised GRX (Hanschmann et al., 2013; Meyer et al., 2012). For example, an *E. coli* GRX mutant with a C_{14}/S mutation of the resolving cysteine is not able to reduce ribonucleotide reductase (Bushweller et al., 1992).

In contrast, the monothiol reaction mechanism (Figure 1C) requires just the catalytic cysteine and is used in deglutathionylation reactions. The catalytic thiol of the GRX attacks the disulfide of the glutathionylated peptide, releases the reduced peptide, and becomes glutathionylated. Subsequently, another molecule of GSH reduces the glutathionylated thiol of GRX resulting in GSSG and the reduced GRX. Generally, all of the above-mentioned reactions are reversible. It was thus proposed that GRXs can also specifically oxidise thiols; however, experimental data are sparse (Bender et al., 2015; Deponte and Lillig, 2015).

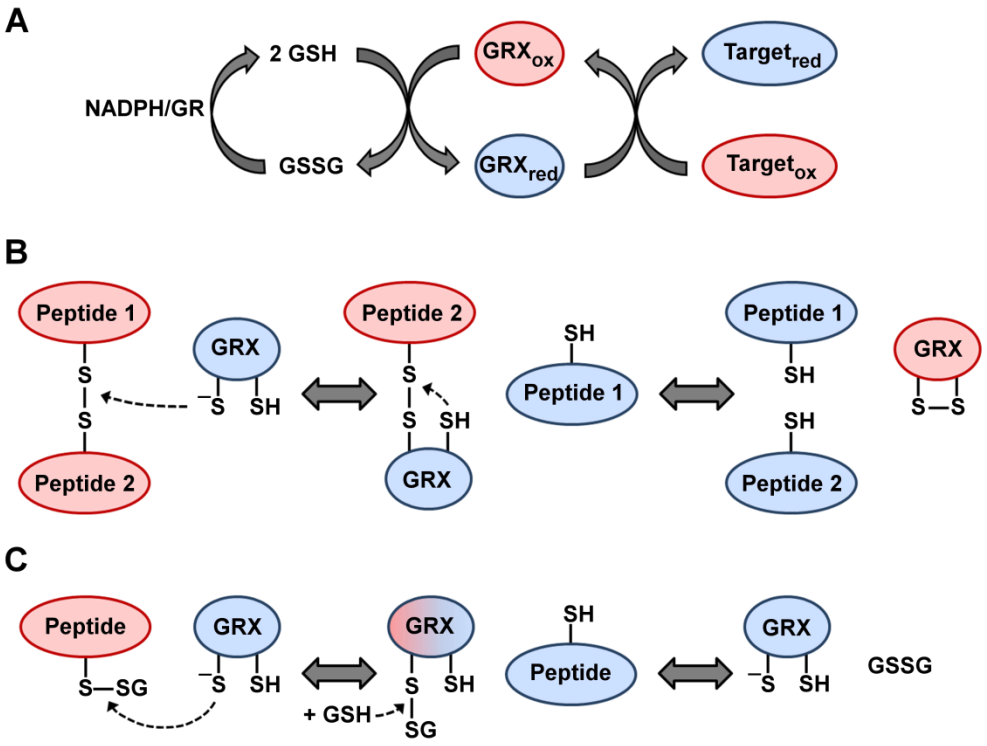

Figure 1: Glutaredoxin reduction mechanism of oxidised target proteins (modified after Meyer et al., 2012).
A: GSH-dependent reduction pathway. NADPH is the major electron source and provides electrons to the glutathione reductase (GR). GR reduces oxidised glutathione (GSSG) yielding two molecules of reduced glutathione (GSH), which serves as a reducing agent for GRXs. Subsequently, the GRXs are able to reduce different types of oxidised cysteines. Red and blue indicate if the substrate is oxidised or reduced, respectively.
B: The dithiol mechanism is used to reduce disulfide bridges of two peptidyl cysteines. The N-terminal active site cysteine of the GRX forms a covalently bound mixed disulfide intermediate with the target protein, which is reduced by the C-terminal active site cysteine, releasing the reduced protein. The oxidised GRX is then reduced by two molecules of GSH.
C: De-/glutathionylation is based on the monothiol mechanism. Here, the N-terminal active site cysteine of the GRX attacks the disulfide of the glutathionylated peptide, releases the reduced peptide, and becomes glutathionylated. Another molecule of GSH reduces the glutathionylated cysteine of the GRX yielding the reduced GRX and GSSG.

To proof the presence and properties of enzymatically active GRXs, a number of biochemical assays have been established. The most prominent assays are using HED, dehydroascorbate (DHA), or insulin as substrates. These monitor GRX activity in a coupled fashion, spectroscopically following NADPH consumption upon GSSG reduction through GR (Begas et al., 2015). Although easily performable with robust outcome, they exclusively report GRX activity that relies on GSH and thus, just the reductive half-reaction. To overcome this, a green fluorescent protein has been engineered with two proximate surface cysteines to yield roGFP2, a redox-sensitive sensor (Dooley et al., 2004; Gutscher et al., 2008; Hanson et al., 2004).

Oxidation or reduction of the engineered disulfide bond triggers small structural changes that affect the protonation of the chromophore resulting in changed spectroscopic properties of roGFP2 (Hanson et al., 2004). Thus, the activity of GRXs can be analysed via the redox equilibration between glutathione and roGFP2 with regard to the oxidative and reductive half-reaction (Meyer et al., 2007). However, based on such standard assays as described above, different GRXs are referred to as "enzymatically active or inactive" for the sake of simplicity without excluding the possibility that inactive GRXs might actually catalyse other reactions with specialised substrates *in vivo* (Begas et al., 2017). Indeed, GRXs have a broad range of functions and distinct substrate specificities that are not just based on the active site motif and the respective redox potential. The specificity is mainly determined by short- and long-range electrostatic interactions as well as a geometric complement of the immediate contact area of the proteins (Berndt et al., 2015). Most notably, at the time when with rising oxygen concentrations the complexity of organisms increased also the occurrence of cysteines increased (Miseta and Csutora, 2000). Concomitant with this, especially in photosynthetic organisms, redox regulatory pathways expanded. Thus, it is not surprising that land plants like *Populus trichocarpa* contain up to 38 GRXs as well as several GRX-like proteins (GRXL) in contrast to baker's yeast *Saccharomyces cerevisiae* that encode just 8 GRXs in their genome indicating a specialisation of the GRXs in their *in vivo* function and physiologically relevant roles (Couturier et al., 2009; Mesecke et al., 2008; Navrot et al., 2006). However, it has to be considered that during the evolution of flowering plants the Type III GRXs (syn. ROXYs) increased massively. For these, however, it is still under debate whether they are really acting as oxidoreductases (Xing et al., 2006).

1.1.2 Glutaredoxins in Arabidopsis

The analysis of the Arabidopsis genome revealed 31 GRXs which are all nuclear-encoded but localised to different subcellular compartments (Rouhier et al., 2004). Arabidopsis GRXs have been found in the cytosol, nucleus, mitochondria, plastids and the secretory pathway (Figure 2). Their subcellular distribution, however, is often still based on bioinformatical prediction (Heazlewood et al., 2007) and the number of isoforms whose localisation has been proven experimentally is limited (Bandyopadhyay et al., 2008; Cheng et al., 2006; Couturier et al., 2011; Knüsting et al., 2015) (Figure 2).

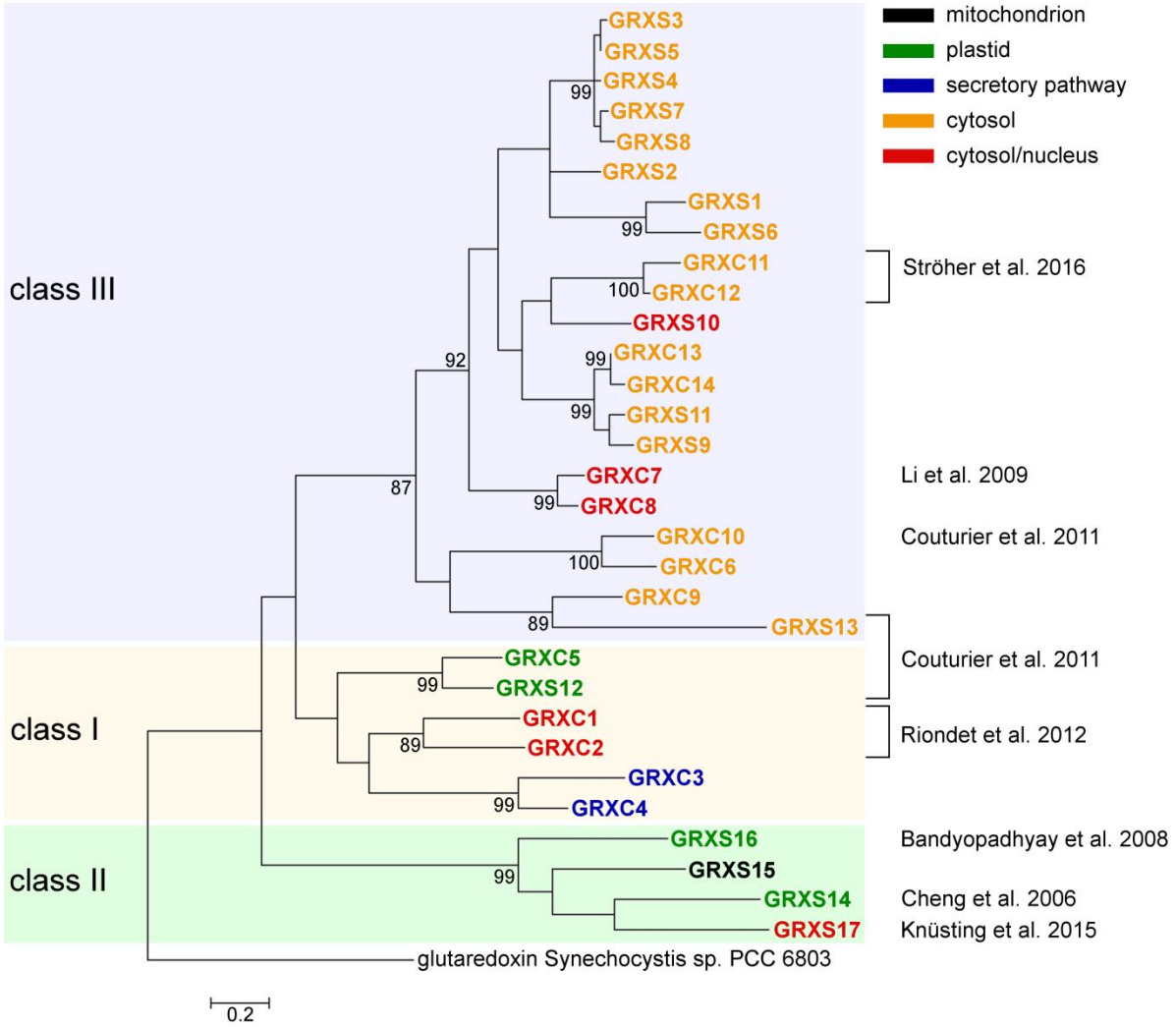

Figure 2: Phylogeny and subcellular localisation of glutaredoxins in Arabidopsis.
The localisation of the respective GRXs indicated by the colour code is based on predictions from SUBA3 (The SUBcellular localisation database for Arabidopsis proteins) or literature when indicated. Bootstrap value: 5,000, Scale bar = 0.2 amino acid substitution per site. Modified after Moseler et al. (2015); accession numbers and synonyms are listed in section 2.8.

The initial classification of GRXs was based on the active site motif defining two types with either a dithiol or monothiol active site motif (Rodríguez-Manzaneque et al., 1999). These "classical" findings were mostly based on bacterial, yeast or mammalian GRXs, which have a limited number of 4, 8 or 4 GRX family members (Hanschmann et al., 2013; Mesecke et al., 2008; Ströher and Millar, 2012). Once much larger numbers of GRXs were discovered in higher plants, a new classification was introduced (Couturier et al., 2009; Rouhier et al., 2004). The first class comprises 5 GRXs termed GRXC1-5 plus a close isoform of GRXC5, GRXS12. GRXC1-4 share a conserved CP/GYC active site motif, whereas GRXC5 and S12 are characterised by a CSYC/S sequence. The nomenclature of the respective GRX (C or S) is

based on the presence of a cysteine or a serine in the fourth position of the active site (CxxC or CxxS) (Rouhier et al., 2006). This GRX class is homologous to the "classical" dithiol GRXs such as *E. coli* Grx1 and Grx3, yeast Grx1p and Grx2p as well as mammalian GLRX1 and GLRX2 (Ströher and Millar, 2012). All class I GRXs tested so far are able to reduce artificial disulfides like HED (Couturier et al., 2013; Couturier et al., 2011; Li et al., 2010; Lundberg et al., 2001). Also Arabidopsis GRXC1 and GRXC2 were able to reduce HED as well as the cytosolic peroxiredoxin-2B (Riondet et al., 2012). Furthermore, Riondet (2012) and colleagues showed that GRXC1 forms a homodimer by coordinating an iron-sulfur cluster (ISC). Coordination of the ISC led to inactivation of the protein similar to findings with the human GLRX2 (Berndt et al., 2007; Lillig et al., 2005). For GLRX2, it was demonstrated that GSH is part of the holo-complex and the cluster is coordinated by the two N-terminal cysteines of the GLRX2 monomers as well as two molecules of GSH bound non-covalently to each of the monomers (Berndt et al., 2007; Johansson et al., 2007) (Figure 3).

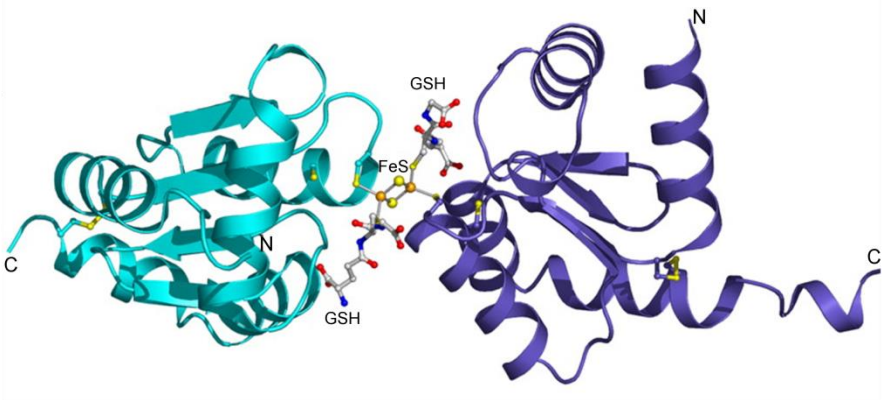

Figure 3: Cluster coordination and glutathione binding of GLRX2 (Johansson et al., 2007).
Monomers A and B of GLRX2 (PDB: 2ht9) are coloured cyan and dark blue, respectively. The glutathione (GSH) and cysteines are represented as sticks. The GRX dimer is bridged by a [2Fe2S] cluster depicted as spheres with grey lines showing the coordination.

Additionally, they showed that the GSH is in constant equilibrium with the pool of free GSH and stability of the ISC depends on the redox environment, because oxidants like GSSG promote disassembly of the holo-complex (Lillig et al., 2005). Thus, it is assumed that under oxidising conditions the dimer would separate into ISC-free active monomers, providing a structural explanation for GRX activation under oxidative stress (Berndt et al., 2007; Johansson et al., 2007). Exchange of the second amino acid in the active site in GRXC1 (CGYC) and GLRX2 (CSYC) into a proline resulted in a loss of the ISC (Berndt et al., 2007; Riondet et al.,

2012). Indeed, Arabidopsis GRXC2, the closest homolog of GRXC1, contains a CPYC active site motif and is not able to coordinate an ISC. Nevertheless, although *grxc1* and *grxc2* mutants have no obvious phenotype, a *grxc1grxc2* double mutant could not be isolated which has been claimed to indicate a functional redundancy of both GRXCs (Riondet et al., 2012). However, the developmental stage of lethality was not shown by Riondet and colleagues although it is mentioned that the *grxc1/grxc1 GRXC2/grxc2* plants showed a high proportion of siliques lacking several seeds. As both genes are coupled to each other on chromosome V, isolation of double null mutants is expected to be rare as it would require chromosomal crossover to link the mutant alleles. Hence, it may well be possible that the number of genotyped seedlings (58) was too low to find a double homozygous mutant.

Another well-studied GRX of class I is the plastidic GRXC5. Similar to GRXC1, it is able to reduce the artificial disulfide substrate HED or the small molecule DHA. Furthermore, it can also reduce putative physiological target proteins like methionine sulfoxide reductase B1 (MsrB1) or peroxiredoxin-2E. Additionally, the protein is able to coordinate an ISC with a similar ligation as GRXC1 resulting in enzymatic inactivation (Couturier et al., 2011). However, the precise function of the class I GRXs *in vivo* has to be analysed.

The second GRX class contains the monothiol GRXS14, S15, S16 and S17 with a conserved CGFS active site motif. They belong to the PICOT-HD (protein kinase C interacting cousin of Trx-homology domain) containing proteins and are homologous to *E. coli* Grx4 as well as yeast Grx3p, 4 and 5 or human GLRX5 (Isakov et al., 2000; Lemaire, 2004). In contrast to class I GRXs or other monothiol GRXs containing a C(P/S)YS active site motif, the CGFS GRXs have a negligible oxidoreductase activity in standard assays assuming essential functions of this class other than acting as a reductase. As GRXS15 is the central point of this study, class II will be described in more detail in section 1.1.3.

The third and most comprehensive class (21 members in Arabidopsis) is class III comprising all GRXs with CCxx active site motif and are also named ROXYs (Gutsche et al., 2015; Li et al., 2009b). This class of GRXs is land plant-specific and interacts with members of the bZIP-type TGA transcription factor family (Zander et al., 2012). Here, ROXY1 and ROXY2 have been intensively studied revealing a function in the regulation of organ primordia initiation, control of organ identity gene expression and progression into meiosis in the male germ line (Li et al., 2009b; Xing et al., 2005; Xing and Zachgo, 2008). Also for maize it was shown that the GRX *male sterile converted anther 1* (msca1) plays a role in archesporial cell formation (Kelliher and Walbot, 2012). Beside the role in floral development, other CC-type GRXs play a role in stress response and plant defence (La Camera et al., 2011; Ndamukong et

al., 2007; Zander et al., 2012). Nevertheless, the exact function and the question why there are so many of the CC-type GRXs have still to be resolved. Furthermore, there is an additional GRX class (class IV) in eukaryotes consisting of proteins with three domains, an N-terminal GRX module followed by two domains of unknown function (Couturier et al., 2009).

1.1.3 The role of CGFS glutaredoxins

Although monothiol class II GRXs share the signature CGFS as their active site motif, members of the family are structurally and functionally versatile. Arabidopsis GRXS14 and GRXS15 are very small proteins with a single GRX domain preceded by an N-terminal signal peptide for plastidic or mitochondrial targeting, respectively (Figure 4). Arabidopsis GRXS16 has an N-terminal extension in addition to a plastid targeting sequence. It has been shown *in vitro* that a putative GIY–YIG endonuclease fold in the N-terminal extension can act as an endonuclease and that the two domains are negatively regulated through the formation of an intramolecular disulfide bond indicating a regulatory mechanism for both nuclease and GRX activity (Liu et al., 2013). The physiological function of GRXS16 nevertheless remains unknown. The last GRX of class II is the multidomain GRXS17 that is characterised by an N-terminal TRX domain followed by three GRX domains (Figure 4).

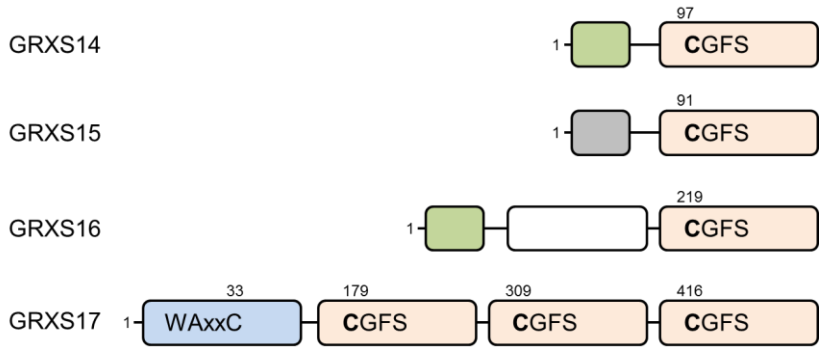

Figure 4: Domain structure of CGFS monothiol GRXs.
The TRX domain (blue) and GRX domains (orange) are shown as boxes, whereas the conserved cysteines in the active sites of the TRX and GRX domains are numbered. Predicted or known plastidic or mitochondrial targeting signals are shown as green or grey boxes, respectively.

Although CGFS GRXs lack the classical oxidoreductase activity *in vitro* (Fernandes et al., 2005; Tamarit et al., 2003), they might be involved in maintaining cellular redox homeostasis *in vivo*. For example, *grxs14* plants have a higher level of protein carbonylation in chloroplasts and seedlings are more sensitive to external oxidants like H_2O_2 (Cheng et al., 2006). Likewise, GRXS15 has been proposed to be involved in the responses to oxidative stress (Cheng, 2008). Tomato plants silenced for the expression of GRXS16 display increased sensitivity to osmotic stress (Guo et al., 2010). Regarding GRXS17, Arabidopsis null mutants showed some degree of hypersensitivity to DNA damage and when growing at 28 °C exhibited impaired primary root growth, impaired flowering as well as altered sensitivity to auxin (Cheng et al., 2011; Inigo et al., 2016; Knüsting et al., 2015). Consistently, ectopic expression of Arabidopsis GRXS17 in tomato plants resulted in enhanced thermotolerance (Wu et al., 2012). Additionally, *grxs17* seedlings are sensitive to oxidative stress and increase ROS production under iron deficiency stress (Yu et al., 2017).

Concerning the subcellular localisation, experimental evidence exists for all isoforms. GFP-tagged GRXS14 and GRXS16 have been localised in plastids (Bandyopadhyay et al., 2008; Cheng et al., 2006; Liu et al., 2013) and GRXS17 in cytosol and nucleus (Knüsting et al., 2015; Wu et al., 2012). The precise localisation for GRXS15 is controversial. Independent targeting experiments have reported GFP-tagged poplar GRXS15 in mitochondria and Arabidopsis GRXS15 in the plastid stroma or dual-targeted plastidic-mitochondrial in bifunctional fluorescence complementation (BiFC) experiments with BolA4 (Bandyopadhyay et al., 2008; Cheng, 2008; Couturier et al., 2014). In proteomic studies, GRXS15 has been repeatedly found in the mitochondria of Arabidopsis and potato, but also in the chloroplast proteome of maize (Huang et al., 2013; Klodmann et al., 2011; Salvato et al., 2014).

The same considerable ambiguity remains for the ability to complement a yeast *Δgrx5* mutant. Yeast Grx5p is a mitochondrial monothiol GRX involved in the maturation of FeS-proteins and displaying distinct growth defects (Rodríguez-Manzaneque et al., 2002). Among poplar monothiol GRXs, GRXS15 is the only isoform failing to rescue most phenotypes of the yeast *Δgrx5* mutant (Bandyopadhyay et al., 2008). In contrast, all Arabidopsis CGFS GRXs are able to fully complement the *Δgrx5* mutant (Cheng et al., 2006; Cheng, 2008; Knüsting et al., 2015; Liu et al., 2013). Based on the ability to complement the yeast mutant, plant CGFS GRXs have been considered to participate in the maturation of FeS-proteins. Indeed, similar to class I GRXs, monothiol class II GRXs are able to coordinate an ISC (Bandyopadhyay et al., 2008; Haunhorst et al., 2010; Picciocchi et al., 2007). Interestingly, multidomain GRXs like GRXS17 are able to incorporate an ISC in each GRX domain (Knüsting et al., 2015). The first crystal

structure of a CGFS GRX was published for *E. coli* Grx4, confirming that two GRX molecules form a homodimer and that two GSH molecules are linked to the cluster, but held in place by non-covalent interactions with the GSH binding pocket of each Grx4 monomer (Iwema et al., 2009). A crystal structure for human GLRX5 reveals a similar coordination environment for the [2Fe-2S] cluster; however, in this structure, two [2Fe-2S]-bridged homodimers interact to form a tetramer (Johansson et al., 2011). Dithiol GRXs, in contrast, are not able to complement the yeast *Δgrx5* mutant indicating a separate role of ISC coordination in the function of GRXs (Bandyopadhyay et al., 2008). The ISC coordination of dithiol GRXs is, indeed, assumed to be a redox sensor since the ISC coordination under oxidative conditions is lost leading to enzymatic active GRXs, whereas CGFS GRXs are implicated in intracellular iron trafficking or sensing via their ISC as well as maturation of FeS-proteins (Lillig et al., 2005; Mühlenhoff et al., 2010; Rodríguez-Manzaneque et al., 2002). A more detailed overview of ISC assembly and FeS-protein biogenesis will be given in the following paragraph.

1.2 Iron-sulfur cluster

Iron is the fourth most abundant element in the Earth's crust and an essential nutrient for virtually all organisms (Beinert, 2000). Especially the electron transfer property of this transition metal makes it fundamental for vital metabolic processes like photosynthesis, respiration or nitrogen fixation. In photosynthetic organisms, the most prominent role of iron is the participation in ISCs acting as a cofactors for several indispensable enzymes (Balk and Schaedler, 2014). The presence of ISCs in both aerobic and anaerobic archaea, bacteria, and eukaryotes and their fundamental requirement for normal metabolism indicates that these clusters were likely integrated into central metabolic pathways early in the evolution of life (Boyd et al., 2014). Indeed, it has been suggested that, prior to the widespread oxidation of Earth's atmosphere, the oxidative formation of pyrite (FeS_2) from hydrogen sulfide (H_2S or HS^-) and Fe^{2+} or iron sulfide (FeS) is the most geochemically plausible source of reducing power for a "chemo-auto-origin" and for the early evolution of life in an "Fe-S World" (Wächtershäuser, 1992). Therefore, ISC can be thought of as "mineral relics" from emerging life bound to rocks that was later incorporated into proteins.

The inorganic cluster consists of iron cations (Fe^{2+}/Fe^{3+}) and sulfide anions (S^{2-}) and can vary in structure and stereochemistry. The simplest clusters are the rhombic [2Fe-2S] and cubic [4Fe-4S] cluster (Figure 5), with the [4Fe-4S] cluster being the most frequent one (Beinert, 2000). More complicated forms, however, have been characterised that can also harbour other metal ions like molybdenum in the Molybdenum cofactor (Moco) or up to 7 Fe atoms as in nitrogenase (Beinert, 2000; Beinert et al., 1997). Interestingly, it has been shown at least *in vitro*, that under elevated oxygen levels, the [4Fe-4S] cluster of *E. coli* fumarate and nitrate reduction (FNR) regulatory protein undergoes a rapid conversion to a [2Fe-2S] cluster, whereas under anaerobic incubation with DTT and Fe^{2+} ion the [4Fe-4S] can be regenerated (Zhang et al., 2012).

ISCs are usually integrated into proteins through coordination of the Fe ions by sulfhydryl groups of cysteine side chains (Figure 5), yet alternative ligands like histidine are known. Substitution of the Cys ligand by other amino acids leads to destabilisation and hence, impairs the cluster assembly (Moulis et al., 1996).

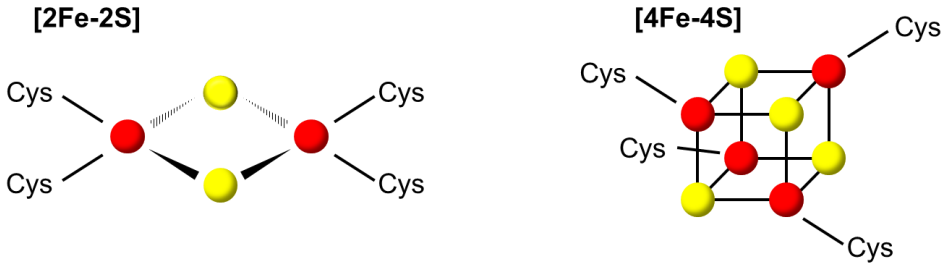

Figure 5: Structures of iron-sulfur clusters.
Iron is shown in red and sulfur in yellow. Depicted are the [2Fe-2S] (left) and the [4Fe-4S] (right) cluster coordinated by 4 Cys ligands. Two [2Fe-2S] clusters can be converted into an [4Fe-4S] cluster by reductive coupling.

ISCs can be spontaneously assembled from the required components under anaerobic conditions (Hagen et al., 1981). However, the spontaneous formation would most likely not happen efficiently *in vivo*. Especially iron has to be treated with caution by the organism. On the one hand, excess iron is a potent source of ROS due to its ability to catalyse the Fenton reaction. On the other hand, although iron is the fourth abundant element, the bioavailability has varied substantially over time and is nowadays marginal. Prior to the Great Oxidation Event, Fe^{2+} was bioavailable because of an absence or very low concentration of O_2 and the solubility of Fe^{2+} being higher than of Fe^{3+}. The increasing O_2 concentration led to spontaneous oxidation of Fe^{2+} to Fe^{3+} which made iron insoluble and nearly inaccessible at physiological pH (Boyd et al., 2014). Thus, based on the dual nature of iron and given that ISCs where introduced early in evolution (i.e. under reducing atmosphere) they now need to be protected and tightly controlled under oxygenic conditions. Therefore, increasing O_2 concentration of the atmosphere also provided the driving force that led to the evolution of sophisticated machineries mediating and controlling the assembly and the transfer of ISCs to acceptor proteins.

1.2.1 Biogenesis of iron-sulfur cluster

Although around one hundred proteins with myriad functions require iron-containing cofactors for activity (Waldron et al., 2009), the machinery responsible for distributing these cofactors remains relatively obscure in parts. Three distinct systems, which are required for the formation and insertion of ISCs into the polypeptide chain, have been initially identified in bacteria and are encoded by the *nif*, *isc* and *suf* operons (Johnson et al., 2005). Hubs of ISC assembly in bacteria are proteins of the *isc* operon, whereas *suf* operon encoded proteins are induced under conditions of oxidative stress or iron limitation (Nachin et al., 2003; Outten et al., 2004). *Nif*-

specific proteins found in *Azotobacter vinelandii* are involved in the assembly of ISCs for nitrogenase (Jacobson et al., 1989; Robinson et al., 1987). The central function of the assembly machinery is to mobilise Fe and S atoms, to assemble them into an ISC form and to transfer the ISCs to their respective apoproteins. In plants, autonomous pathways for this multistep process are present in plastids and mitochondria whereas the cytosolic machinery relies on the export of bound sulfide from mitochondria (Figure 6).

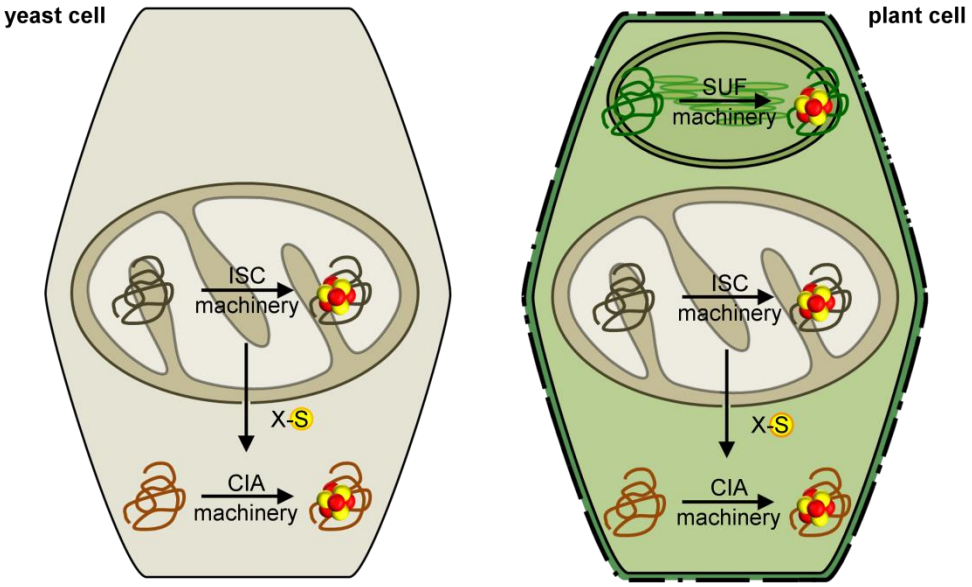

Figure 6: Iron-sulfur cluster assembly machineries in eukaryotes.
Mitochondria contain the ISC assembly machinery and are also essential for the cluster assembly in the cytosol in association with the CIA machinery. A hitherto undefined sulfur-containing compound in a glutathione-dependent fashion (termed X-S) is exported from the mitochondrial ISC machinery to the cytosolic CIA machinery as a sulfur donor for ISC assembly because of the absence of a cytosolic cysteine desulfurase. Plastids harbour the SUF machinery which operates independently.

Because homologs of some bacterial SUF proteins have been discovered in plastids of algae and higher plants, the plastidic assembly pathway is called SUF (**su**l**f**ur mobilisation) assembly machinery (Takahashi and Tokumoto, 2002; Xu et al., 2005). This machinery is essential for the maturation of plastidic FeS-proteins. In contrast, homologs to the bacterial *isc* genes have been found in yeast, mammals, and plants (Supplementary Table 1). Here, the mitochondrion harbours the respective nuclear-encoded proteins as the machinery was likely inherited from α-proteobacteria, the evolutionary ancestor of the organelle (Lill and Kispal, 2000). The system is named ISC (**i**ron-**s**ulfur **c**luster) assembly machinery and is essential for the maturation of mitochondrial FeS-proteins. The machinery is, additionally, indispensable for the **c**ytosolic

iron-sulfur protein **a**ssembly (CIA) machinery as cysteine desulfurases that generate sulfur for ISCs, are strictly localised in the plastids and mitochondria, respectively. It has been suggested that a mitochondrial ABC transporter of the inner membrane, named ATM3 in Arabidopsis or Atm1p in yeast, is able to export glutathione polysulfide to supply the CIA machinery with a sulfur donor for cytosolic-nuclear FeS-protein maturation (Bernard et al., 2009; Schaedler et al., 2014). This substrate, however, is questionable and both the actual molecule as well as export mechanism remain puzzling (Lill et al., 2014). At least in yeast, the crystal structure of the respective ABC transporter Atm1p has been resolved displaying a putative substrate binding pocket for GSH or derivatives (Srinivasan et al., 2014). In addition, yeast lacking Gsh1p, the enzyme that catalyses the first step of glutathione biosynthesis, show decreased activity of cytosolic but not mitochondrial FeS-proteins (Sipos et al., 2002). This indicates that the sulfur-containing compound is exported from the mitochondrial ISC machinery in a glutathione-dependent fashion.

Despite the chemical simplicity of ISCs, the biosynthesis is rather complex. Intensive studies of the assembly process in bacteria and yeast have clarified key steps in the biogenesis of FeS-proteins (Blanc et al., 2015; Lill et al., 2012). Nevertheless, the detailed molecular mechanism of each step has yet to be identified more precisely. In the first step, a [2Fe-2S] cluster is assembled *de novo* on the scaffold protein ISU1 (Leon et al., 2005). Sulfur is delivered by the cysteine desulfurase complex NFS1-ISD11 that catalyses the removal of S^0 from L-cysteine. The sulfur is bound as persulfide (-SSH) on NFS1 and next transferred to ISU1 (Turowski et al., 2012; Zheng et al., 1993). In this step, S^0 is reduced to S^{2-}. Here, it is suggested that electrons are provided by ferredoxin together with the ferredoxin reductase and NADPH (Webert et al., 2014). How and when Fe is inserted remains elusive. Metal delivery, however, is assisted by Frataxin (FH) that binds to the ISC-assembly complex consisting of ISU1 and NFS1-ISD11 and thus leads to a tetrameric complex (Cook et al., 2010; Gerber et al., 2003), whereas binding of FH can regulate the activity of NFS1 (Turowski et al., 2012).

In the second step, the cluster has to be released from the scaffold protein and transferred to the respective apoprotein. In yeast, the dissociation is facilitated by a chaperone system comprising the ATP-dependent Hsp70 chaperone Ssq1p, its co-chaperone Jac1p as well as the nucleotide exchange factor Mge1p (Mühlenhoff et al., 2003; Xu et al., 2009). The released ISC might be transferred to the monothiol Grx5p via specific association of the GRX with Ssq1p (Uzarska et al., 2013). It has been suggested that Grx5p acts as a carrier protein transferring a cluster from the core ISC machinery to recipient apoproteins or to other late acting components of the ISC machinery that are essential for the maturation of [4Fe-4S] containing proteins. As the

respective acceptor proteins are extremely diverse in terms of their structure, their surface properties and the type of cluster they require, it is assumed that the remaining ISC components are acting more specific. For example, the proteins Isa1p and Isa2p are interacting with Grx5p as well as specifically with Iba57p. The Isa/Iba57 complex is dedicated to the maturation of [4Fe-4S] proteins like aconitase or biotin and lipoyl synthase (Gelling et al., 2008; Mühlenhoff et al., 2011; Waller et al., 2012). Another late-acting component of the ISC machinery is IND11 that is essential for the maturation of complex I (Bych et al., 2008; Wydro et al., 2013). Furthermore, NFU1 is needed for maturation of specific targets such as lipoyl synthase and succinate dehydrogenase (Leon et al., 2003; Navarro-Sastre et al., 2011). How the ISC is inserted in the respective polypeptide chain and how the carrier proteins are interacting with the target proteins remains ambiguous. Given the essential functions of FeS-proteins, it is not surprising that disruption of most genes involved in ISC assembly results in lethality (Busi et al., 2006; Frazzon et al., 2007; Waller et al., 2012). To further explore the essential roles of ISCs, FeS-proteins whose maturation depend on the mitochondrial ISC machinery will be described in the following.

1.2.2 Iron-sulfur proteins in Arabidopsis

Based on the ability of iron to switch between Fe^{2+} and Fe^{3+}, the most obvious function of the ISC is the participation in electron transfer reactions, where just a glance at the mitochondrial respiration chain highlights the pivotal role of several ISCs. The NADH:ubiquinone oxidoreductase[3] (Complex I), succinate dehydrogenase (Complex II) as well as cytochrome c reductase (Complex III) contain ISCs comprising [2Fe-2S], [3Fe-4S] as well as [4Fe-4S] cluster (Balk and Lobreaux, 2005; Imsande, 1999). Lack of functional ISCs in these proteins frequently causes lethality, e.g. NDUFS1 (At5G37510) that is an ISC binding subunit of complex I is assumed to be embryo defective (Heazlewood et al. (2003); www.seedgenes.org).

However, non-electron transfer functions of the ISC are also essential for life. ISCs can also act as an active site of enzymes like in aconitase (ACO), where one of the irons of the [4Fe-4S] cluster serves as a Lewis acid (Kennedy et al., 1983) catalysing the isomerisation of citrate to isocitrate via *cis*-aconitate in the tricarboxylic acid (TCA) cycle. In Arabidopsis, ACO is encoded by three genes *ACO1*, *ACO2* and *ACO3*[4], with ACO1 located in the cytosol, ACO2 in the mitochondria and ACO3 being dual targeted to cytosol and mitochondria (Hooks et al.,

[3] respective EC numbers of enzymes are listed in Supplementary Table 3
[4] ACO1 (At4g35830), ACO2 (At4g26970), ACO3 (At2g05710)

2014; Peyret et al., 1995). When grown under controlled conditions single mutants displayed no macroscopic phenotype but an *aco1aco3* double mutant was found to be lethal resulting in aborted seeds (Arnaud et al., 2007). Other [4Fe-4S] cluster containing proteins are the radical S-adenosyl-L-methionine (SAM) enzymes biotin synthase and lipoyl synthase (Ollagnier-De Choudens et al., 2000). The enzymes are required for the C-S bond formation at non-activated carbon in the biosynthesis of biotin and lipoic acid, respectively. The precise role of the ISCs is not yet fully understood, but it is assumed that they serve as a sulfur donor (Booker et al., 2007; Tse Sum Bui et al., 1998). However, null mutants of biotin synthase are embryo lethal underlining the importance of this protein *in planta* (Arnal et al., 2006). Another SAM enzyme containing an [4Fe-4S] cluster is CNX2 (Cofactor of Nitrate reductase and Xanthine dehydrogenase 2). This protein, along with CNX3, catalyses the conversion of GTP into cyclic pyranopterin monophosphate (cPMP) in the first step of Moco biosynthesis (Bittner, 2014; Hänzelmann et al., 2004). Moco-dependent enzymes function in nitrogen assimilation (nitrate reductase; NR), abscisic acid synthesis (abscisic aldehyde oxidase 3; AAO3), purine catabolism (xanthine dehydrogenase; XDH1) and sulfite detoxification (sulfite oxidase; SO). Interestingly, cPMP is exported from mitochondria to the cytosol via ATM3, which is also involved in the synthesis of cytosolic ISCs (Bernard et al., 2009; Teschner et al., 2010). Furthermore, AAO3 and XDH1 contain both, in addition to Moco, an ISC whose assembly depends on the CIA machinery (Figure 7) (Bittner, 2014).

A third general function of the ISC is the stabilisation of proteins. This structural role is assumed for several enzymes involved in DNA recombination and repair like DNA helicases or glycosylases[5] (Hinks et al., 2002; White, 2009).

[5] DNA helicases RAD3 (UVH6); At1g03190, (RAD-like proteins: At1g20720, At1g20750, At1g79950); DNA glycosylases DME; At5g04560, DML1-3; At2g36490, At3g10010, At4g34060)

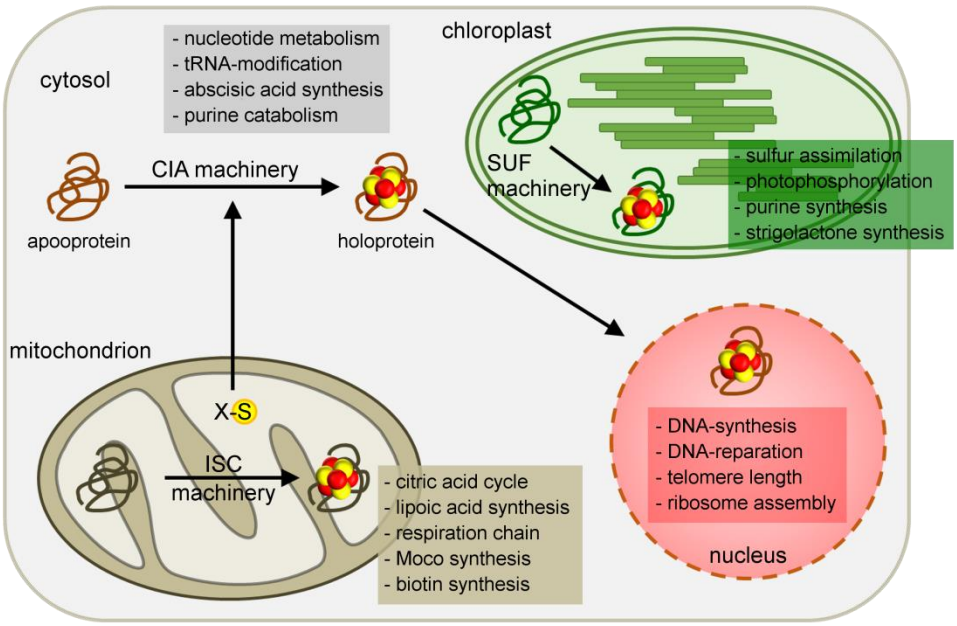

Figure 7: Subcellular localisation of FeS-protein in Arabidopsis.
In plants, FeS-proteins are localised in mitochondria, plastids, cytosol and nucleus. Numerous FeS-proteins are known, but in many cases the precise role of the ISC is still not determined. The ISC can serve in electron transfer, as active site of catalytic enzymes, structural component or sensor for intracellular iron as well as oxidative and nitrosative stress.

Additionally, ISCs are exploited in sensing and signalling reactions. Because ISCs are extremely vulnerable, cluster destruction can trigger complex responses regulating thereby enzyme activity itself as described previously for dithiol GRXs or gene expression (Crack et al., 2014). The best example of post-transcriptional regulation of gene expression is the mammalian cytosolic iron-regulatory protein 1 (IRP1). When iron is abundant, the protein contains a [4Fe-4S] cluster and acts as aconitase metabolising citrate to isocitrate. In contrast, when the protein loses its cluster under iron deprivation it can bind to stem-loop structures (termed iron-responsive elements (IREs)) in certain messenger RNAs coding for proteins involved in iron uptake, storage as well as distribution in the cell and thus, can regulate the synthesis of the respective proteins (Rouault, 2006; Walden et al., 2006). However, such regulatory function has not yet been described for the respective FeS-proteins in Arabidopsis (Arnaud et al., 2007). Interestingly, in baker's yeast, two monothiol GRXs function in iron regulation, namely Grx3p and Grx4p (Li et al., 2009a). Here, the expression of iron uptake and storage genes, collectively known as the iron regulon in yeast, is primarily controlled by the iron-responsive transcription factor Aft1p and its paralog Aft2p (Yamaguchi-Iwai et al., 1996). Under iron-replete conditions, Aft1p resides in the cytosol, whereas under iron-deficient

conditions the protein accumulates in the nucleus and activates the iron regulon. Grx3/4p are able to interact with Aft1p and thereby negatively regulate the transcriptional function of Aft1p (Ojeda et al., 2006). Indeed, in *Δgrx3Δgrx4* double null mutants the iron regulon was activated constitutively resulting in an over-accumulation of iron (Pujol-Carrion et al., 2006). Although iron accumulates in the cytosol, the double mutant exhibits a decreased mitochondrial iron pool as well as a decreased enzyme activity of iron-dependent enzymes like FeS-proteins indicating an essential role of Grx3/4p in iron trafficking (Mühlenhoff et al., 2010). Intriguingly, Grx3/4p can bind an ISC and mutations that affect the cluster binding result in a similar phenotype as the double knock-out indicating that the ISC is essential for proper iron sensing (Mühlenhoff et al., 2010; Ojeda et al., 2006). Thus, it is assumed that the GRX-bound ISC functions as a sensor for the iron-responsive transcription factor Aft1p signalling the status of the cytosolic iron pool (Chen et al., 2004; Lill et al., 2012; Rutherford et al., 2005).

1.2.3 Role of glutaredoxins in the iron-sulfur cluster assembly machineries

In contrast to yeast, Arabidopsis has only one monothiol GRX, GRXS17, in the cytosol. GRXS17 is so far the best-characterised monothiol GRX in Arabidopsis. *GRXS17* is ubiquitously but strongly expressed in very different cell types localised in meristematic areas or in reproductive and vascular organs (Knüsting et al., 2015). Moreover, consistent with the previously mentioned thermo-sensitivity of the *grxs17* line (Cheng et al., 2011), Knüsting and colleagues showed that GRXS17 is central for the plant response to environmental changes such as length of photoperiod and temperature. Upon heat stress, GRXS17 migrates from the cytosol to the nucleus (Wu et al., 2012) where it supposedly interacts with the transcriptional regulator NF-YC11/NC2α. As a mutant deficient in NF-YC11/NC2α phenocopied the *grxs17* null mutant depending on the photoperiod, it was proposed that GRXS17 together with NF-YC11/NC2α relay a redox signal generated by the photoperiod to maintain meristem function (Knüsting et al., 2015).

Although GRXS17 has, similar to yeast Grx3/4p, an additional TRX domain and can bind ISCs, GRXS17 plays only a minor role in iron trafficking and the ISC machinery, as the activities of cytosolic FeS-proteins like aconitase or aldehyde oxidase were not substantially altered in *grxs17* null mutants (Knüsting et al., 2015). Nevertheless, Inigo and colleagues showed that GRXS17 can interact with cytosolic FeS-proteins like XDH1 or Cytsolic Thiouridylase Subunit 1 (CTU1) and CTU2, which are essential for the thiolation of tRNAs (Inigo et al., 2016). However, the authors also showed that the enzymatic activity of XDH1 or tRNA thiolation was

not markedly reduced in the *grxs17* mutant, albeit metabolic profiling of the *grxs17* mutant reflected a perturbed flux through the purine salvage pathway. In addition, the *grxs17* mutant phenocopied mutants in the elongator subunit ELO3, essential for effective thiolation of tRNAs (Inigo et al., 2016). These findings as well as the ability of GRXS17 to complement the yeast Grx5p mutant points to a contribution of GRXS17 in the maturation of cytosolic FeS-proteins even though it apparently plays no essential role. Astonishingly, the yeast Grx3p and Grx4p were not able to fully complement the growth defect of the *Δgrx5* mutant (Rodríguez-Manzaneque et al., 2002).

As mentioned previously, yeast Grx5p is located in the mitochondrial matrix and the *Δgrx5* mutant reveals a distinct growth phenotype. Initially, it was assumed that Grx5p is involved in regulating protein glutathionylation since the *Δgrx5* mutant displays an increased protein carbonyl content as well as a dramatic increase in sensitivity to oxidants although no transcriptional changes of Grx5p were observed during stress conditions (Rodríguez-Manzaneque et al., 1999). Furthermore, this role was underlined with the suggestion that Grx5p is involved in the efficient de-thiolation of the Tdh3 GAPDH isoenzyme (Shenton et al., 2002). Additionally, Grx5p is able to reduce glutathionylated rat carbonic anhydrase III (Tamarit et al., 2003) and indeed, the active-site cysteine residue is necessary for Grx5p as its substitution results in the same phenotype as that seen for the null mutant (Belli et al., 2002). However, the rate of Grx5p to be reduced by GSH was at least 20 times slower than observed for the reduction of the dithiol Grx1 from *E. coli* (Tamarit et al., 2003). Moreover, a closer look on the *Δgrx5* mutant displayed an iron accumulation in the cell, a condition which in turn could promote oxidative damage. In addition, the lack of Grx5p negatively influenced the activity of several FeS-proteins like aconitase or succinate dehydrogenase (Rodríguez-Manzaneque et al., 2002). The ability of Grx5p to coordinate an ISC as well as the ISC accumulation on the scaffold protein Isu1p in Grx5p-depleted cells led to the conclusion that Grx5p functions as a late-acting component of the mitochondrial core ISC machinery linking the ISC synthesis reaction on Isu1p with late assembly steps involving ISC targeting to dedicated apoproteins (Mühlenhoff et al., 2003; Uzarska et al., 2013). Furthermore, the activity of cytosolic FeS-proteins is also diminished in Grx5p-depleted cells indicating that Grx5p is somehow involved in the generation or export of the sulfur-containing compound X-S (Figure 7) (Uzarska et al., 2013). Interestingly, deletion of Grx5p is not lethal unlike that of most other core ISC assembly genes (Lill et al., 2012; Rodríguez-Manzaneque et al., 1999). In multicellular organisms like zebrafish or humans, however, mutations in GLRX5 are lethal (Wingert et al., 2005) or lead to severe diseases like sideroblastic anemia (Camaschella et al., 2007; Ye et al., 2010). Functional

analysis of human GLRX5 mutants revealed that different amino acid mutations led to distinct effects on downstream target proteins like aconitase, succinate dehydrogenase or lipoyl synthase, which was measured indirectly by activity of lipoylated proteins namely of pyruvate dehydrogenase complex (PDC) and α-ketoglutarate dehydrogenase complex (OGDHC) (Liu et al., 2016). A phenotype with similar defects in lipoic acid-containing proteins was reported for individuals with a mutation in the gene BOLA3, encoding a mitochondrial protein of the BolA protein family (Cameron et al., 2011). Little is known about the function, but BolA family members have been postulated to act as reductases, interacting with the monothiol GRX family via heterodimerisation (Huynen et al., 2005; Roret et al., 2014). In Arabidopsis, four proteins containing a BolA domain are present. BOLA1, BOLA2 and BOLA4 as well as a fusion protein between an N-terminal SufE domain and a C-terminal BolA domain named SUFE1[6] (Couturier et al., 2014). BOLA4 and SUFE1 are both dual targeted to chloroplasts and mitochondria (Couturier et al., 2014; Xu and Møller, 2006). SUFE1 interacts with and activates the cysteine desulfurases, SUFS in plastids and NFS1 in mitochondria, and both activations are vital during embryogenesis (Xu and Møller, 2006; Ye et al., 2006). In a yeast two-hybrid approach, GRXS15 is able to interact with both BOLA4 and the BolA domain of SUFE1 (Couturier et al., 2014). This result, however, could not be confirmed *in planta* using bimolecular fluorescence complementation (BiFC). Whereas for BOLA4 and GRXS15 a BiFC signal was present in mitochondria, no fluorescence reconstitution for SUFE1 and GRXS15 was obtained (Couturier et al., 2014).

[6] SUFE1-BolA (At4g26500)

1.3 Aims of the study

Monothiol glutaredoxins have been considered as core components of the iron-sulfur protein assembly machinery. In plants, experimental evidence for monothiol GRXs providing similar functions is lacking due to the lack of suitable mutants and partial functional redundancy between GRXs. The key aim of this work was to understand the precise function of GRXS15 with respect to the ISC machinery as well as putative alternative functions in metabolic pathways. To experimentally address these functions, a combination of genetic, physiological, and biochemical approaches was used.

In the first part, the function of GRXS15 in the ISC assembly machinery and maturation of FeS-proteins will be described. First, ambiguities concerning the subcellular localisation as well as the ability of GRXS15 to complement the yeast *Δgrx5* mutant were to be clarified. Moreover, the ability of GRXS15 to bind an ISC was investigated and the respective results are complemented with data from GRXS15 variants that carry amino acid exchanges at the putative ISC and GSH coordination site *in vivo* and *in vitro*. To elucidate the general function of GRXS15 in Arabidopsis, mutants have been generated and characterised. Given that T-DNA insertion mutants have been described as viable in homozygous form with a weak oxidation-sensitive phenotype (Cheng, 2008), additional T-DNA mutants were to be isolated and analysed with regards to the activity of FeS-proteins and respective downstream effects. Additionally, mutants expressing GRXS15 variants were analysed for FeS-protein activities.

In the second part, the influence of glutathione on GRXS15 function and maturation of FeS-proteins will be reported. Glutathione might act as a co-factor of GRXS15 to coordinate an ISC and a phenotypic comparison between glutathione-depleted and *grxs15* mutants were used to judge how important that is for GRXS15 function. Additionally, glutathione is required for export of an undefined sulfur-containing compound X-S that links the mitochondrial and cytosolic iron-sulfur cluster machineries. A knock-down mutant of the mitochondrial ATM3 was to be crossed with a specific mutant of glutathione reductase that has a more oxidised mitochondrial glutathione pool. The double mutant was then to be used to investigate if an increased amount of GSSG influences the maturation of cytosolic FeS-proteins.

In the last part, GRXS15 was to be analysed regarding its oxidoreductase activity. It was investigated whether recombinant GRXS15 has an oxidoreductase function by testing the impact on the redox state of HED and redox-sensitive GFP2 *in vitro*. Here, it was examined, if GRXS15 can mediate the reversible electron flow between glutathione and reduced or oxidised roGFP2. For comparison, both assays were performed with the dithiol GRXC1 as positive

control. In addition, it was questioned whether roGFP2 can be optimised regarding the kinetic properties of the GRX-roGFP2 interaction.

2. Material and Methods

2.1 Laboratory equipment and materials

2.1.1 Consumables and Chemicals

General chemicals were purchased from Sigma-Aldrich (www.sigmaaldrich.com/germany), Duchefa Biochemie (www.duchefa-biochemie.nl), Merck (www.merckmillipore.de), Roth (www.carlroth.com) or AppliChem (www.applichem.com). General plastic ware was purchased from Sarstedt (www.sarstedt.com/php/main.php) and VWR (de.vwr.com/store).

2.1.2 Kits and enzymes

NucleoSpin® Plasmid	Macherey-Nagel[7]
NucleoSpin® Gel and PCR Clean-up	Macherey-Nagel
NucleoSpin® RNA	Macherey-Nagel
Q5® Site-Directed Mutagenesis	New England BioLabs[8]
Gateway®BP clonase II enzyme mix	Thermo Scientific[9]
Gateway® LR clonase II enzyme mix	Thermo Scientific
M-MLV Reverse Transcriptase (200 U μL^{-1})	Thermo Scientific
Phusion High-Fidelity DNA Polymerase (2 U μL^{-1})	Thermo Scientific
Taq DNA Polymerase (5 U μL^{-1})	New England BioLabs
FastDigest ApoI	Thermo Scientific
FastDigest NheI	Thermo Scientific

2.1.3 Working concentrations of antibiotics and herbicides

Ampicillin	100 $\mu g\ mL^{-1}$
Gentamycin	100 $\mu g\ mL^{-1}$
Kanamycin	50 $\mu g\ mL^{-1}$
Rifampicin	100 $\mu g\ mL^{-1}$
Spectinomycin	100 $\mu g\ mL^{-1}$
Sulfadiazine sodium salt	5.25 $mg\ L^{-1}$
Basta®	240 $mg\ L^{-1}$
Hygromycin B	20 $\mu g\ mL^{-1}$

[7] www.mn-net.com
[8] www.neb-online.de
[9] www.thermofisher.com

2.1.4 Oligonucleotides

Oligonucleotides (Supplementary Table 4) were synthesised by MWG (www.eurofinsgenomics.eu). Salt-adjusted oligonucleotide melting temperatures were calculated at http://biotools.nubic.northwestern.edu/OligoCalc.html. Lyophilised oligonucleotides were resuspended in dH_2O to working concentrations of 10 pmol μL^{-1}. Primer stocks and working solutions were stored at -20 °C.

2.2 Plant methods

2.2.1 Plant material

Seeds of *grxs15-1* (SALK_112767C) and *grxs15-3* (GK-837C05) T-DNA insertion alleles were obtained from the Nottingham Arabidopsis Stock Centre. Seeds of the *grxs15-2* allele (SAIL_431_H03) were kindly provided by Ninghui Cheng, Baylor College of Medicine, Houston. Furthermore, the mutant lines *atm3-4* (Bernard et al., 2009), *atm3-1* (Teschner et al., 2010), *zir1* (Shanmugam et al., 2012) and *rml1* (Vernoux et al., 2000) were used in this study. To phenotypically compare the complemented *grxs15-3* mutant, segregated wild-type ecotype Col-0 from the T-DNA line *grxs15-3* was used. Other lines were compared with wild-type ecotype Col-0 (Lehle seeds (2014) WT-02-46.01) was used.

2.2.2 Growth conditions

Where not indicated otherwise, surface-sterilised seeds were grown on vertical culture plates containing nutrient medium (Somerville and Ogren, 1982) with 0.1 % (w/v) sucrose and 0.8 % (w/v) agar under long-day conditions with a diurnal cycle of 16 h light at 22 °C and 8 h dark at 18 °C. The light intensity and relative air humidity were 75 $\mu E\ m^{-2}\ s^{-1}$ and 50 %, respectively. Arabidopsis plants were grown on a soil:sand:vermiculite mixture in the ratio 10:1:1. The soil was obtained from Floragard, Oldenburg (Floradur® Anzuchtssubstrat). Plants were kept in controlled growth chambers under long-day conditions with a diurnal cycle of 16 h light at 19 °C and 8 h dark at 17 °C. The light intensity and relative air humidity were 100-120 $\mu E\ m^{-2}\ s^{-1}$ and 50 %, respectively.

2.2.3 Stable transformation of Arabidopsis

For floral dip transformation, the method of Clough and Bent (1998) was used. A liquid culture of *A. tumefaciens* containing the respective construct was inoculated from a 5 mL overnight-culture and grown to an OD_{600} of ~1.0. The cells were harvested by centrifugation with 3,000 *g*

for 10 min at 4 °C and resuspended in floral-dip medium containing 5 % (w/v) sucrose and 0.02 % (v/v) Silwet L-77 (Vac-In-Stuff, Lehle Seeds). The medium was added to a beaker and plants were dipped into this suspension for 5–10 s. Plants were left at high humidity in a closed chamber in the dark overnight and returned to the growth chamber the next day. The dipping procedure was repeated after 7 d to increase the transformation rate.

2.2.4 Screening for transformed Arabidopsis

Plants transformed with constructs containing the BAR gene as selection marker were grown on soil under long-day conditions. After two weeks of growth, the plants were sprayed with a 240 mg L^{-1} glufosinate ammonium solution (Basta®). The treatment was repeated one week later.

Plants transformed with constructs containing the NPT, SUL or HPT gene were screened *in vitro* following the protocol of Harrison et al, 2006. Seeds were therefore surface sterilised with 70 % (v/v) EtOH and grown on plates with Arabidopsis medium supplemented with 0.8 % (w/v) agar and 50 µg mL^{-1} kanamycin, 5.25 mg L^{-1} sulfadiazine sodium salt or 20 µg mL^{-1} hygromycin B, respectively.

Fluorescent plants were detected on a stereomicroscope (Leica M165 FC) equipped with a GFP filter of 470 ± 40 nm excitation and emission at 525 ± 50 nm or DsRed filter of 545 ± 30 nm excitation and emission at 620 ± 30 nm and documented with an attached camera (Leica DFC425 C).

2.2.5 Analysis of germination rate and root length

Germination rate was determined on vertical culture plates using a stereomicroscope (Leica M165 FC).

Root growth was documented photographically on vertical culture plates containing 0.8 % (w/v) phytagel and 0.1 % (w/v) sucrose. 5 and 8 d after stratification, root length was documented and measured using Adobe Illustrator CS5.1.

Influence of the nitrogen source on root length was analysed on plates containing 5 mM KNO_3 or 2.5 mM $(NH_4)_2SO_4$, 2.5 mM KH_2PO_4, 2 mM $MgSO_4$, 2 mM $CaCl_2$, 50 µM Fe-EDTA, 70 µM H_3BO_4, 14 µM $MnCl_2$, 0.5 µM $CuSO_4$, 1 µM $ZnSO_4$, 0.2 µM $NaMoO_4$, 10 µM NaCl, 0.01 µM $CoCl_2$, 0.8 % (w/v) Phytagel and 0.1 % (w/v) sucrose, pH 5.8.

2.2.6 Detection of reactive oxygen species

For detection of increased H_2O_2 production, leaves were stained with DAB (3, 3-diaminobenzidine) (Thordal-Christensen et al., 1997). Leaves were vacuum-infiltrated in a solution containing 0.1 mg mL^{-1} DAB, 50 mM potassium phosphate buffer pH 7.6 and 0.1 % (v/v) Silwet L-77. After infiltration, the leaves were incubated for 20-24 h in the dark and destained by lactic acid:glycerol:EtOH (1:1:3) for 30 min at 70 °C.

For histochemical staining of superoxide, NBT (nitro blue tetrazolium) was used (Hoffmann et al., 2013). Leaves were vacuum-infiltrated in a solution containing 0.1 mg mL^{-1} NBT, 50 mM potassium phosphate buffer pH 7.6 and 0.1 % (v/v) Silwet L-77. After infiltration the leaves were incubated for 30 min in the dark and destained by lactic acid:glycerol:EtOH (1:1:3) for 30 min at 70 °C.

2.2.7 Isolation of Mitochondria and Chloroplasts

Arabidopsis mitochondria were purified from 2-week-old seedlings as described before (Escobar et al., 2006) with slight modifications. All steps were performed on ice or at 4°C. Seedlings were homogenised using mortar and pestle and the homogenate was filtered (Miracloth; Merck Millipore) before cellular debris was pelleted by centrifugation for 5 min at 1,200 *g*. The supernatant was centrifuged for 20 min at 18,000 *g*, and the pellet of crude mitochondria was gently resuspended in wash buffer (0.3 M sucrose, 0.1 % (w/v) BSA and 10 mM TES, pH 7.5) and centrifuged for 5 min at 1,200 *g*. The supernatant was transferred into a new tube and centrifuged for 20 min at 18,000 *g*. The pellet was gently resuspended in final wash buffer (0.3 M sucrose, 10 mM TES, pH 7.5), loaded directly on a 0–6 % Percoll gradient and centrifuged for 40 min at 40,000 *g*. For isolation of plastids, the same extraction buffer was used. After homogenisation of the seedlings, the homogenate was filtered (Miracloth; MerckMillipore) and cellular debris was pelleted by centrifugation for 5 min at 1,100 *g*. The pellet was resuspended in wash buffer (0.33 M sorbitol, 20 mM tricine, 2.5 mM EDTA, 5 mM $MgCl_2$, pH 7.6). After centrifugation for 1 min at 2,500 *g*, the plastid fraction was loaded on a step gradient of 50 % and 80 % Percoll and centrifuged for 10 min at 2,500 *g*. Chloroplasts were transferred into a new tube and washed once with wash buffer.

2.2.8 Respiration analysis of roots and mitochondria

Oxygen consumption of intact Arabidopsis roots and isolated mitochondria was measured in Oxytherm Clark-type electrodes (Hansatech; www.hansatech-instruments.com) as described before (Wagner et al., 2015). Whole roots from seedlings vertically grown on agar plates were

cut below the hypocotyl-root junction and assayed in a volume of 1.2 mL containing 5 mM KCl, 10 mM MES, and 10 mM $CaCl_2$, pH 5.8, and after addition of 4 mM KCN and 0.2 mM pGal.

O_2 consumption of isolated mitochondria (2.2.7) was measured in a volume of 1 mL containing 0.3 M mannitol, 10 mM TES-KOH pH 7.5, 5 mM KH_2PO_4, 10 mM NaCl, 2 mM $MgSO_4$ and 0.1 % (w/v) bovine serum albumin. O_2 consumption rate was measured before (blank) addition of mitochondria and after addition of mitochondria (mito) or respective substrate (state II; succinate (10 mM succinate, 0.25 mM ATP) or pyruvate/malate (10 mM pyruvate, 10 mM malate, 0.3 mM NAD and 0.1 mM thiamine pyrophosphate), state III; ADP (50 µM ADP). Additionally, O_2 consumption rate was analysed after ADP consumption (state IV) and after addition of 10 µM carbonyl cyanide m-chlorophenylhydrazone (CCCP).

2.2.9 Determination of metabolite levels via HPLC

Aliquots (45-55 mg) of freshly ground plant tissue were used for absolute quantification of amino acid, α-ketoacid and organic acid content each.

Free amino acids and α-ketoacids were extracted with 0.5 mL ice-cold 0.1 M HCl in an ultrasonic ice-bath for 10 min. Cell debris and insoluble material were removed by centrifugation for 10 min at 25,000 *g*. For the determination of α-ketoacids, 150 µL of the resulting supernatant were mixed with an equal volume of 25 mM OPD (o-phenylendiamine) solution and derivatised by incubation at 50 °C for 30 min. After centrifugation for 10 min, the derivatised ketoacids were separated by reversed phase chromatography on an Acquity HSS T3 column (100 mm x 2.1 mm, 1.7 µm, Waters) connected to an Acquity H-class UPLC system. Prior separation, the column was heated to 40 °C and equilibrated with 5 column volumes of solvent A (0.1 % (v/v) formic acid in 10 % (v/v) acetonitrile) at a flow rate of 0.55 mL min^{-1}. Separation of ketoacid derivates was achieved by increasing the concentration of solvent B (acetonitrile) in solvent A (2 min 2 % B, 5 min 18 % B, 5.2 min 22 % B, 9 min 40 % B, 9.1 min 80 % B and hold for 2 min, and return to 2 % B in 2 min). The separated derivates were detected by fluorescence (Acquity FLR detector, Waters, excitation: 350 nm, emission: 410 nm) and quantified using ultrapure standards (Sigma). Data acquisition and processing were performed with the Empower3 software suite (Waters). Derivatisation and separation of amino acids was performed as described by Yang et al. (2015).

Total organic acids were extracted with 0.5 mL ultra-pure water for 20 min at 95 °C. Organic acids were separated using an IonPac AS11-HC (2 mm, ThermoScientific) column connected to an ICS-5000 system (ThermoScientific) and quantified by conductivity detection after cation

suppression (ASRS-300 2mm, suppressor current 95-120 mA). Prior separation, the column was heated to 30 °C and equilibrated with 5 column volumes of solvent A (ultra-pure water) at a flow rate of 0.38 mL min^{-1}. Separation of anions and organic acids was achieved by increasing the concentration of solvent B (100 mM NaOH) in buffer A (8 min 4 % B, 18 min 18 % B, 25 min 19 % B, 43 min 30 % B, 53 min 62 % B, 53.1 min 80 % B for 6 min, and return to 4 % B in 11 min). Soluble sugars were separated on a CarboPac PA1 column (ThermoScientific) connected to the ICS-5000 system and quantified by pulsed amperometric detection (HPAEC-PAD). Column temperature was kept constant at 25 °C and equilibrated with five column volumes of solvent A (ultra-pure water) at a flow rate of 1 mL min^{-1}. Baseline separation of carbohydrates was achieved by increasing the concentration of solvent B (300 mM NaOH) in solvent A (from 0 to 25 min 7.4 % B, followed by a gradient to 100 % B within 12 min, hold for 8 min at 100 % B, return to 7.4 % B and equilibration of the column for 12 min). Data acquisition and quantification was performed with Chromeleon 7 (ThermoScientific).

2.2.10 Fatty acid methyl ester measurement

Fatty acid methyl ester (FAME) analysis was performed as described before (Browse et al., 1986). 1 mL 1 N HCl in MeOH was added to 5 seeds or ~50 mg homogenised seedlings as well as 5 µg pentadecanoic acid as internal standard. Samples were incubated at 80 °C for 2 h (seeds) or 30 min (seedlings). After cooling down, 1 mL 0.9 % (w/v) NaCl and 1 mL hexane were added. Samples were mixed vigorously and centrifuged with 1,000 *g* for 3 min. Hexane phase was transferred to a GC vial. GC-MS data were analysed by Regina Wehler and Peter Dörmann.

2.3 Molecular biological techniques

2.3.1 DNA extraction from Arabidopsis tissue

DNA was extracted as described by Edwards et al. (1991). Plant tissue was homogenised in 400 µL buffer containing 200 mM Tris-HCl (pH 7.5), 250 mM NaCl, 25 mM EDTA and 0.5 % (w/v) SDS. After centrifugation (at 20,000 *g* for 10 min), the supernatant was transferred into a new tube, 400 µL isopropanol was added and the samples were centrifuged as before. The supernatant was discarded and the DNA was washed with 70 % (v/v) EtOH. The air-dried DNA was resuspended in 50 µL dH_2O, heated for 5 min at 95 °C, spun down and stored at -20 °C. DNA was quantified with the spectrophotometer NanoDrop 2000 (Thermo Scientific).

2.3.2 Polymerase chain reaction

For polymerase chain reactions (PCR), two different protocols were used. For cloning, the reaction was performed in a total volume of 50 µL containing 1x Phusion buffer, 200 µM dNTPs, 0.5 µM oligonucleotide A, 0.5 µM oligonucleotide B, 0.02 U μL^{-1} Phusion® high fidelity DNA polymerase and 0.5 µL template DNA. The thermocycling conditions, described below, were applied with the C1000™ thermal cycler from BIO-RAD (www.bio-rad.com).

step	temperature	time	
initial denaturation	98 °C	180 s	
denaturation	98 °C	30 s	34x
annealing	52-60 °C	30 s	
elongation	72 °C	60 s per kbp	
final extension	72 °C	300 s	
hold	12 °C	∞	

For genotyping and RT-PCR the reaction was executed in a total volume of 20 µL with 0.025 U μL^{-1} *Taq* DNA polymerase (New England BioLabs), 1x Standard *Taq* Reaction Buffer, 200 µM dNTPs, 0.2 µM oligonucleotide A, 0.2 µM oligonucleotide B and 2 µL template DNA. The following PCR-program was used:

step	temperature	time	
initial denaturation	95 °C	120 s	
denaturation	95 °C	30 s	20/30x
annealing	52-60 °C	30 s	
elongation	72 °C	60 s per kbp	
final extension	72 °C	420 s	
hold	12 °C	∞	

2.3.3 Genotyping of Arabidopsis mutants

For genotyping, genomic DNA was isolated (2.3.1) and PCR performed (2.3.2) as described previously. The oligonucleotides were designed with the T-DNA Primer Designer from SignalSalk (http://signal.salk.edu/tdnaprimers.2.html) and are listed with the respective sequence in Supplementary Table 4. Wild-type and T-DNA insertion alleles were identified with left and right genomic oligonucleotides or with the T-DNA oligonucleotide combined with a genomic oligonucleotide specified in Table 1. To identify mutants with deletion or mutation, the respective PCR products were digested as described below (2.3.4).

Table 1: Oligonucleotides used for genotyping of Arabidopsis mutants.

mutant name	combination for wild-type allele	combination for T-DNA insertion
grxs15-1	#2710; #2711	#2711; #1401
grxs15-2	#2747; #2748	#2748; #321
grxs15-3	#2708; #2709	#2709; #432
gr2	#328; #329	#328; #1401
rml1	#641; #642: digestion with ApoI	
atm3-4	#3523; #3524; digestion with NheI	

2.3.4 Digestion of DNA with restriction endonucleases

For DNA cleavage restriction enzymes cutting double-stranded DNA from Fermentas or New England BioLabs were used. Digestion was performed in 30 µL final volume with 1-2 U of enzyme pro 1 µg DNA. Reaction conditions (buffer, incubation time and temperature) were applied according to manufacturer's manual.

2.3.5 Isolation of RNA from Arabidopsis tissue

RNA was isolated with the NucleoSpin® RNA isolation kit (Macherey-Nagel) following the manufacturer's protocol. RNA was eluted in 50 µL dH_2O and quantified with the spectrophotometer NanoDrop 2000.

2.3.6 cDNA synthesis and semiquantitative RT-PCR

For reverse transcription of mRNA to cDNA, M-MLV Reverse Transcriptase Transcriptase (Thermo Scientific) was used following the manufacturer's protocol. 1 µg total RNA (see 2.3.5) was mixed with 2 µL of 50 mM oligo(dT) and filled up with dH_2O to achieve a volume of 12 µL. The samples were spun down briefly and incubated at 70 °C for 3 min. The tubes were placed back onto ice and 2 µL 10x First Strand Synthesis buffer, 4 µL dNTP mix (2.5 mM each), 1 µL dH_2O and 1 µL M-MLV Reverse Transcriptase were added. The samples were mixed gently and spun briefly. After incubation for 1 h at 42 °C the samples were incubated for 10 min at 92 °C to inactivate the M-MLV Reverse Transcriptase. The cDNA was subsequently amplified by a semi-quantitative PCR reaction to analyse the gene expression of *GRXS15* using gene-specific oligonucleotides #3218 and #3219 (2.1.4). *SAND* family protein (At2g28390) transcript was amplified with the oligonucleotides #2455 and #2456 as a constitutively expressed reference gene.

2.3.7 DNA Gel electrophoresis

Agarose gel-electrophoresis was employed to separate PCR products. Depending on the size of the expected PCR product 0.6-2 % (w/v) agarose was melted in 0.5x TBE-buffer (90 mM Tris-HCl pH 8, 90 mM boric acid, 0.5 mM EDTA) and ethidium bromide was added to a final concentration of 0.5 µg mL^{-1}. Before loading, DNA was mixed with loading buffer (0.025 % (w/v) bromophenol blue, 0.025 % (w/v) xylene cyanole and 4 % (v/v) glycerol). DNA was separated by applying a current of 120 V in 0.5x TBE running buffer. The gel was documented using MF-ChemiBIS 2.0 (DNR Bio-Imaging Systems).

2.3.8 PCR product purification from agarose gel

DNA fragments of interest were excised from agarose gels (2.3.7) and purified with the NucleoSpin® Gel and PCR Clean-up kit (Macherey-Nagel) according to the manufacturer's recommendations. DNA was eluted in 20 µL dH_2O.

2.3.9 Mutagenesis of GRXS15

Substitutions of specific amino acids were defined with a codon usage database (www.kazusa.or.jp/codon). The mutations were introduced by overlapping PCR using the oligonucleotides described in Table 2 in combination with the oligonucleotide #2594 or reverse #2592, respectively. The fragments were fused by a subsequent PCR using the oligonucleotide combination #2594 + #2592 and cloned into the respective entry clones.

Table 2: Oligonucleotides with base substitutions to introduce amino acid exchanges in GRXS15 through overlapping PCR reactions.

mutation	oligonucleotide combination[10]	nucleotide substitution
GRXS15 $C_{91}S$	#2753; #2754	TGT → TCT
GRXS15 K_{83}/A	#2841; #2842	AAA → GCT
GRXS15 K_{83}/E	#2839; #2840	AAA → GAA
GRXS15 K_{120}/A	#2849; #2850	AAA → GCT
GRXS15 K_{120}/E	#2847; #2848	AAA → GAA
GRXS15 K_{124}/A	#2853; #2854	AAA → GCT
GRXS15 K_{124}/E	#2851; #2852	AAA → GAA
GRXS15 D_{146}/A	#2845; #2846	GAC → GCT
GRXS15 D_{146}/R	#2843; #2844	GAC → AGA

[10] Detailed primer sequences are provided in Supplementary Table 4

Another procedure to substitute specific amino acids was performed by using the Q5® Site-Directed Mutagenesis Kit (BioLabs) following the manufacturer's instruction. Mutagenic oligonucleotides were designed using the NEBaseChanger™ and are listed in Table 3.

Table 3: Oligonucleotides with base substitutions to introduce amino acid exchanges in GRXS15 through site-directed mutagenesis on plasmid DNA.

mutation	oligonucleotide[11]	nucleotide substitution
GRXS15 K_{83}/A C_{91}/S	#3654; #3655	AAA → GCT

2.3.10 Gateway® cloning

For Gateway® cloning, the sequence of interest was amplified with *attB*-flanking sites and cloned into an entry vector using the Gateway® BP clonase II enzyme mix following the manufacturer's instruction. After transformation into *E. coli* DH5α (2.4.3), colonies were double checked by PCR for the presence of the respective gene construct and purified plasmids (2.4.4) were sequenced for validation (2.3.11).

Table 4: Vectors used for Gateway® cloning.

vector	selectable markers			description
	bacteria	plants	yeast	
pDONR201	Kan	-	-	entry clone for further Gateway® cloning
pDONR207	Gen	-	-	entry clone for further Gateway® cloning
pSS01	Kan	Kan	-	Fusion of roGFP2 to the protein's C-terminus (Brach et al., 2009)
pSS02	Kan	Hygr	-	derivative of pMDC3 (Curtis and Grossniklaus, 2003)
pB7GW2.0	Kan	BASTA	-	over-expression of gene of interest (Karimi et al., 2002)
pETG-10A	Amp	-	-	over-expression of gene of interest; EMBL Heidelberg
pAG415	Amp	-	Leu	over-expression of gene of interest; Susan Lindquist (Addgene plasmid # 14146)
pAG415-HA	Amp	-	Leu	over-expression of gene of interest; Susan Lindquist (Addgene plasmid # 14242)

[11] Detailed primer sequences are provided in Supplementary Table 4

The gene of interest was subcloned into a destination vector by the LR-reaction using the Gateway® LR clonase II enzyme mix. *E. coli* DH5α were transformed with the recombined vector and subsequently the plasmid was purified and used for transformation of the respective acceptor organism (Table 5).

To clone the TP_{GRXS15}:roGFP2 or GRXS15:roGFP2 construct into the respective entry vector, the oligonucleotides #2592 and #2659 were used. For GRXS15 and its variants the oligonucleotides #2592 and #2593 or #2594 were used dependent on a required stop-codon. Regarding $GRXS15_{38\text{-}169}$, #2626 was used to truncate the target peptide.

Table 5: Donor and expression vectors generated in this study.

entry clone	**expression clone**	**usage**	**finale organism**
pDONR201	pB7GW2 TP_{GRXS15}:roGFP2	localisation	*A. thaliana* wild-type
pDONR207	pSS01 GRXS15	localisation	*A. thaliana* wild-type
pDONR207	pSS02 GRXS15	Overexpression/ Complementation	*A. thaliana* wild-type, *grxs15-2*, *grxs15-3*
pDONR201	pAG415 TP_{GRXS15}:roGFP2	localisation	yeast wild-type
pDONR207	pAG415 GRXS15:roGFP2	localisation	yeast wild-type
pDONR201	pAG415 GRXS15	complementation	yeast *Δgrx5*
pDONR201	pETG-10A $GRXS15_{38\text{-}169}$	protein purification	*E.coli* Lemo21(DE3)
pDONR201	pETG-10A $GRXS15_{38\text{-}169}$ K_{83}/A	protein purification	*E.coli* Lemo21(DE3)
pDONR201	pETG-10A $GRXS15_{38\text{-}169}$ C_{91}/S	protein purification	*E.coli* Lemo21(DE3)
pDONR201	pAG415-HA GRXS15 C_{91}/S	complementation	yeast *Δgrx5*
pDONR201	pAG415-HA GRXS15 K_{83}/A	complementation	yeast *Δgrx5*
pDONR201	pAG415-HA GRXS15 K_{83}/E	complementation	yeast *Δgrx5*
pDONR201	pAG415-HA GRXS15 K_{120}/A	complementation	yeast *Δgrx5*
pDONR201	pAG415-HA GRXS15 K_{120}/E	complementation	yeast *Δgrx5*
pDONR201	pAG415-HA GRXS15 K_{124}/E	complementation	yeast *Δgrx5*
pDONR201	pAG415-HA GRXS15 K_{124}/A	complementation	yeast *Δgrx5*
pDONR201	pAG415-HA GRXS15 D_{146}/A	complementation	yeast *Δgrx5*
pDONR201	pAG415-HA GRXS15 D_{146}/R	complementation	yeast *Δgrx5*
pDONR207	pSS02 GRXS15 K_{83}/A	complementation	*grxs15-3*
pDONR207	pSS02 GRXS15 K_{120}/E	complementation	*grxs15-3*

2.3.11 DNA sequencing

Donor vectors (Table 5) recombined with gene of interest were verified by sequencing using the oligonucleotides #689 and #690. DNA sequencing was done by GATC Biotech® (Köln; www.gatc-biotech.com).

2.4 Microbiological methods

2.4.1 Bacterial and yeast strains

Table 6: Bacterial and yeast strains.

strain	genotype
E. coli DH5α	F– Φ80*lac*ZΔM15 Δ(*lac*ZYA-*arg*F) U169 *rec*A1 *end*A1 *hsd*R17 (rK–, mK+) *pho*A *sup*E44 λ– *thi*-1 *gyr*A96 *rel*A1
E. coli DB3.1	F– *gyr*A462 *end*A1 Δ(sr1-*rec*A) *mcr*B *mrr hsd*S20(rB–, mB–) *sup*E44 *ara*-14 *gal*K2 *lac*Y1 *pro*A2 *rps*L20(SmR) *xyl*-5 λ– *leu mtl*1
E. coli Origami (DE3)	Δ(ara-leu)7697 Δ lacX74 Δ phoA PvuII phoR ara Δ 139 ahpC galE galK rpsLF′[lac+ lacIq pro] (DE3)gor522::Tn10 trxB (KanR, StrR,TetR
E. coli Lemo21(DE3)	fhuA2 [lon] ompT gal (λ DE3) [dcm] ΔhsdS/ pLemo*(Cam^R)* λ DE3 = λ sBamHIo ΔEcoRI-B int::(lacI::PlacUV5::T7 gene1) i21 Δnin5 *pLemo = pACYC184*-PrhaBAD-lysY
A. tumefaciens C58C1	C58 background; T_i-plasmid cured (RifR, AmpR; Deblaere et al., 1985)
S. cerevisiae BY4742	*MATα ; his3Δ1; leu2Δ0; lys2Δ0; ura3Δ0* Wild-type, S288C derivative strain, EUROSCARF
S. cerevisiae YPL059w	*MATa; grx5 :: kanMX4* Deletion of *Grx5* in BY4742; EUROSCARF
S. cerevisiae CML235	*MATa ura3-52 leu2Δ1 his3Δ200* Wild-type (Rodríguez-Manzaneque et al., 1999); spore from FY1679 (S288C derivative strain)
S. cerevisiae MML1500	*MATa grx5 :: kanMX4* Deletion of *Grx5* in CML235
S. cerevisiae W303.1A	*MATa ura3-1 ade2-1 leu2-3,112 trp1-1 his3-11,15* Wild-type (Rodríguez-Manzaneque et al., 2002), W303 derivative strain
S. cerevisiae MML100	*MATa grx5 :: kanMX4* Deletion of *Grx5* in W303-1A (Rodríguez-Manzaneque et al., 2002)

2.4.2 Growth conditions for bacteria

Bacteria strains were cultured in LB-Medium (1 % (w/v) tryptone, 0.5 % (w/v) yeast extract, 1 % (w/v) NaCl, pH 7 with NaOH) at 37 °C (*E. coli*) or 28 °C (*A. tumefaciens*). For solid plates, media was supplemented with 1 % (w/v) agar before autoclaving. Antibiotics were sterile-filtrated and added after autoclaving (see 2.1.3 for concentrations). For an overnight-culture, a single colony was inoculated in 5 mL LB-medium.

2.4.3 Heat shock transformation of *E. coli*

100 µL chemically competent *E. coli* were incubated together with 1 µL of the respective plasmid or 5 µL of the BP/LR reaction for 50 s at 42 °C. Afterwards, 500 µL LB-medium was added and the culture was incubated for at least 30 min at 37 °C. Finally, the culture was plated on LB-agar plates containing the appropriate antibiotics and incubated overnight at 37 °C.

2.4.4 Isolation of plasmid DNA from *E. coli*

For plasmid extraction, 5 mL LB medium containing the appropriate antibiotics was inoculated with bacteria and placed in a 37 °C shaking incubator overnight. The plasmids were isolated with the NucleoSpin® Plasmid kit (Macherey-Nagel) following the manufacturer's protocol. The DNA was eluted in 50 µL dH_2O and quantified with the spectrophotometer NanoDrop 2000.

2.4.5 Electropulse transformation of *A. tumefaciens*

40 µL of electrically competent *A. tumefaciens* were mixed with 1 µL of the respective plasmid and transferred to the electroporation cuvette. Cells were pulsed with 2,500 V for approximately 5 ms. Subsequently, 500 µL LB-medium was added and the bacteria were incubated for at least 2-3 h at 28 °C. Afterwards, 50-100 µL of the culture was plated on agar plates containing the selective antibiotics and incubated for 2 d at 28 °C.

2.4.6 Growth conditions for *S. cerevisiae*

A single colony of the yeast strain was inoculated in YPD-medium (1 % (w/v) Bacto yeast extract, 2 % (w/v) peptone from casein and 2 % (w/v) glucose). For selection of positive yeast transformation, synthetic complete drop-out (SC) medium (0.67 % (w/v) yeast nitrogen base (YNB) without amino acids, 0.136 % (w/v) yeast synthetic drop-put medium and 2 % (w/v) glucose) was used lacking the specific amino acid depending on the used plasmid. For plates, 2 % (w/v) Bacto Agar was added. The cells were grown 2-3 d at 30 °C. Sensitivity to oxidants

was determined onto SC plates containing the indicated concentration of the agent, by spotting 1:5 serial dilutions of exponential cultures and recording growth after 2 d of incubation at 30 °C with a stereomicroscope (Leica M165 FC) equipped with a camera (DFC 425 C). Growth rates were measured in a volume of 260 µL at 28 °C on a plate reader (POLARstar Omega) monitoring the increase in absorbance at 600 nm.

2.4.7 Transformation of *S. cerevisiae*

The yeast transformation was performed using the lithium acetate/single-stranded carrier DNA/PEG method following the protocol from Gietz and Schiestl (2007) with slight modifications. A single colony of the yeast strain was inoculated into 10 mL liquid YPD medium and incubated overnight on a rotary shaker at 190 rpm and 30 °C. On the next day the culture was diluted to an OD_{600} of 0.1 and grown to an OD_{600} of 0.4-0.6. The cells were harvested with a volume for 1 OD by centrifugation at 3,000 *g* for 1 min. The pellet was resuspended in 1 mL sterile water and centrifuged again as before. The pellet was resuspended in 360 µL of transformation mix (0.1 M LiAc, 33 % (v/v) PEG4000, 2 mg mL^{-1} single-stranded carrier DNA and 34 µL plasmid DNA plus sterile water). The samples were incubated for 20-30 min at 42 °C. Thereafter, the tubes were centrifuged at 13,000 *g* for 1 min. The supernatant was discarded and the pellet was resuspended in 100 µL sterile water. The cell suspension was plated onto the appropriate SC selection medium and incubated for 3-4 d at 30 °C.

2.5 Protein methods and enzyme assays

2.5.1 Modelling of GRXS15 based on GLRX5

A homology model of Arabidopsis GRXS15 was built by using Phyre2 (Kelley et al., 2015) and human mitochondrial monothiol GLRX5 (PDB ID code: 2WUL) as a template. The coordinates of GSH and ISC were copied into the GRXS15 model after superimposition with GLRX5. Candidate side chains stabilising GSH within GRXS15 and their existence/biological relevance in other GRXs were compared with *At*GRXS14 (3IPZ), *Pt*GRXS14 (2LKU), *Hs*GLRX3 (3ZYW), *Hs*GLRX5 (2WUL), *Sc*Grx5p (3GX8), *Tb*Grx1 (2LTK), *Ec*Grx4 (1YKA), *At*GRXC5 (3RHB), *Pt*GRXC1 (1Z7P), *Pt*GRXS12 (3FZA), *Hs*GLRX2 (2HT9), *Sc*Grx1 (3C1R), *Sc*Grx2 (3CTF), *Sc*Grx6 (3L4N), and *Ec*Grx3 (3GRX).

2.5.2 Affinity-based purification of recombinant proteins

All recombinant proteins were expressed in *E. coli* and purified via affinity chromatography using an N-terminal His_6-tag. Cells were grown at 37 °C to an OD_{600} of ~0.8 in selective LB-medium and high level of protein expression was achieved by addition of IPTG to a final concentration of 1 mM. The cultures were harvested after 18-24 h at 20 °C. Cells were pelleted by centrifugation at 13,000 *g* for 10 min and resuspended in binding buffer (50 mM Tris-HCl, pH 8, 250 mM NaCl, 20 mM imidazole supplemented with 0.5 mM PMSF). After sonication the cell debris was pelleted by centrifugation and the supernatant filtered through a 0.45 µm sterile filter. Soluble proteins were loaded on a 1 mL Ni^{2+} loaded HisTrap™ HP affinity column (GE Healthcare) by cycling over the column for at least 30 min with a constant flow rate of 1 mL min^{-1}. The loaded column was washed several times with wash buffer (50 mM Tris-HCl, pH 8, 250 mM NaCl containing increasing concentrations of imidazole from 20 to 80 mM). Finally, the protein was eluted with buffer containing 250 mM imidazole.

2.5.3 SDS- PAGE

To separate individual proteins by molecular weight, the discontinuous gel system of Laemmli was used (Laemmli, 1970). For most purposes a 4 % stacking gel and 10 to 16 % resolving gel was prepared. Before gel loading, samples were heated for 5 min at 95 °C in 1x Laemmli sample buffer (2 % (w/v) SDS, 20 mM Tris HCl pH 6.8, 0.02 % (w/v) bromophenol blue, 0.4 M DTT and 10 % (v/v) glycerol). Sample and size standard (PageRuler Unstained Protein Ladder; Thermo Scientific) were loaded and the gel was run in running buffer (25 mM Tris-HCl pH 8.3, 192 mM Glycine, 0.1 % (v/v) SDS) at 110 V.

2.5.4 Staining of protein gels

Protein gels were stained with Coomassie (SERVA blue R, SERVA Electrophoresis). After electrophoretic separation, the gels were incubated at least for 1 h in staining solution (0.1 % (w/v) Coomassie, 10 % (v/v) acetic acid and 45 % (v/v) MeOH) on a shaker. The gels were discoloured with destaining solution containing 10 % (v/v) acetic acid and 30 % (v/v) EtOH or in water overnight.

2.5.5 Determination of protein content

The protein content was quantified by the Bradford assay (Bradford, 1976) with bovine serum albumin (BSA) as standard. 10 µL of protein solution was mixed with 260 µL Bradford reagent in 96-well plates (Sarstedt, flat base, transparent) and incubated for 5 min at RT. Optical density

(OD_{595}) of the samples was measured with a plate reader (POLARstar Omega; BMG) and the amount of protein was determined from the standard curve.

2.5.6 Protein gel blot and antibodies

For protein gel blot analysis, total cell extract or purified organelles were heated for 5 min and separated on standard SDS-PAGE gels. Proteins were transferred to a membrane (BioTrace PVDF Transfer Membrane; Pall Corporation) and labelled with antibodies (1:2,500 dilution GRXS15; 1:8,000 dilution ACO; 1:1000 dilution AOX1/2 (AS04054 Agrisera); 1:20,000 dilution Streptavidin HRP (ab7403 Abcam)). Immunolabelling was detected by chemiluminescence using secondary horseradish peroxidase-conjugated antibodies (1:20,000) and Pierce ECL Western Blotting Substrate. The GRXS15 antibody was a kind gift of Nicolas Rouhier (Nancy) and the ACO antibody the kind gift of Janneke Balk (Norwich).

Post-staining of membrane was performed by incubating the membrane for 5 min in amido black staining solution (0.1 % (w/v) amido black, 45 % (v/v) EtOH, 10 % (v/v) acetic acid) and washing it with water until background was white again.

2.5.7 HED assay

Reduction of HED was measured as the change in A_{340} in the following mixture: 0.1 M potassium phosphate buffer pH 7.8 containing 0.5 mM HED, 0.1 U GR, 500 µM NADPH, and 3 µM GRX. GSH (in 0.1 M phosphate buffer, pH 7.0) was automatically injected to a final concentration of 0.5 mM by using the built-in injector of the plate reader (POLARstar Omega; BMG, www.bmglabtech.com).

2.5.8 roGFP2 interaction assay

Interaction of GRX with roGFP2 was analysed as described previously (Aller et al., 2013) *in vitro* by ratiometric time-course measurements on a fluorescence plate reader (POLARstar Omega®; BMG) with filter-based excitation at 390 ± 10 nm and 480 ± 10 nm and detection of emitted light at 520 nm with a bandwidth of 10 nm. 0.1 M potassium phosphate buffer pH 7.8 containing 1 µM roGFP2 and 3 µM of the respective GRX was pipetted into the wells of a 96-well plate with flat bottom (Sarstedt). Ratiometric time-course measurements were carried out with initially oxidised or reduced roGFP2, respectively. For the latter, the protein was reduced with 10 mM DTT for 20 min. The remaining DTT was removed by desalting spin columns according to the manufacturer's manual (Zeba™ Spin Desalting Columns, Thermo Scientific). For interaction analysis with oxidised roGFP2, GSH (in 0.1 M potassium phosphate

buffer, pH 7.0) was automatically injected after 10 cycles to a final concentration of 2 mM using the built-in injectors. When working with oxidised roGFP2, a highly negative redox state of the glutathione buffer was maintained by addition of 1 U GR and 100 µM NADPH. For oxidation of roGFP2 40 µM GSSG was injected into the wells. Furthermore, H_2O_2 and DTT were used at a final concentration of 10 mM to preset roGFP2 to the fully oxidised and fully reduced state, respectively, and determine maximum and minimum fluorescence ratios of roGFP2 as reference values. A basal background fluorescence of buffer or buffer containing 100 µM NADPH was subtracted from fluorescence reads for all samples. The reduction and oxidation kinetics of roGFP2 in the presence of GRXC1 served as a positive control.

2.5.9 Aconitase and malate dehydrogenase assay

Arabidopsis seedlings were homogenised in extraction buffer (50 mM Tris-HCl pH 8.0, 50 mM KCl, 0.2 % (v/v) Triton X-100, 2 mM sodium citrate, 1 mM DTT) and centrifuged for 10 min at 4 °C. Extracts from yeast cells growing exponentially in SD medium were prepared in 0.1 M HEPES, pH 7.8, 0.1 % (w/v) ascorbate, 0.05 % (v/v) β-mercaptoethanol, 10 mM EDTA and 0.01 % (v/v) Triton X-100 by using glass beads to break the cells.

Aconitase activity was analysed in a coupled assay measuring NADPH formation by monitoring the increase in absorbance at 340 nm using a plate reader (CLARIOstar®; BMG). The reaction mixture contained 50 mM HEPES pH 7.8, 2.5 mM $NADP^+$, 5 mM $MnCl_2$, 0.1 % (v/v) Triton X-100 and 0.05 U isocitrate dehydrogenase. The mixture was allowed to come to equilibrium after addition of protein extract. The reaction was started by adding 8 mM cis-aconitic acid.

For measuring the malate dehydrogenase activity, the rate of change in A_{340} was monitored in the following mixture: 0.1 M HEPES pH 7.8, 0.5 mM NADH, 5 mM $MgCl_2$, 0.65 % (v/v) Triton X-100. The reaction was started by the addition of 750 µM oxaloacetic acid.

2.5.10 Nitrate reductase assay

Nitrate reductase (NR) assay was performed as described previously (Scheible et al., 1997) with slight modifications. Leaves were homogenised in extraction buffer (50 mM MOPS, pH 7.0, 50 mM KCl, 5 mM Mg-acetate, 1 mM CaCl, 2 mM Na-citrate and 1 mM DTT) and centrifuged for 10 min at 20,000 *g* and 4 °C. NR activity was measured in a reaction mixture containing 50 mM MOPS, pH 7.0, 50 mM KCl, 5 mM Mg-acetate, 1 mM CaCl, 10 mM KNO_3 and 0.4 mM NADH. At various time points, 150 µL aliquots were removed from the mixture and the reaction was stopped by adding 54 mM zinc acetate and 37.5 µM phenazine methosulfate.

Thereafter, 0.475 % (v/v) sulphanilamide in 1 N HCl and 0.005 % (v/v) N-(1-naphthyl)-ethylendiamine was added. Samples were allowed to stand for 15 min at RT in the dark and the absorbance of the produced azo-dye was measured at 540 nm.

2.5.11 Aldehyde oxidase and xanthine dehydrogenase assay

Aldehyde oxidase (AO) and xanthine dehydrogenase (XDH) assays were performed similar as described previously by Koshiba et al. (1996) and Hesberg et al. (2004). For determination of AO and XDH activities Arabidopsis seedlings were homogenised in extraction buffer (0.1 M potassium phosphate buffer pH 7.5, 2.5 mM EDTA and 5 mM DTT) and centrifuged for 10 min at 4 °C. Enzyme activities of AO and XDH in the resulting supernatant were detected after native PAGE by activity staining. Activity of AO was developed in a reaction mixture containing 0.1 M potassium phosphate buffer pH 7.5, 1 mM 1-naphthaldehyde, 1 mM indole-3-carboxaldehyde, 0.1 mM phenazine methosulfate (PMS), and 0.4 mM MTT (3-(4,5-dimethylthiazol-2-yl)-2,5-diphenyltetrazolium bromide) at RT. Activity of XDH was analysed with a staining solution of 1 mM hypoxanthine, 1 mM MTT and 0.1 mM PMS in 250 mM Tris-HCl, pH 8.5.

2.5.12 Pyruvate dehydrogenase complex assay

To estimate the activity of pyruvate dehydrogenase complex, mitochondria were isolated as described previously (2.2.7) and reduction of NAD^+ was measured at 340 nm in a reaction mixture containing ~10 µg mitochondria in 100 mM MOPS pH 7.4, 1 mM $CaCl_2$, 1 mM $MgCl_2$, 4 mM cysteine, 0.45 mM thiamine pyrophosphate, 0.18 mM Coenzyme A, 3 mM NAD^+ and 0.1 % (v/v) Triton X-100. The reaction was started with 7.5 mM pyruvate.

2.5.13 Reconstitution assay

The reconstitution assay was performed similar to the protocol described in Berndt et al. (2007). 0.1 M potassium phosphate buffer, pH 7.4 containing 200 mM NaCl, 0.01 molar equivalents of *E. coli* IscS, 2 equivalents of $Fe(NH_4)_2(SO_4)_2$, 2.5 equivalents of cysteine, 1 mM GSH, 5 mM dithiotreitol (DTT), 10 µM pyridoxal phosphate and 50 µM GRX was incubated under argon atmosphere at RT. After 2 h the mixture was desalted using Zeba™ Spin Desalting Columns (Thermo Scientific) according to the manufacturer's manual. UV-VIS spectra of the reconstitution was recorded on a plate reader (CLARIOstar® BMG) monitoring the absorbance at 250-750 nm.

2.6 Microscopic methods

2.6.1 GSH visualisation *in vivo*

The *in vivo* GSH content was determined as previously reported by Cairns et al. (2006). Plants were germinated for 4 d on 0.5 MS plates containing 2 mM BSO (L-buthionine-[S, R] sulfoximine) before being transferred for 24 h to 0.5 MS plates without BSO to initiate GSH recovery. Seedlings were stained with 100 µM monochlorobimane and 50 µM propidium iodide for 30 min before performing confocal laser scanning microscopy analysis.

2.6.2 Silique imaging

Defective seed development was noted by dissecting siliques of self-pollinated plants and counting the number of normal and aborted seeds present in each silique. To determine the phenotypes of embryos, whole siliques were destained with Hoyer's solution (7.5 g gum arabic, 100 g chloral hydrate, 5 mL glycerol and 60 mL dH_2O) overnight. Siliques were analysed with a stereomicroscope (Leica M165 FC) equipped with a camera (DFC 425 C) by using the software LAS V3.8 (Leica Application Suite).

2.6.3 GUS staining

Histochemical staining of pollen was performed for the confirmation of T-DNA mutants (SAIL-431-H03) containing the T-DNA pCSA110 with a Lat52 promoter-β-glucuronidase fusion. Pollen were placed in a solution containing 10 µM X-Gluc (Duchefa Biochemie), 50 mM potassium ferricyanide and 50 mM potassium ferrocyanide in 0.1 M sodium phosphate buffer pH 7.0 and incubated in the dark at 37 °C overnight. After 24 h, pollen were analysed by bright field microscopy (Axio Observer.Z1, Carl Zeiss Microscopy) equipped with a 20x lens (LD Plan-Neofluar® 20x/0.4 Korr, Carl Zeiss Microscopy) and with a camera (Zeiss AxioCam MRc) using the software Palm Robo V4.5.

2.6.4 Subcellular localisation and fluorescence microscopy

Fluorescent plants and yeast colonies were detected on a stereomicroscope (Leica M165 FC) equipped with a GFP or DsRed filter and documented with an attached camera (Leica DFC425 C). For co-localisation in mitochondria, samples were incubated with 0.5 µM MitoTracker Orange CM-H_2TMRos for at least 15 min. Yeast cells were transferred to a slide and immobilised with 0.1 % (w/v) agarose. A confocal laser scanning microscope (Zeiss LSM 780, attached to an Axio Observer.Z1; Carl Zeiss Microscopy) was used for confocal imaging. Images were collected with a 40× (C-Apochromat 40×/1.2 W Korr) or a 63× lens (Plan-

Apochromat 63×/1.40 Oil DIC). For localisation studies, GFP was excited at 488 nm and MitoTracker at 543 nm. roGFP2 fluorescence was collected with a 505-530 nm bandpass filter and MitoTracker fluorescence with a bandpass filter of 560-620 nm. Chlorophyll autofluorescence was excited at 488 nm and detected with a bandpass filter of 647-745 nm.

For ratiometric analyses of mitochondrial localised roGFP2:hGRX1 or roGFP2:Orp1, roGFP2 was excited at 405 and 488 nm. For both excitation wavelengths, roGFP2 fluorescence was collected with a bandpass filter of 505-530 nm.

The cytosolic ATeam was excited at 458 nm and emission of FRET-pair proteins CFP (mseCFP) and YFP (cp173-mVenus) was collected at 499-544 nm and 579-615 nm, respectively.

Cytosolic NADH/NAD^+ redox state was assessed with the Peredox-mCherry sensor, exciting tSapphire and mCherry at 405 and 543 nm, respectively and collecting the emission at 499-544 nm and 579-615 nm.

2.7 Phylogenetic analysis

An alignment of GRX full-length amino acid sequences, which were retrieved from TAIR (Lamesch et al., 2012), was generated with MUSCLE (Edgar, 2004). The evolutionary history was inferred by using the maximum likelihood method based on the JTT matrix-based model. The tree with the highest log likelihood (−3940.9281) is shown. The percentage of trees in which the associated taxa clustered together is shown next to the branches. Initial tree(s) for the heuristic search were obtained automatically by applying neighbour-join and BioNJ algorithms to a matrix of pairwise distances estimated by using a JTT model, and then selecting the topology with superior log likelihood value. A discrete gamma distribution was used to model evolutionary rate differences among sites [five categories (+G, parameter = 4.3811)]. The rate variation model allowed for some sites to be evolutionarily invariable ([+I], 2.7321 % sites). The tree is drawn to scale, with branch lengths measured in the number of substitutions per site. The analysis involved 32 amino acid sequences. All positions with less than 95 % site coverage were eliminated. Thus, less than 5 % alignment gaps, missing data, and ambiguous bases were allowed at any position. In total, 92 positions remained in the final dataset. Evolutionary analyses were conducted in MEGA6 (Tamura et al., 2013). Bootstrap value: 5,000.

2.8 Synonyms and AGI locus code of used Arabidopsis genes

GRXC1 (At5g63030), GRXC2 (At5g40370), GRXC3 (At1g77370), GRXC4 (At5g20500), GRXC5 (At4g28730), GRXC6 (ROXY21; At4g33040), GRXC7 (ROXY1; At3g02000), GRXC8 (ROXY2; At5g14070), GRXC9 (ROXY19; At1g28480), GRXC10 (ROXY20; At5g11930), GRXC11 (ROXY4; At3g62950), GRXC12 (ROXY5; At2g47870), GRXC13 (ROXY9; At2g47880), GRXC14 (ROXY8; At3g62960), GRXS1 (ROXY16; At1g03020), GRXS2 (ROXY10; At5g18600), GRXS3 (ROXY11; At4g15700), GRXS4 (ROXY13; At4g15680), GRXS5 (ROXY12; At4g15690), GRXS6 (ROXY17; At3g62930), GRXS7 (ROXY14; At4g15670), GRXS8 (ROXY15; At4g15660), GRXS9 (ROXY7; At2g30540), GRXS10 (ROXY3; At3g21460), GRXS11 (ROXY6; At1g06830), GRXS12 (At2g20270), GRXS13 (ROXY18; At1g03850), GRXS14 (GRXcp, CXIP1, At3g54900), GRXS15 (GRX4, At3g15660), GRXS16 (GRX2, CXIP2, At2g38270), GRXS17 (At4g04950), ScGrx5p (NP_015266), MFDX1 (At4g05450).

3. Results

3.1 Functional characterisation of GRXS15

3.1.1 Subcellular localisation of GRXS15 in mitochondria

During the last decade, the subcellular distribution of several GRXs has been proven experimentally (Figure 2), but still the compartmentation of most GRXs is based on predictions derived from bioinformatic algorithms. Regarding Arabidopsis GRXS15 the subcellular localisation is ambiguous as discussed above. Because the site of action is a prerequisite for an understanding of protein function, we investigated the localisation of GRXS15 more precisely. Sequence analysis with TargetP 1.1 (Emanuelsson et al., 2000) predicted that GRXS15 contains a N-terminal mitochondrial target peptide with a length of 37 amino acids. To resolve the controversial uncertainty of the subcellular localisation, the predicted 37-aa target peptide (TP_{GRXS15}) and the full-length sequence of GRXS15 were cloned in frame with GFP under control of the *35S* promoter and stably expressed in Arabidopsis. In both cases, the GFP signal was exclusively localised in mitochondria as visualised through co-localisation of GFP with the mitochondrial marker MitoTracker (Figure 8A).

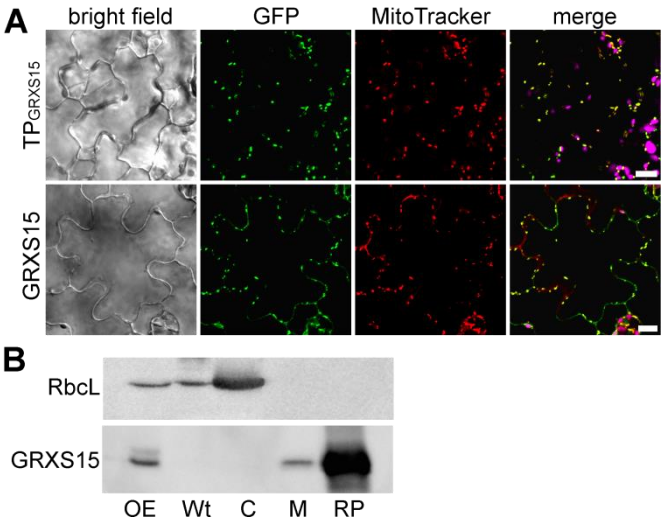

Figure 8: Subcellular localisation of GRXS15 in Arabidopsis.
A: Expression of *35S*$_{pro}$:TP_{GRXS15}:GFP and *35S*$_{pro}$:GRXS15:GFP in leaf epidermal cells. GFP, green; MitoTracker, red; chlorophyll autofluorescence, magenta. Scale bars = 1 µm.
B: Protein gel blot analysis with antiserum raised against Arabidopsis GRXS15. 15 µg of protein isolated from whole leaves of a GRXS15 overexpression plant (OE) and a wild-type plant (Wt) as well as proteins of isolated wild-type chloroplasts (C) and wild-type mitochondria (M) were loaded along with 0.5 µg of recombinant protein (RP). Immunoreactivity of the large subunit of RuBisCO (RbcL) served as control for purity of the mitochondrial preparation.

This result was further corroborated through protein gel blot analysis in which GRXS15 was only detectable in isolated mitochondria but not in chloroplasts (Figure 8B). In whole-leaf extracts of wild-type plants, no GRXS15 was detectable consistent with decreased relative abundance of mitochondrial proteins.

3.1.2 Disruption of GRXS15 causes early embryo abortion

To gain insight into the physiological role of GRXS15 in Arabidopsis, three transfer DNA insertion lines for the gene locus At3g15660 were isolated. These mutants included two lines with insertions in the 5′-UTR, denominated as *grxs15-1* and *grxs15-3* as well as a line with an insertion in the first intron of the gene sequence (*grxs15-2*; Figure 9A). Left border flanking sequences of the T-DNA insertions in *grxs15-1, grxs15-3* and *grxs15-2* were sequenced and the insertion sites were mapped to positions −141, −173, and +322 bp relative to the start codon, respectively. Homozygous *grxs15-1* plants were phenotypically indistinguishable from wild-type under normal growth conditions (Figure 9C and Supplemental Figure 1). Whereas in wild-type plants the gene is transcribed into two different transcripts annotated as At3g15660.1 and At3g15660.2 (Lamesch et al., 2012), *grxs15-1* contains only one transcript with a truncated 5′-UTR without obvious changes in transcript abundance (Supplemental Figure 1). Because this result implies that *grxs15-1* is not a null mutant, it was excluded from further analysis.

The only phenotype of *grxs15* null mutants described thus far is sensitivity toward H_2O_2, which led to the suggestion that GRXS15 may be involved in the maintenance of growth and development under oxidative stress conditions. Interestingly, no homozygous *grxs15-2* and *grxs15-3* mutants were found, although the *grxs15-2* line was described as viable in homozygous form before (Cheng, 2008). In both cases, selfed heterozygous plants segregated in a 1:2 (susceptible:resistant) pattern (Figure 9B). Furthermore, the mutant *grxs15-2* was generated with a T-DNA containing a GUS gene driven by a pollen-specific promoter in the quartet (*qrt*) background that prevents separation of pollen after meiosis. Here, heterozygous plants always produced pollen tetrads with two GUS-positive pollen, which strongly suggests the absence of a second unlinked T-DNA insertion (Figure 9D). Analysis of developing seeds from selfed *grxs15-2* and *grxs15-3* plants revealed frequent abortion (Figure 9B, C). Whereas 23 % of aborted *grxs15-2* seeds were still supporting the hypothesis of a 3:1 (viable:aborted) segregation excluding an effect of gametogenesis, abortion in *grxs15-3* was slightly less frequent with approximately 20 % (Figure 9B). Interestingly, abortion *in grxs15-2* occurred at an early stage after fertilisation, whereas the presumed homozygous seeds in *grxs15-3*

progressed significantly further in development and even initiated endosperm formation. The seeds nevertheless stayed transparent because embryo development was arrested at globular stage (Figure 9E).

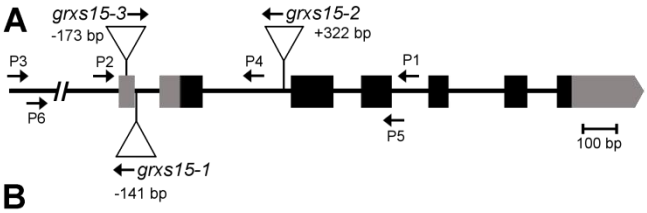

B

progeny genotype				
parental line	*GRXS15*/*GRXS15*	*GRXS15*/*grxs15*	*grxs15*/*grxs15*	χ^2- value
grxs15-2	23	49	0	0.06 (p = 0.97)
grxs15-3	18	38	0	0.04 (p = 0.98)
seed development				
parental line	aborted seeds	normal seeds		χ^2- value
grxs15-2	273	910		2.4 (p = 0.3)
grxs15-3	177	688		9.5 (p = 0.008)

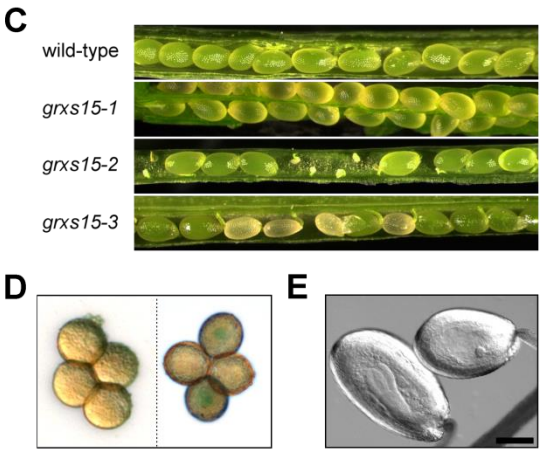

Figure 9: Isolation and characterisation of *grxs15* mutants.
A: Physical map of the *GRXS15* gene according to the gene model At3g15660.2. Introns are represented by lines and exons as boxes. Both UTRs are depicted in gray. The primers used for genotyping are indicated by numbered arrows. The T-DNA insertions of the mutant lines *grxs15-1*, *grxs15-2* and *grxs15-3* are shown as inverted triangles with the identified insertion site relative to the start codon indicated. Blank arrows depict the left border (LB) primers used for genotyping and indicate the orientation of the T-DNA.
B: Segregation pattern and seed development of *grxs15* T-DNA insertion mutants. X^2 values for the progeny genotype are calculated on an expected ratio of 1:2 and for seed development on an expected ratio of 3:1. The degree of freedom in both cases is 2.
C: Opened siliques from wild-type, *grxs15-1*, *grxs15-2* and *grxs15-3* plants.
D: GUS labelling of *qrt* pollen tetrads from a segregated plant homozygous for the wild-type allele *GRXS15* (Left) or from a heterozygous *grxs15-2* plant (Right).
E: Differential interference contrast image of normal (Left) and transparent (Right) seed from the same silique of a *grxs15-3* plant. Scale bar = 150 µm.

To further confirm that the observed early embryo arrest was caused specifically by disruption of *GRXS15*, both null mutants were complemented with wild-type *GRXS15* driven by the *UBQ10* promoter, while complementation driven by the *35S* promotor failed. All complemented plants were phenotypically normal, demonstrating the importance of GRXS15 for plant growth and development (Figure 10A, B).

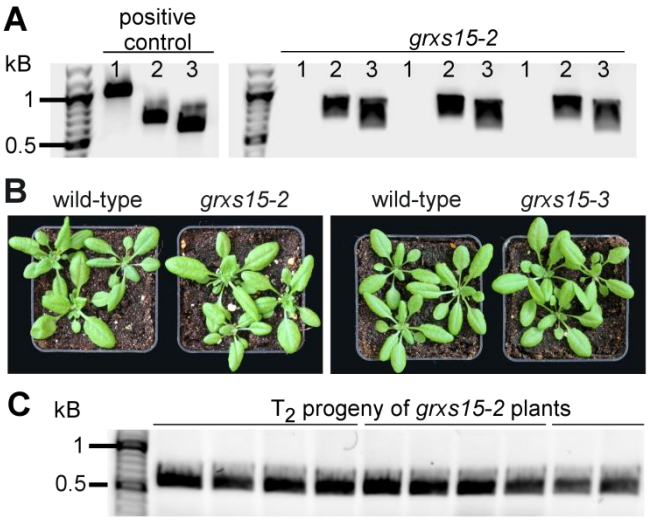

Figure 10: Complementation of *grxs15* null mutants.
A: Isolation of homozygous T-DNA mutants complemented with *GRXS15* by genotyping. Plants were screened with primer combination for the wild-type allele (1), T-DNA insertion (2) and complementation construct (3) using a forward primer binding in the $UBQ10_{pro}$ and an exon-exon spanning reverse primer annealing to exon 2 and exon 3 in the coding region of *GRXS15*.
B: Homozygous *grxs15* $UBQ10_{pro}$:GRXS15 T_2 plants and the respective wild-type were grown for 4 weeks on soil, revealing no obvious differences under these growth conditions.
C: PCR analysis of T_2 progeny from three independent homozygous *grxs15-2* $UBQ10_{pro}$:GRXS15 plants. Using a forward primer binding in the $UBQ10_{pro}$ and an exon-exon spanning reverse primer annealing to exon 2 and exon 3 in the coding region of *GRXS15* consistently results in the anticipated PCR product of 591 bp.

The viable T_2 progeny of complemented *grxs15-2* plants all contain the *GRXS15* transgene (Figure 10C) indicating that a loss of the complementation construct due to segregation causes lethality. These complementation data validate the conclusion that the embryo lethality is due to GRXS15 deficiency.

3.1.3 ISC binding of GRXS15

As shown above, GRXS15 is an indispensable mitochondrial protein in Arabidopsis and the unknown link between embryo lethality and lack of GRXS15 raises questions concerning its function. Monothiol GRXs have been considered as components of the FeS-protein assembly machinery. However, the involvement of GRXS15 in the maturation of FeS-proteins in mitochondria remains elusive in plants because, among all poplar monothiol CGFS GRXs, it is the only isoform failing to rescue most phenotypes of the yeast *Δgrx5* mutant (Bandyopadhyay et al., 2008). Here again, conflicting results were published with the Arabidopsis GRXS15, showing a full complementation of the yeast *Δgrx5* mutant (Cheng et al, 2008). Thus, distinct growth defects displayed by the yeast *Δgrx5* strain were exploited for functional complementation studies. The original GRXS15 target peptide of 37-aa is sufficient for targeting GFP or a GRXS15:GFP fusion to mitochondria in yeast (Figure 11A), as in plants.

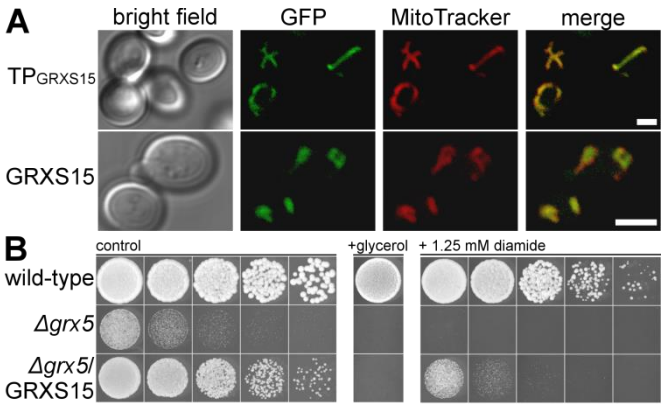

Figure 11: Complementation of the yeast *Δgrx5* mutant by Arabidopsis GRXS15.
A: Subcellular localisation of TP_{GRXS15}:GFP or GRXS15:GFP in *Saccharomyces cerevisiae* cells. Cultures were grown in liquid drop-out medium before incubation with the mitochondrial marker MitoTracker. GFP, green; MitoTracker, red. Scale bars = 2 μm.
B: Yeast growth on drop-out medium. Serial fivefold dilutions of wild-type (BY4742) and the respective *Δgrx5* mutant (YPL059w), transformed with an empty vector, and the *Δgrx5* mutant transformed with GPD_{pro}:GRXS15 were spotted on plates containing glucose (Left) or glucose with 1.25 mM diamide (Right) and grown at 30 °C. No growth was observed on drop-out medium containing glycerol instead of glucose to enforce respiratory growth (Center). One representative experiment from three independently performed experiments is shown.

To test for yeast complementation we thus used the full-length sequence of GRXS15 for detailed complementation studies. Indeed, the complementation resulted in partial rescue of *Δgrx5*. Moreover, expression of GRXS15 also diminished the sensitivity of *Δgrx5* to the

oxidative agent diamide but not the respiratory growth defect on glycerol (Figure 11B). These observations strongly point at a partial functional conservation between yeast Grx5p and Arabidopsis GRXS15.

To support the hypothesis that GRXS15 is involved in supplying ISC to mitochondrial proteins, the capacity of recombinant GRXS15 for binding an ISC was analysed. *Escherichia coli* cells expressing GRXS15 did not display the strong characteristic brownish colour associated with the presence of an ISC in overexpressed proteins. However, when the recombinant protein was purified in the presence of 4 mM GSH, the UV-visible spectrum showed a pronounced shoulder at 420 nm, indicating that ISC coordination by GRXS15 occurred in *E. coli* and is stabilised by GSH. Because GRXS15 ISC incorporation was likely far from completion, an *in vitro* reconstitution assays was performed under anaerobic conditions by using the purified apoprotein. In this case, the visible part of the absorption spectrum of the reconstituted protein presented a prominent absorbance peak at approximately 420 nm compared with the apoprotein (Figure 12A), which is characteristic for the presence of an $[2Fe\text{-}2S]^{2+}$ cluster or a mixture of $[2Fe\text{-}2S]^{2+}$ and linear $[3Fe\text{-}4S]^{+}$ clusters.

Based on the ability of GRXS15 to coordinate an ISC *in vitro*, a homology model was built with human GLRX5 as template (Figure 12B) and GRXS15 candidate residues were compared for noncovalent binding of GSH as a prerequisite for ISC coordination to other GRX structures (Figure 12C). Whereas position K_{83} is fully conserved in all analysed GRX structures, position K_{120} is more variable but usually retains residues that may participate in GSH binding through hydrogen bonding. However, especially K_{83} that resides near the catalytic cysteine might influence via ionic interactions of the positively charged residues the stability of the cysteine thiolate of C_{91} and thus lowering the ability to coordinate an ISC (Deponte, 2013). Based on the modelled structure, several substitutions were carried out to manipulate the direct environment of the putative ISC binding in a targeted manner. The mutations included charge inversions to gain drastic effects and substitutions by alanine that were anticipated to be less severe. Indeed, a K_{83}/A mutant variant was still able to coordinate an ISC, albeit less efficient than the wild-type but better than the C_{91}/S mutant (Figure 12A).

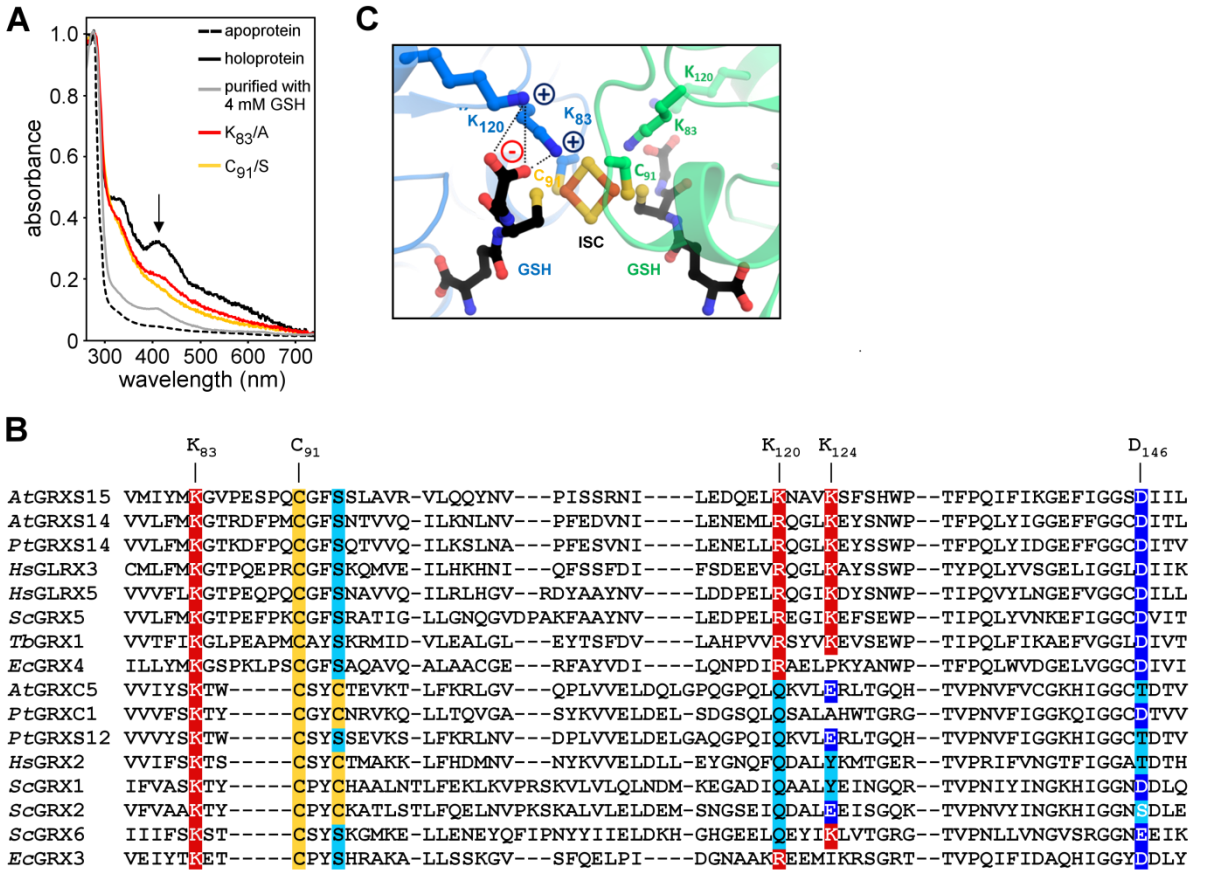

Figure 12: Coordination of an ISC by GRXS15.
A: Reconstitution of an ISC in GRXS15. UV-visible spectra of apo- (dashed line) and holo-GRXS15 (straight black line), the K_{83}/A (red), and the C_{91}/S substituted protein (yellow) 2 h after reconstitution or directly after purification from *E. coli* in the presence of 4 mM GSH (grey). The spectra were normalised to the absorbance at 278 nm.
B: Amino acid alignment of GRXS15 and other ISC binding GRXs core region. The sequence alignment was performed with MUSCLE. Enumeration of the amino acids is based on GRXS15.
C: Structure modelling of GRXS15. A homology model was built by using Phyre2 with human mitochondrial GLRX5 as template. Highlighted are the amino acids K_{83} and K_{120} that may form hydrogen bonds with the carboxyl group of GSH as well as C_{91} that directly interacts with the ISC.

3.1.4 Diminished ISC coordination by GRXS15 limits the ability to complement

To explore the functional impact of GRXS15 on cellular ISC homeostasis and maintenance of FeS-proteins, *Δgrx5* yeast strains expressing the mutant GRXS15 variants were analysed for complementation of growth defects and the activity of ISC-containing aconitase. Mutants lacking the active site cysteine (C_{91}) or carrying a K_{83}/E substitution were no longer able to complement the *Δgrx5* mutant, indicating the essential role of both amino acids (Figure 13A). Substitution K_{83}/A turned out to be less severe and still allowed for residual complementation, whereas mutations of K_{120} generally had only diminutive effects on the ability of GRXS15 to

complement *Δgrx5*. In contrast, mutations of K_{124} or D_{146} had no effect resulting in a similar complementation as the native GRXS15 (Supplemental Figure 2).

Furthermore, ACO activity strongly depended on the mutations, while malate dehydrogenase (MDH), a mitochondrial non-ISC enzyme used as control, showed similar activity in all complemented lines and wild-type. Less severe mutations led to a minor proportional decrease in ACO/MDH activity ratio, while mutant variants that did not rescue *Δgrx5* growth showed only low ACO activity (Figure 13B).

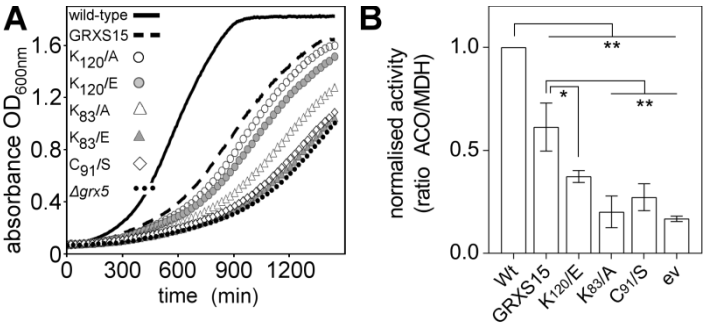

Figure 13: Rescue of the yeast *Δgrx5* mutant defects by mutated GRXS15.

A: Growth of the yeast *Δgrx5* mutant, complemented with different versions of *GRXS15*. The absorbance at 600 nm was followed over time. One representative experiment from three independently performed experiments is shown.

B: Normalised ratio of aconitase (ACO)/malate dehydrogenase (MDH) activity. Enzyme activity was measured in total yeast cell extract of complemented *Δgrx5* mutant. (n = 3 ± SEM), Asterisks indicate statistically significant differences (Student's t test: *P ≤ 0.1; **P ≤ 0.05) compared with wild-type or GRXS15-complemented *Δgrx5* mutant.

To analyse whether the diminished function of GRXS15 has also an influence on the maturation of FeS-proteins in the plant context, we complemented the Arabidopsis *grxs15-3* null mutant with the mutated GRXS15 variants K_{120}/E and K_{83}/A based on the observation that both mutations lead to different degrees of partial complementation of the yeast *Δgrx5* mutant. In both cases homozygous plants for the *grxs15-3* null allele were obtained. The *grxs15-3 UBQ10pro:GRXS15 K_{120}/E* plants showed no obvious differences in phenotype, whereas the *grxs15-3 UBQ10pro:GRXS15 K_{83}/A* complemented lines showed severely reduced growth. Analysis of root length in the *grxs15* mutant lines showed also a reduction of primary root length compared to wild-type (Figure 14A, B). As line #3 seems to grow best and line #4 worse these two lines were chosen for further analysis. To further test whether the reduced root length of GRXS15 K_{83}/A complemented null mutants was a true growth retardation or only a

phenotype caused by a delay of development, we determined the germination rate in the two complemented lines #3 and #4. The absence of any difference between wild-type and mutant suggests that the growth phenotype indeed reflects a *bona fide* growth retardation (Figure 14C).

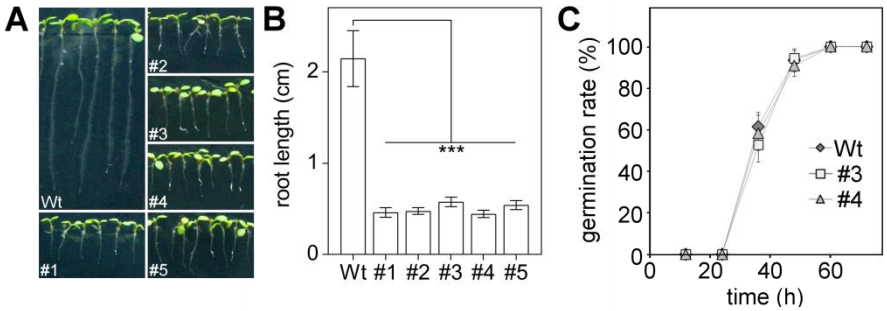

Figure 14: Rescue of the *grxs15-3* mutant by GRXS15 K_{83}/A.
A: 8-d-old wild-type (Wt) seedlings compared with *grxs15-3 UBQ10:GRXS15 K_{83}/A* mutants grown on vertical agar plates under long-day conditions.
B: Primary root length of 8-d-old *grxs15-3 UBQ10:GRXS15 K_{83}/A* mutants compared to wild-type (n = 35 ± SD). Student's t-Test analysis showed significant differences between wild-type and all mutant lines *** = P<0.001.
C: Germination rate of *grxs15-3 UBQ10:GRXS15 K_{83}/A* line #3 and #4 compared to the wild-type after 1 d stratification (n = 6 with 20-25 seeds each ± SD).

3.1.5 GRXS15 K_{83}/A does not affect biotin-dependent enzymes

We were wondering if the dwarfed phenotype is based on an inefficient ISC transfer to specific mitochondrial FeS-proteins. One putative candidate is the biotin synthase (BIO2, At2g43360) catalysing the final step in the biotin biosynthetic pathway. Biotin is an essential cofactor for several enzymes and *bio2* null mutants were previously described as embryo lethal arresting mostly at the globular or heart stage (Arnal et al., 2006; Patton et al., 1998). Biotin-dependent methylcrotonoyl-CoA carboxylase (MCCase) is involved in leucine degradation in mitochondria which might be affected in mutants with diminished GRXS15 activity. However, there was just a slight decrease in protein abundance of the biotinylated MCCase subunit MCCA (Figure 15A). Biotin is also exported to the cytosol and chloroplasts where it is required for synthesis and elongation of fatty acids by hetero- and homomeric acetyl-CoA carboxylase (ACCase). Here, also just a slight decrease of protein amount was observed, which had no influence on fatty acid amount or ratio of specific fatty acids in seeds or young seedlings in the worst growing mutant line #4 (Figure 15B-D, Supplemental Figure 3A-C).

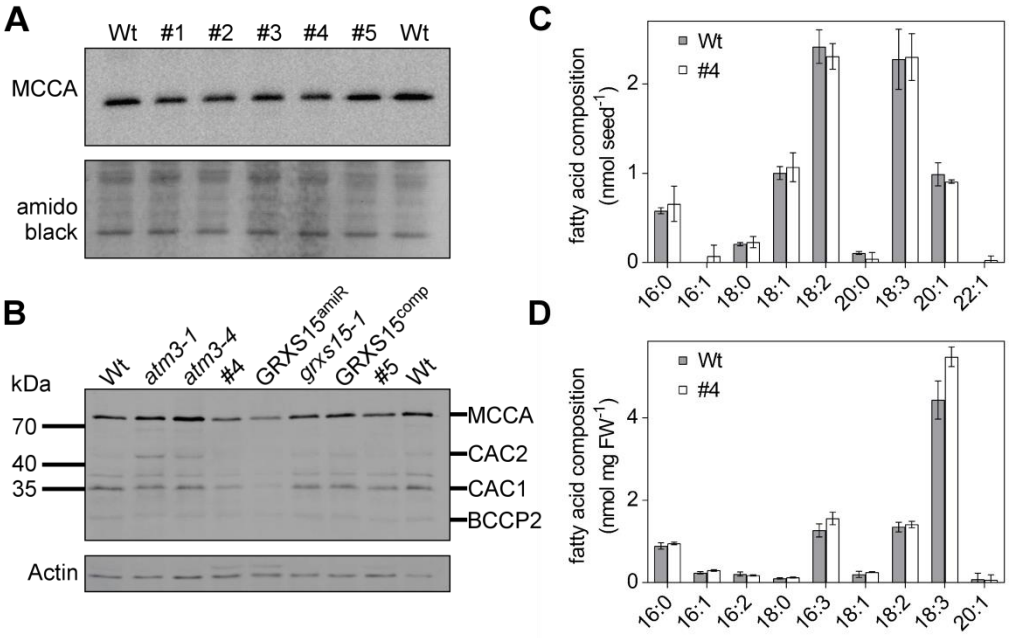

Figure 15: GRXS15 K_{83}/A mutation has no impact on the biotin pathway.
A: Immunoblot analysis of biotinylated MCCA in mitochondria of GRXS15 K_{83}/A mutants compared with wild-type. In the upper panel, biotinylated MCCA was detected by streptavidin HRP (ab7403 Abcam) in isolated mitochondria (9 µg protein was loaded). In the lower panel, amido black staining of the membrane is shown as a control for protein loading.
B: Protein expression of biotinylated proteins in total proteins of GRXS15 K_{83}/A mutants line #4 and #5, a knock-down line (GRXS15^{amiR}), the T-DNA insertion line *grxs15-1*, and the *grxs15-1* mutant complemented with GRXS15 (GRXS15^{comp}) compared with wild-type and *atm3* mutants. In the upper panel, biotinylated proteins were detected by streptavidin HRP in total proteins. In the lower panel, expression of actin is shown as a control for protein loading. Data were provided by Inga Kruse and Janneke Balk.
C, D: Fatty acid profiles (FAMEs) quantified by GC-MS of seeds and 8-d-old seedlings of GRXS15 K_{83}/A line #4 compared with wild-type. FAMEs were measured by GC-FID using pentadecanoic acid as internal standard. (n = 3-4 ± SD).

Furthermore, it has been shown that *bio1* as well as *bio2* mutants can be rescued by the addition of biotin to arrested embryos cultured *in vitro* and to mutant plants grown on soil (Patton et al., 1998; Schneider et al., 1989). However, growing the *grxs15* mutants on biotin-containing medium did not rescue the growth defect, indicating that a defect in the biotin synthesis is not the cause of the phenotype of *grxs15* mutants (Supplemental Figure 3D).

3.1.6 Moco-dependent enzymes are not affected in the K_{83}/A mutant

Another mitochondrial FeS-protein is CNX2 (At2g31955) that catalyses the first step of Moco biosynthesis in which GTP is converted to cPMP (Bittner, 2014; Hänzelmann et al., 2004). The most abundant Moco-dependent enzymes include nitrate reductase (NR; At1g37130), aldehyde oxidase (AAO3; At2g27150), xanthine dehydrogenase (XDH1; At4g34890) and sulfite oxidase (SO; At3g01910). Interestingly, we found that the growth retardation of the K_{83}/A mutant roots is more pronounced on nitrate (KNO_3), than on ammonium ($(NH_4)_2SO_4$) as only nitrogen source (Figure 16A-C). Similar results were obtained when seedlings were grown on NH_4Cl instead of $(NH_4)_2SO_4$ to exclude possible impacts of the respective counter anions on the growth behaviour (Supplemental Figure 4B, C).

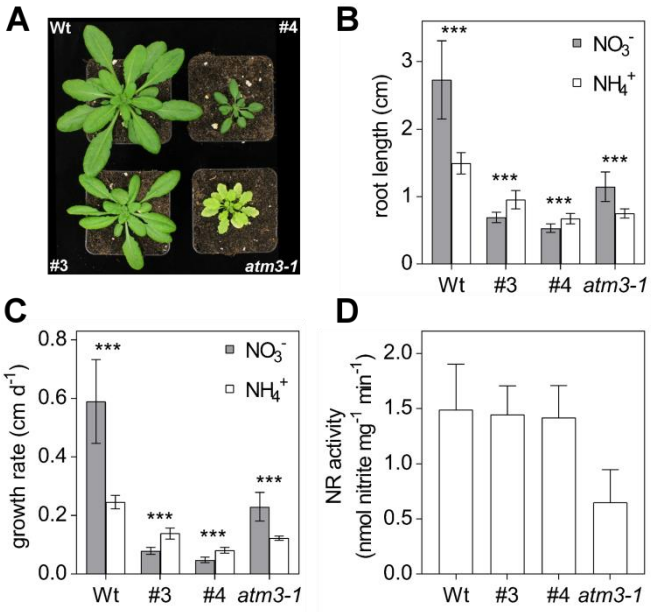

Figure 16: The nitrogen source influences growth of GRXS15 K_{83}/A mutants.
A: Representative 4-week-old wild-type plant compared with GRXS15 K_{83}/A line #3 and #4 as well as *atm3-1* grown on soil under long-day conditions.
B: Primary root length of GRXS15 K_{83}/A line #3 and #4 as well as *atm3-1* seedlings compared to wild-type (Wt) grown on vertical agar plates for 8 d under long-day conditions containing 5 mM KNO_3 or 2.5 mM $(NH_4)_2SO_4$ as N-source (n = 30 ± SD). Student's t-Test analysis showed significant differences between the growth on the different N-sources in all lines *** = P<0.001.
C: Growth rate calculations from root length measurements at day 5 and day 8 under long-day conditions (n = 30 ± SD) from seedlings depicted in B. Student's t-Test analysis showed significant differences between the growth on the different N-sources in all lines *** = P<0.001.
D: Nitrate reductase activity in wild-type, line #3 and #4 mutants as well as in the *atm3-1* line. Activity was analysed in 4-week-old plants grown on soil by measuring the presence of nitrite via the Griess reaction (n = 4 ± SD).

This could be indicative of a severe NR deficiency, because *nia1nia2* double mutants grow poorly on media containing nitrate as the only nitrogen source characterised by very small, yellowish plants (Wilkinson and Crawford, 1993). Therefore, we compared the growth of *grxs15* roots with *atm3-1*, which has a decreased NR activity and a similar macroscopic phenotype as *nia1nia2* (Teschner et al., 2010) as well as a decreased activity of other Moco-dependent enzymes (Bernard et al., 2009). The *grxs15* mutants do not phenocopy the *atm3* mutants and surprisingly, in contrast to *grxs15* mutants, root growth of *atm3-1* was still better on nitrate than on ammonium (Figure 16B, C). The result suggests that the residual NR activity in *grxs15* mutants is sufficient to use nitrate as the sole nitrogen source. Nevertheless, the *grxs15* mutant grew slightly better under short-day conditions similar to mutants which have a diminished nitrate storage capacity (Krebs et al., 2010) (Supplemental Figure 4A) suggesting that the *grxs15* mutants struggle with nitrate as nitrogen source in some other way.

The severe growth retardation on medium with nitrate as the sole N-source prompted us to measure the NR activity and the amount of nitrate and nitrite in the *grxs15* mutants complemented with GRXS15 K_{83}/A. As expected, we found a severe decrease in NR activity in *atm3-1*, but interestingly not in the mutant lines #3 and #4 (Figure 16D). Similarly, other Moco-dependent enzymes like the AAO or XDH showed no decrease in activity in the *grxs15* mutants compared to wild-type (Supplemental Figure 4D). Consistently, no increase in nitrate content could be found. The nitrate content in the *grxs15* mutants was rather slightly decreased compared to wild-type (Figure 17A). Nitrite and other anions like chloride, sulfate or phosphate were not altered between the complementation lines and wild-type (Figure 17B).

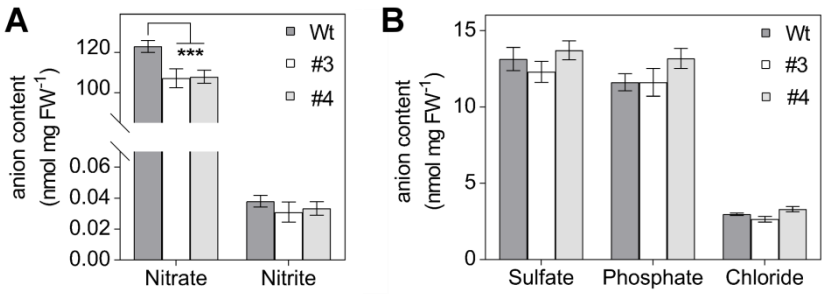

Figure 17: Anion content of *grxs15* mutant lines compared to wild-type.
A: Nitrate and nitrite content of 8-d-old Arabidopsis wild-type and line #3 and #4 seedlings grown on agar plates ($n = 4 \pm$ SEM).
B: Amount of sulfate, phosphate and chloride in Arabidopsis wild-type and line #3 and #4 seedlings ($n = 4 \pm$ SEM). The statistical analysis (two way ANOVA with post hoc Holm-Sidak comparisons for wild-type vs. *grxs15* mutant) indicated no significant ($P \leq 0.05$) change, except in one case; ***$P \leq 0.001$.

3.1.7 K_{83}/A mutants have less root respiration and an altered metabolism

The results strongly suggest that the bottleneck limiting growth of GRXS15 K_{83}/A plants is not the NR activity but rather a shortage in either metabolites or energy provision required for nitrate assimilation which is known to require huge amounts of reducing equivalents. Hence, we were wondering whether the *grxs15* mutants are affected in respiration or in the TCA cycle. Because mitochondrial respiration is the fundamental energy-conserving process, generating ATP needed for cell maintenance and growth, and furthermore, because respiration is based on several enzyme complexes containing ISCs, we measured the respiration of isolated roots. Indeed, roots of the mutant line #3 had a decreased respiration of 1.31 ± 0.35 nmol O_2 min^{-1} mg DW^{-1} compared with the wild-type respiring 2.92 ± 0.62 nmol O_2 min^{-1} mg DW^{-1} (Figure 18A). Interestingly, protein amount of AOX1/2 was slightly higher in the mutants in contrast to the wild-type (Figure 18B). To investigate if the decreased root respiration is based on an inefficient respiratory machinery, we purified mitochondria from whole seedlings and energised them with succinate or pyruvate/malate. Succinate provides electrons to the ubiquinone pool of the electron transport chain via complex II whereas pyruvate/malate predominantly via NAD(P)H generated by malate dehydrogenase and the pyruvate dehydrogenase complex, and, in turn, complex I. However, no differences in the respiration of isolated mitochondria were found and thus, differences in respiration were not based on decreased complex I and complex II capacity (Figure 18C, D). Hence, we assume that the dwarf phenotype is not caused by an improper ISC transfer of GRXS15 to the complexes in the electron transport chain.

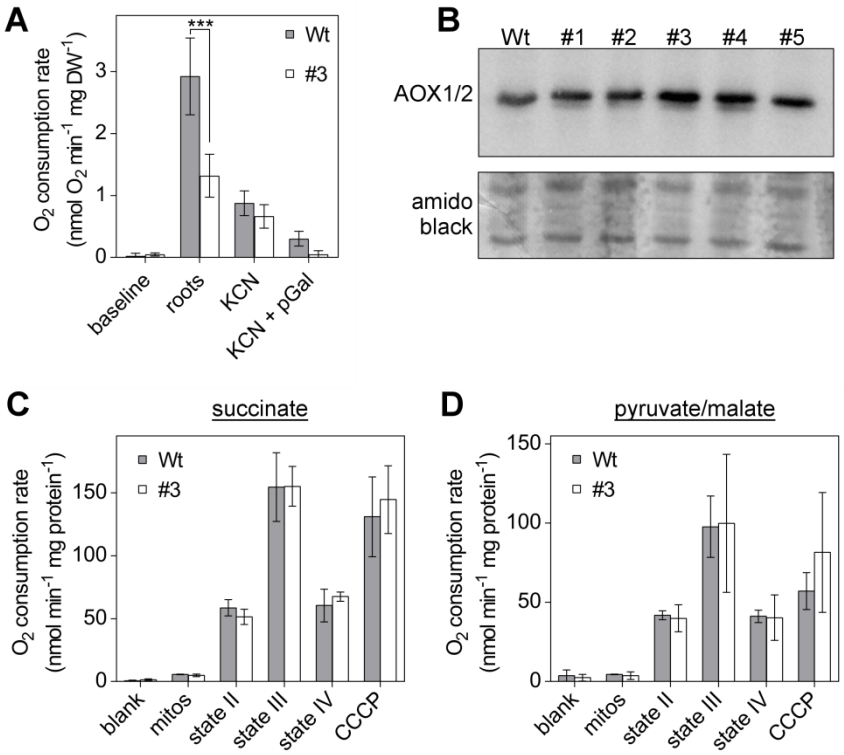

Figure 18: Respiration and AOX expression in complemented *grxs15* mutants.
A: Root respiration rate of *grxs15-3 UBQ10:GRXS15 K_{83}/A* line #3 (4.5-week-old) and the respective wild-type (2-week-old) after addition of KCN (4 mM) and KCN (4 mM) + pGal (propylgallate; 0.2 mM). (n = 4 ± SD). The statistical analysis (two way ANOVA with post hoc Holm-Sidak comparisons for wild-type vs. *grxs15* mutant) indicated one significant change; ***P ≤ 0.001.
B: Immunoblot analysis of alternative oxidase 1 and 2 in mitochondria of GRXS15 K_{83}/A mutants compared with wild-type. In upper AOX expression in isolated mitochondria of wild-type and *grxs15-3 UBQ10:GRXS15 K_{83}/A* lines was detected by a specific AOX antibody (AS04054 Agrisera). 10 µg isolated mitochondria were loaded. In lower the membrane was stained with amido black as a control for protein loading.
C, D: Oxygen consumption rates for purified mitochondria from wild-type and *grxs15-3 UBQ10:GRXS15 K_{83}/A* line #3 energised with succinate or pyruvate/malate. O_2 consumption rate was measured before (blank) and after addition of mitochondria (mito), the respective substrate (state II; succinate (10 mM succinate, 0.25 mM ATP) or pyruvate/malate (10 mM pyruvate, 10 mM malate, 0.3 mM NAD and 0.1 mM thiamine pyrophosphate), ADP (state III; 50 µM ADP), after ADP consumption (state IV) and after addition of CCCP (10 µM carbonyl cyanide m-chlorophenylhydrazone). (n = 3 ± SEM)

Nevertheless, the availability of a high capacity for electron flow does not mean that the electron transport chain is working at normal speed *in planta* and hence, we were wondering if the decreased respiration had any impact on the ATP level. During respiration energy is released and transiently stored in ATP, which is used by cellular reactions for maintenance and development. For analyses of the ATP level wild-type as well as the *grxs15* mutant complemented with GRXS15 K_{83}/A were transformed with a fluorescence resonance energy

transfer (FRET)-based sensor named ATeam (Adenosine 5'-Triphosphate indicator based on epsilon subunit for analytical measurements; Imamura et al. (2009)) targeted to the cytosol. Targeting of the sensor to the mitochondrial matrix led to a strong stunted phenotype (De Col et al., 2017). As cytosolic ATP is mainly provided by the mitochondria (Igamberdiev et al., 2001), we assumed that a disturbance in the mitochondrial ATP synthesis is displayed by changed ATP levels in the cytosol. For the ATeam sensor, variants of CFP and YFP are connected by the ε subunit of *Bacillus subtilis* F_oF_1-ATP synthase. In the ATP-free form, the two fluorescent proteins are separated, resulting in low FRET efficiency. In the ATP-bound form, the subunit retracts to draw the two fluorescent proteins close to each other, which increases FRET efficiency. However, although FRET across the seedlings revealed differences between cotyledons and roots as shown previously (De Col et al., 2017), the YFP/CFP emission ratio did not differ between wild-type and mutants indicating a similar ATP level in mutants and wild-type in the cytosol (Figure 19).

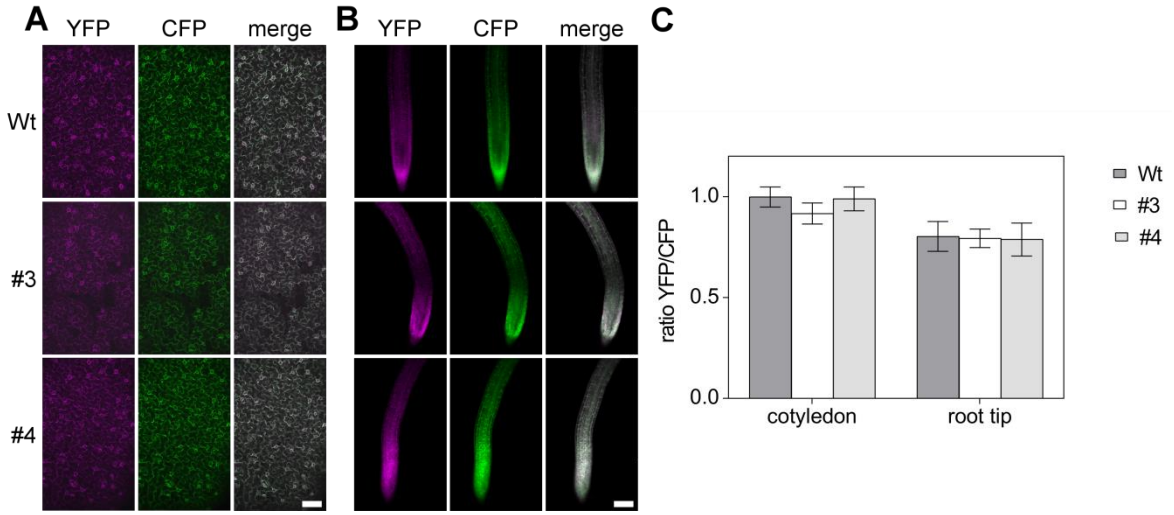

Figure 19: *In vivo* monitoring of ATP levels in the cytosol of *grxs15* mutants.
ATeam was stably expressed under a *35S* promoter in the cytosol of wild-type and *grxs15-3 UBQ10:GRXS15 K_{83}/A* line #3 and #4 and analysed in cotyledons (**A**) and roots (**B**). Scale bar = 100 µm. Fluorescence of YFP (magenta) and CFP (green) was recorded and the ratio was calculated (**C**) from fluorescent images of cotyledons and root tips of 7-d-old seedlings from two independent lines (n = 10 ± SD). Autofluorescence was subtracted from both channels.

Because of the functional respiratory chain in the *grxs15* mutants, we were wondering if the TCA cycle is somehow affected in *grxs15* mutants leading to a lack of reducing agent like NADH. Thus, to further investigate the impact of altered GRXS15 function on major

mitochondrial FeS-proteins, we analysed the activity of aconitase, of which the two isoforms ACO2 and ACO3 are affiliated with the TCA cycle and mitochondrial energy metabolism. Despite similar amounts of ACO protein detectable in isolated mitochondria, ACO activity was decreased to a similar degree of approximately 35 % residual activity in total protein extracts of complemented mutant plants (Figure 20), but just to ~60 % in isolated mitochondria. In contrast, activity of malate dehydrogenase was the same.

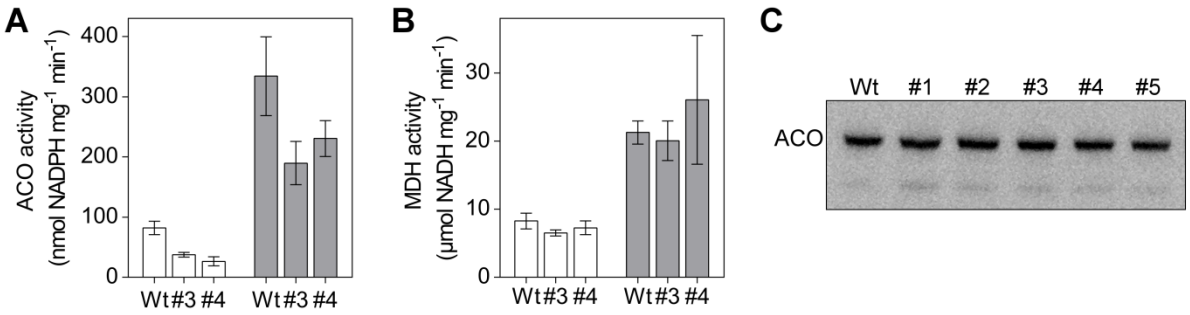

Figure 20: Aconitase activity in total and purified mitochondria.
A: Aconitase (ACO) activity in total protein extracts of 7-d-old seedlings (white bars) and in purified mitochondria (grey bars) of 14-d-old wild-type and *grxs15-3 UBQ10:GRXS15 K_{83}/A* line #3 and #4 (*n* = 3 ± SEM).
B: Malate dehydrogenase (MDH) activity in total protein extracts of 7-d-old seedlings and in purified mitochondria of 14-d-old wild-type and *grxs15-3 UBQ10:GRXS15 K_{83}/A* line #3 and #4 (*n* = 3 ± SEM).
C: Protein gel blot analysis with antiserum raised against Arabidopsis aconitase. 9 µg of protein isolated from mitochondria of a wild-type plant as well as *grxs15-3 UBQ10:GRXS15 K_{83}/A* line #1-5 were loaded.

However, aconitase is highly sensitive against oxidative stress (Navarre et al., 2000; Verniquet et al., 1991) and there might be iron-mediated ROS formation because of an improper ISC transfer of the GRXS15 K_{83}/A variant similar to the yeast *Δgrx5* mutant. To address this problem, leaves were stained with DAB and NBT to analyse a potential global increase of H_2O_2 or superoxide production, respectively, in the *grxs15* mutants as another plausible cause for aconitase inhibition. However, no differences could be detected in leaves between wild-type and *grxs15* mutants neither by the DAB nor NBT staining (Figure 21A).

In addition, to analyse mitochondria-specific changes in H_2O_2 concentration or glutathione redox potential (E_{GSH}), the genetically encoded sensors roGFP2:Orp1 and roGFP2:hGRX1 were expressed in the mitochondrial matrix of both wild-type and mutant plants. CLSM analysis of the T_2 generation showed exclusive targeting of both constructs to mitochondria (Supplemental Figure 5).

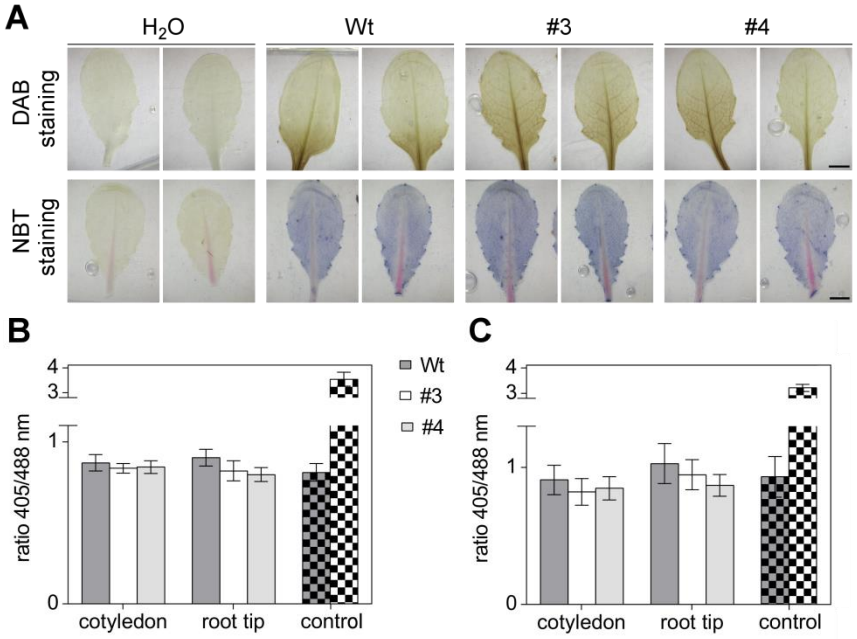

Figure 21: Analysis of the oxidation state of the *grxs15* mutants.
A: DAB (upper) and NBT (lower) staining for detection of increased ROS production in leaves. Wild-type and mutants were grown for 4 weeks under long-day growth conditions. Scale bar = 0.5 cm.
B: Measuring changes in mitochondrial H_2O_2 concentration using the biosensor roGFP2:Orp1. Ratiometric analysis was performed with 7-d-old seedlings of wild-type and *grxs15-3 UBQ10:GRXS15 K_{83}/A* line #3 and #4 expressing mitochondrial roGFP2:Orp1 by CLSM. As control wild-type seedlings were incubated in 10 mM DTT (grey squared) or 10 mM H_2O_2 (white squared) and fluorescence of roGFP2 in the hypocotyl was analysed.
C: Measurement of the mitochondrial E_{GSH} using roGFP2:hGRX1. Ratiometric analysis was performed with 7-d-old seedlings of wild-type and *grxs15-3 UBQ10: GRXS15 K_{83}/A* line #3 and #4 expressing mitochondrial roGFP2:hGRX1 by CLSM. As control wild-type seedlings were incubated in 10 mM DTT (grey squared) or 10 mM H_2O_2 (white squared) and fluorescence of roGFP2 in the root tips was analysed.

Regarding roGFP2:Orp1, a peroxidase (Orp1), which is fused to roGFP2, reacts with H_2O_2 and is getting oxidised. The proximity between both proteins allows that the oxidation is passed efficiently from Orp1 to roGFP2 and thus, increased H_2O_2 concentration are expected to lead to more oxidised roGFP2. By comparing the 405/488 nm fluorescence ratio of roGFP2, however, no differences between wild-type and *grxs15* mutants were observed neither in cotyledons nor in roots indicating the absence of increased mitochondrial H_2O_2 levels (Figure 21B). As control, the minimal and maximal fluorescence ratio was measured after incubation with DTT or H_2O_2, respectively. It should be noted though that the lack of pronounced changes in fluorescence may also be caused by a dominating reduction system which might masks a putative increase in H_2O_2. Furthermore, redox-dependent fluorescence of roGFP2 fused to hGRX1 was analysed. The fused hGRX1 mediates the redox equilibration of roGFP2 with the

glutathione redox buffer and thus, mitochondrial E_{GSH} can be compared of wild-type and *grxs15* mutants. Here, similar to the wild-type, roGFP2 was highly reduced indicating no oxidation of the mitochondrial glutathione pool (Figure 21C).

To further investigate whether the decreased activity of aconitase had consequences on the rate of TCA cycle organic acid production and thus, NADH production, we analysed the amount of organic acids in the *grxs15* mutants. Interestingly, we found virtually all analysed organic acids in the complemented *grxs15* mutants #3 and #4 to be increased which may reflect a perturbed flux. Especially pyruvate accumulated to high levels. While 31.5 ± 2.4 pmol mg FW^{-1} pyruvate was present in the wild-type, the pyruvate amount increased more than 4-fold up to 131.76 ± 3.8 pmol mg FW^{-1} in mutant line #3 and 153.97 ± 16.5 pmol mg FW^{-1} in line #4 (Figure 22). In contrast, the accumulation of citrate was just about significant in the *grxs15-3 UBQ10: GRXS15 K_{83}/A line* #4 but not in line #3. Similarly, also isocitrate accumulated in the mutant line #4.

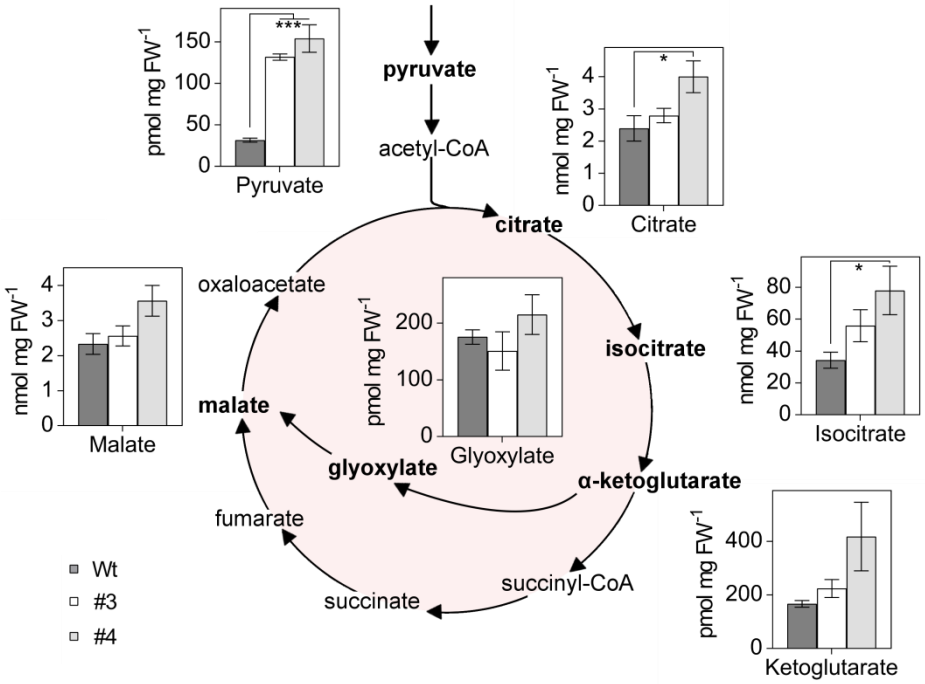

Figure 22: Organic acids of the TCA cycle accumulate in the GRXS15 mutant.
Organic acids were analysed in 8-d-old seedlings of wild-type compared to *grxs15-3 UBQ10:GRXS15 K_{83}/A* line #3 and #4 (n = 4-5 ± SEM). The statistical analysis (one way ANOVA with post hoc Holm-Sidak comparisons for wild-type vs. *grxs15* mutant) indicated significant changes; *P ≤ 0.05; ***P ≤ 0.001.

In the TCA cycle the stepwise oxidation of pyruvate mobilises the major amount of reducing power in form of NADH and $FADH_2$. To investigate if the perturbed flux had any influence on the NADH metabolism, we expressed the fluorescence biosensor Peredox-mCherry for monitoring the free NADH/NAD^+ ratio (Hung et al., 2011) in the cytosol of wild-type and the *grxs15* mutants. The cytosolic NADH/NAD^+ is highly connected with the mitochondrial via a malate/OAA shuttle as well as a malate/aspartate shuttle (Journet et al., 1981; Krömer and Heldt, 1991). As the malate/OAA shuttle is regulated in a way that avoids a depletion of NADH in the matrix (Krömer, 1995), disturbance of the mitochondrial NADH/NAD^+ pool should also be reflected in the cytosol. However, no changes in cytosolic NADH/NAD^+ redox states were observed neither in the cotyledons nor in the roots of the mutants compared to the wild-type (Figure 23).

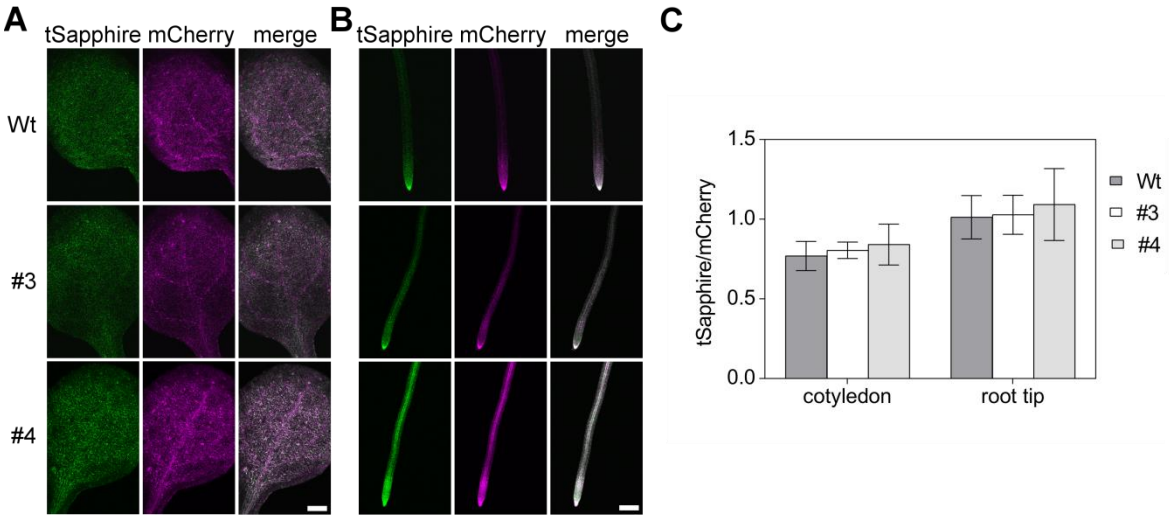

Figure 23: Imaging the cytosolic NADH/NAD^+ redox state in *grxs15* mutants.
Peredox-mCherry was stably expressed under a *UBQ10* promoter in the cytosol of wild-type and *grxs15-3 UBQ10:GRXS15* K_{83}*/A* line #3 and #4 and analysed in cotyledons (**A**) and roots (**B**). Scale bar = 200 µm. Fluorescence of tSapphire and mCherry was recorded and the ratio was calculated (**C**) from fluorescent images of cotyledons and root tips of 7-d-old seedlings from two independent lines (*n* = 10 ± SD).

However, the amount of free NADH is low in mitochondria and most is bound to proteins. Therefore, the unchanged ratio of free NADH/NAD^+ might be because free NADH in the mitochondrial matrix is maintained at a relatively constant level irrespective of respiratory state (Kasimova et al., 2006). Thus, probably differences in the mitochondrial NADH/NAD^+ ratio between wild-type and *grxs15* mutants are too little and also do not affect the level of the cytosolic NADH/NAD^+ ratio.

3.1.8 The GRXS15 K_{83}/A mutation influences lipoic acid-dependent enzymes

The pronounced pyruvate accumulation may be caused by a diminished activity of pyruvate dehydrogenase complex (PDC) which catalyses the irreversible reaction of pyruvate into acetyl-CoA. Interestingly, the E2 subunit of this multienzyme complex needs lipoic acid as a cofactor. Lipoic acid (LA) is synthesised in mitochondria by the FeS-protein lipoyl synthase and an essential cofactor for other proteins in the mitochondrial matrix: α-ketoglutarate dehydrogenase, branched-chain α-ketoacid dehydrogenase complex (BCKDC) or glycine decarboxylase complex (GDC) (Figure 24A) (Taylor et al., 2004). Indeed, the amount of lipoyl proteins of GDC was decreased in the GRXS15 K_{83}/A mutant (Figure 24B). GDC is a multimeric complex comprising three individual enzymes, P-, T-, and L-protein, that interact with a fourth subunit, the lipoylated H-protein (Heineke et al., 2001). Immuno-detection of proteins with an antibody against LA showed a clear decrease in H-protein isoforms H1, H2 and H3, whereas immuno-labelling of H protein showed that the protein levels are only very slightly decreased if at all. For H2 no LA was detectable, while there was still some left for H1 + H3. This might be to differences in the total protein amount as you can also not differ between the H1 and H3 isoforms. No difference in the total protein amount of LIP1 was detectable between *grxs15* mutants and wild-type. Since during this study a publication was published where a GRXS15 knock-down ($GRXS15^{amiR}$) showed an effect of lipoylated enzymes (Ströher et al., 2016), the knock-down mutant was used as positive control.

To further test whether the accumulation of pyruvate was because of a less active mtPDC, we measured the activity of the mtPDC in isolated mitochondria. Interestingly, there was just a slight reduction of activity, but not significant ($p = 0.077$). While the wild-type displayed a mtPDC activity of 92.7 ± 16.1 nmol NADH mg^{-1} min^{-1} that is in a similar range as described before for Arabidopsis mtPDC (Lee et al., 2010) the *grxs15* mutant line #3 had just a activity of 72.40 ± 15.6 nmol NADH mg^{-1} min^{-1} (Figure 24C).

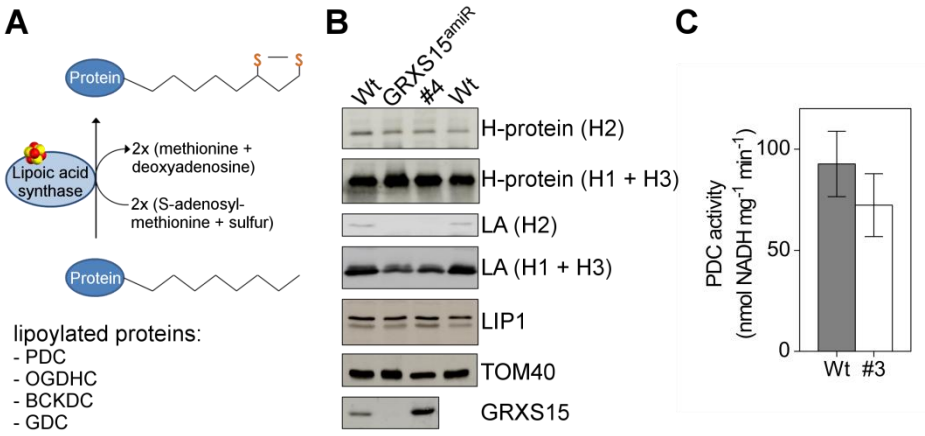

Figure 24: Lipoic acid dependent enzymes are affected in the mutant lines.
A: Lipoyl synthase catalyses the lipoylation of the octanoylated apoprotein by using SAM and sulfur. Lipoylated proteins of the mitochondrial matrix are PDC = Pyruvate dehydrogenase complex; OGDHC = α-ketoglutarate dehydrogenase, BCKDC = branched-chain α-ketoacid dehydrogenase complex and GDC = glycine decarboxylase complex.
B: Immunoblot analysis using antibodies against H-protein (H1-3), lipoic acid (LA) and LIP1 as well as TOM40 and GRXS15. Data were provided by Inga Kruse and Janneke Balk.
C: Pyruvatedehydrogenase complex activity in isolated mitochondria. Reduction of NAD^+ was measured in isolated mitochondria of 14-d-old wild-type seedlings and *grxs15-3 UBQ10:GRXS15* K_{83}*/A* line #3 (n = 5 ± SD).

Similar to an Arabidopsis mutant with a mutation in the E2 subunit of the pyruvate dehydrogenase complex containing only 30 % of the wild-type mtPDC activity (Yu et al., 2012) the *grxs15* mutants showed a dwarf phenotype (Figure 14) as well as an accumulation of TCA intermediates (Figure 22). Furthermore, the mutant in E2 subunit of the mtPDC showed an accumulation of nearly all amino acids, while null mutants of the BCKDC subunit E1 showed a specific accumulation of the branched chain amino acids (BCAA) (Peng et al., 2015). The BCAAs are leucine, isoleucine and valine and are classified by their small branched hydrocarbon residues. BCKDC catalyses the second step of BCAA degradation in the mitochondrial matrix and hence leads to conversion of branched-chain ketoacids into acyl-CoA esters (Figure 25) (Peng et al., 2015; Taylor et al., 2004).

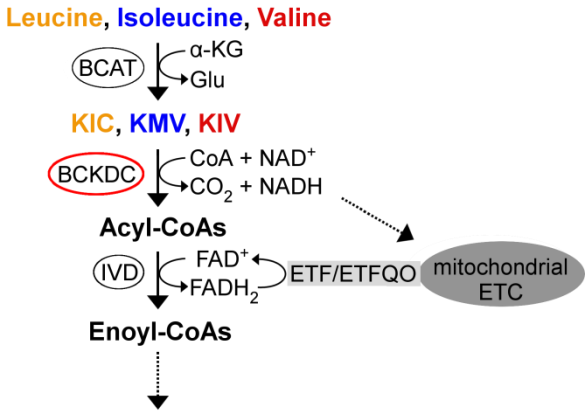

Figure 25: Catabolism of branched chain amino acids.
First, the branched chain amino acids leucine, isoleucine and valine are deaminated by the BCAT (Branched-chain aminotransferase), which uses largely α-KG (α-ketoglutarate) forming the branched chain keto acids α-ketoisocaproic acid (KIC), α-keto-β-methylvaleric acid (KMV) and α-ketoisovaleric acid (KIV) as well as glutamate. The ketoacids are further degraded by BCKDC (branched-chain ketoacid dehydrogenase), which catalyses the oxidative decarboxylation producing thereby acyl-CoA and NADH. IVD (isovaleryl-CoA dehydrogenase) catalyses the third step providing electrons to the ETC (electron transport chain) via ETF (electron transfer flavoprotein)/ETFQO (electron transfer flavoprotein ubiquinone oxidoreductase) (modified after Peng et al. (2015)).

Analysis of the amino acids in the GRXS15 K_{83}/A mutant showed an increase of nearly all amino acids (Figure 26A). Interestingly, however, the BCAAs leucine, isoleucine and valine as well as the small amino acids glycine, alanine and serine accumulated to high levels (Supplementary Table 5). This accumulation correlates also with the growth phenotype of the mutant line; the worst growing line #4 accumulates slightly more amino acids in contrast to the better growing line #3. At the first glance, the 2-fold glycine accumulation in the *grxs15* mutants would suggest a perturbation in photorespiration as GDC is part of the photorespiratory cycle catalysing the catabolism of glycine. Potato plants with a reduction of the P-protein of GDC also show high glycine accumulation (Heineke et al., 2001) and the amount of the lipoylated subunit is decreased in the *grxs15* mutant (Figure 24). Nevertheless, the Gly/Ser ratio was not changed remarkably. For line #3 the ratio was 0.41 and for the line #4 0.35 compared to the wild-type with a ratio of 0.33.

For leucine, the respective amount increased in the mutant lines up to 2-fold. Valine and isoleucine accumulated 1.5-2 times. Furthermore, the ketoacids KIC, KMV and KIV derived from the branched chain amino acids accumulated highly in the *grxs15* mutant (Figure 26B). Here, KIC accumulated in the *grxs15* mutants up to 14 times leading to a total amount of 3.5 ± 0.11 pmol mg FW^{-1} in line #3 and 3.8 ± 0.6 pmol mg FW^{-1} in line #4 compared to the wild-type with 0.25 ± 0.032 pmol mg FW^{-1}. While the amount of KIV and KMV increased up to 6-7 fold

in the *grxs15* mutants. This result inevitably supports the hypothesis of a decreased activity of BCKDC in this mutant. The higher accumulation of KIC might be because BCKDC has a slight preference for the Val derivative (Taylor et al., 2004) and thus, KIV is faster metabolised and accumulate less.

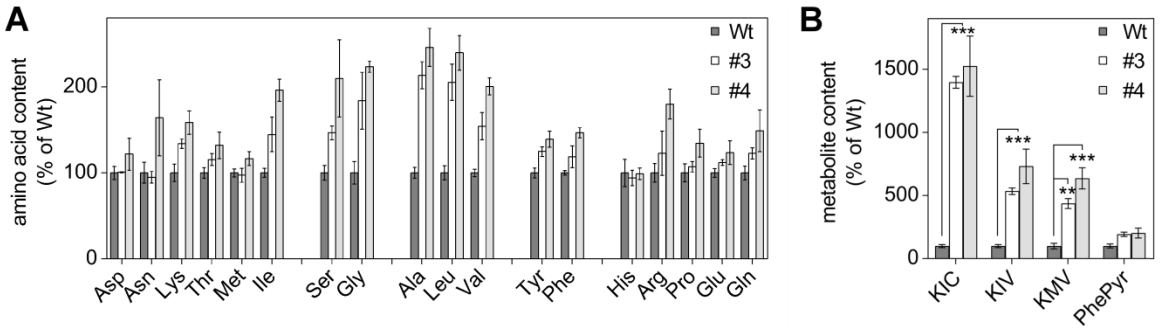

Figure 26: GRXS15 K_{83}/A mutants accumulate BCAA and their derivatives.
A: Amino acids were analysed in 8-d-old seedlings of wild-type compared *grxs15-3 UBQ10:GRXS15 K_{83}/A* line #3 and #4. Wild-type was set to 100 % (*n* = 4-5 ± SEM).
B: Analysis α-ketoisocaproic acid (KIC), α-ketoisovaleric acid (KIV), α-keto-β-methylvaleric acid (KMV) and phenylpyruvate (PhePyr) in seedlings of wild-type compared to *grxs15-3 UBQ10:GRXS15 K_{83}/A* line #3 and #4. Wild-type was set to 100 % (*n* = 4-5 ± SEM). The statistical analysis (two way ANOVA with post hoc Holm-Sidak comparisons for wild-type vs. *grxs15* mutant) indicated significant changes; **P. ≤ 0.01; ***P ≤ 0.001.

Since cysteine was not included in the amino acid measurement, we aimed at measuring the cysteine availability in a different way. Because cysteine is a limiting factor in GSH synthesis, we monitored the recovery of GSH after initial depletion of the GSH pool. For this, Arabidopsis seedlings were grown on 2 mM BSO for 4 days and subsequently transferred to BSO-free medium for 24 h. At the end of this recovery phase GSH was stained in the roots of wild-type as well as *grxs15* seedlings by conjugation with monochlorobimane and GSH levels were monitored by confocal laser scanning microscopy. There was a similar replenishment of the glutathione pool by *de novo* biosynthesis in the root tips of wild-type and *grxs15* mutants (Figure 27) indicating that at least no decrease in the cysteine amount occurs in the mutants.

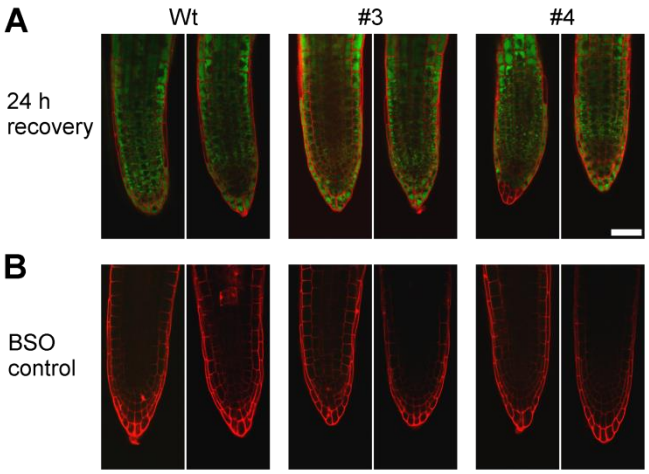

Figure 27: GSH content of BSO treated and recovered *grxs15* mutants.
A: *In vivo* determination of GSH pool recovery in root tips of wild-type (Wt) and *grxs15-3 UBQ10:GRXS15* K_{83}*/A* line #3 and #4 after transfer from BSO-containing (2 mM) to BSO-free plates for 24 h. Control plants were kept on BSO to show the specificity of the GSH labelling **(B)**. Roots were stained with 100 µM monochlorobimane (green) and 50 µM propidium iodide (red) for 30 min before imaging. Scale bar = 50 µm.

3.2 The effect of the GSH pool on GRXS15 function and FeS-protein maturation

3.2.1 GSH-depleted mutants do not show an accumulation of BCAAs and their derivatives

Glutathione is present in low millimolar concentrations in most eukaryotic cells performing numerous tasks (Rouhier et al., 2008). One important role of GSH is the function as a cofactor of GRXs in the coordination of an ISC. As shown previously, GRXS15 coordinates an ISC in the presence of GSH. Indeed, although GSH is only synthesised in plastids and the cytosol, immunocytochemical staining suggested that mitochondria contain particularly high glutathione concentrations (Zechmann et al., 2008). Furthermore, the mitochondrial glutathione pool is kept highly reduced by GR2. To determine if the availability of GSH has any influence on the GRXS15 function, the phenotypes of the GSH-depleted mutants *rml1* and *zir1* were compared with the complemented *grxs15-3* mutants. *rml1* and *zir1* have both a decreased amount of total glutathione with less than >5 % GSH in *rml1* and ~15 % in *zir1* compared to the wild-type based on mutations in GSH1, which catalyses the first step of GSH biosynthesis (Shanmugam et al., 2012; Vernoux et al., 2000). The allele with the lowest glutathione level, *rml1*, exhibited the most severe developmental defects (Vernoux et al., 2000). Since the accumulation of branched chain amino acids and the respective ketoacids are characteristic for the restricted activity of GRXS15 K_{83}/A, we analysed the composition of amino acids in the GSH mutants. Here, *zir1* showed absolutely no accumulated amino acids, rather, there was a significant decrease of Asp. In contrast, *rml1* displayed an accumulation of nearly all amino acids except glutamine when compared to the wild-type (Figure 28A). Here, serine accumulated sparsely 1.7 fold, while the total amount of lysine increased mostly up to 2.4 fold. The BCAAs accumulated all approximately two times. To further investigate if at least the accumulation of the branched chain amino acids also leads to an increase of KIC, KIV and, KMV, the respective ketoacids were analysed in *rml1* compared to wild-type and *grxs15-3 UBQ10:GRXS15 K_{83}/A line #4*. Here, no accumulation of the ketoacids were detected in the *rml1* seedlings (Figure 28B) indicating that a depletion of the GSH pool in the *rml1* mutant has no influence on the BCKDC in contrast to the GRXS15 K_{83}/A variant.

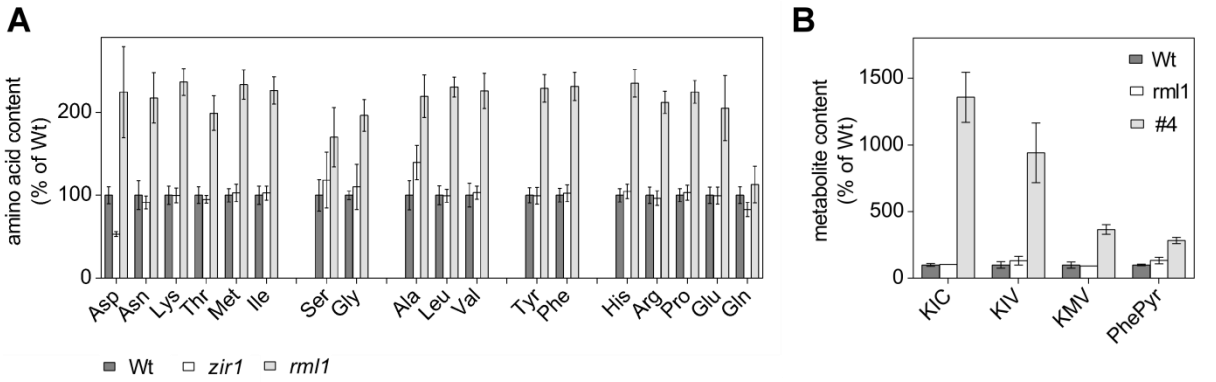

Figure 28: *rml1* accumulates amino acids but not the respective derivatives.
A: Amount of amino acids of *zir1* and *rml1*. Wild-type was set to 100 % (n = 5 ± SD).
B: Analysis α-ketoisocaproic acid (KIC), α-ketoisovaleric acid (KIV), α-keto-β-methylvaleric acid (KMV) and phenylpyruvate (PhePyr) in seedlings of wild-type compared to *rml1* and *grxs15-3 UBQ10:GRXS15 K$_{83}$/A* line #4. Wild-type was set to 100 % (n = 1-5 ± SEM).

Interestingly, *rml1* does not just contain a reduced amount of total glutathione, but, regarding mitochondria, also has an increased oxidised glutathione pool (Sajid Bangash, personal communication). Therefore, we were wondering if an altered GSH:GSSG ratio has any influence on the ISC coordination of GRXS15 as addition of GSSG can destroy ISC coordination of human GLRX2 *in vitro* (Berndt et al., 2007). Reconstituted GRXS15 gradually lost the ISC under aerobic conditions resulting in a decrease of absorbance of ~50 % after 3 h, whereas addition of GSH led to a stabilisation of the holoprotein resulting in a decrease of just ~20 %. In contrast, addition of oxidised glutathione enhanced the decrease in absorbance to 50 % already after 2 h (Figure 29). Thus, GSSG just led to slight destabilisation of the ISC.

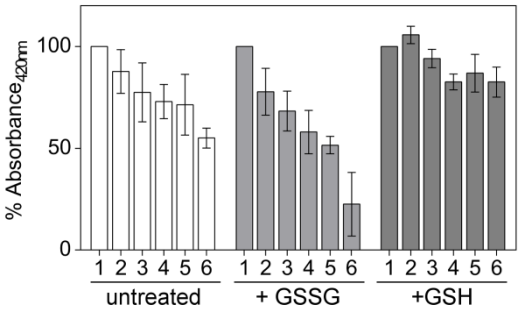

Figure 29: The GRXS15 holoprotein is slightly destabilised by GSSG.
Absorbance of reconstituted GRXS15 at six different time points (1 = 0 min; 2 = 10 min; 3 = 30 min; 4 = 60 min; 5 = 120 min; 6 = 180 min) in the absence or presence of 5 mM GSSG and GSH (n = 4 ± SD). Time point 0 was set to 100 %.

3.2.2 High mitochondrial GSSG aggravates the *atm3* phenotype

Since GSSG has no or just a slight effect on GRXS15 and its function, we were wondering if a more oxidised glutathione pool has an influence on FeS-protein maturation in the cytosol. As the mitochondrial ABC-transporter ATM3 is involved in the export of a sulfur-compound for cytosolic ISC maturation in a glutathione dependent fashion, the severely compromised but still viable mutant *atm3-4* (Bernard et al., 2009) was crossed with the mutant *gr2epc2* which lacks endogenous GR2 in mitochondria and plastids but has been complemented with plastids-targeted GR2 to ensure viability. The lack of GR2 in mitochondria has been shown to cause a local increase in GSSG in the matrix (L. Marty and A.J. Meyer, unpublished results). Here it is hypothesised that the increase in matrix GSSG can compete as a putative substrate of ATM3 with the export of the unknown sulfur-compound X-S from the matrix (Schaedler et al., 2014). It is further assumed that such a competition may have more severe consequences in ATM3 that is genetically compromised. The cross of these mutants led to a viable double mutant. Intriguingly, several seeds of the single mutant *gr2epc2* display a brighter testa compared to the seeds from plants grown side-by-side of wild-type or *atm3-4*, whereas all seeds of the double mutant *atm3-4gr2epc2* were brighter (Figure 30A).

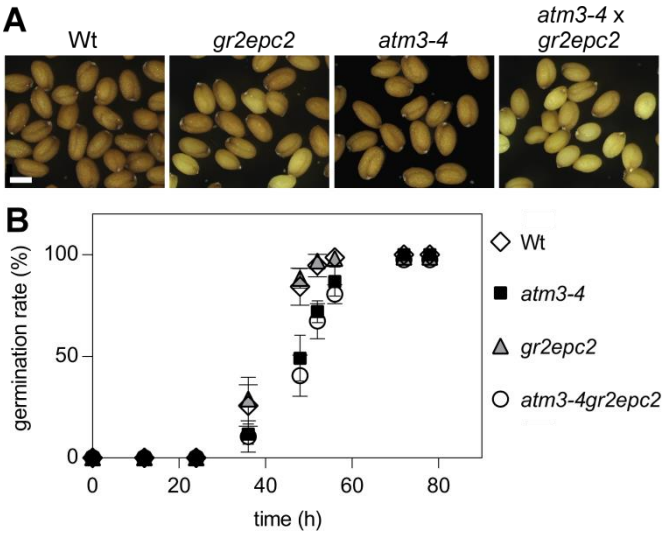

Figure 30: Deletion of mitochondrial GR2 does not augment the delayed germination of *atm3-4*.
A: Seeds of the double mutant compared to wild-type and single mutants. Scale bar = 0.5 mm.
B: Germination rate of the mutants compared to wild-type. Plants were grown on 0.5 MS medium containing 0.5 % (w/v) sucrose and 0.8 % (w/v) phytagel under long-day conditions after 1 d stratification (shown is the mean ± SD of four experiments with 20-30 seeds each). Germination was assessed with the emergence of the radicle.

Moreover, the *atm3-4* single mutant showed a delayed germination compared to the wild-type, but *atm3-4gr2epc2* behaved similar to *atm3-4* (Figure 30B). After 36 h around 25 % of wild-type and *gr2epc2* seeds germinated, while just ~11 % of the seeds of *atm3-4* and *atm3-4gr2epc2* germinated. The delay in germination was even more obvious after 48 h when already more than 80 % of wild-type and *gr2epc2* seeds germinated but less than 50 % of the *atm3-4* and *atm3-4gr2epc2* seeds.

Further macroscopic analysis of mutant seedlings revealed a pronounced root growth phenotype. While the single mutants *gr2epc2* and *atm3-4* developed primary roots that were only 80 % of the length of wild-type control seedlings after 5 days of germination or 60 % after 8 days of germination the *atm3-4gr2epc2* double mutant displayed a pronounced additive effect (Figure 31A, B). Five days after germination the average root length of the double mutant was almost 40 % less than in wild-type seedlings. Eight days after germination the length roots of the double mutant was only 30 % compared to the length of wild-type roots. In addition, the chlorotic phenotype of *atm3-4* that has been described before by Bernard and colleagues was aggravated in *atm3-4gr2epc2* (Figure 31C) (Bernard et al., 2009). Concomitant with this, photosynthetic activity, measured via maximum quantum efficiency of PSII (F_v/F_m), was significantly decreased in *atm3-4* and even more in the double mutant (Figure 31D). The wild-type displayed a F_v/F_m value of 0.78 ± 0.012 that is similar to what has been reported in the literature for unstressed leaves with values of ~0.83, and correlates to the maximum quantum yield of photosynthesis (Björkman and Demmig, 1987). The value of F_v/F_m for *atm3-4* was reduced to 0.749 ± 0.031 and even more to 0.718 ± 0.027 in the *atm3-4gr2epc2* double mutant, while no significant changes were observed between *gr2epc2* and wild-type.

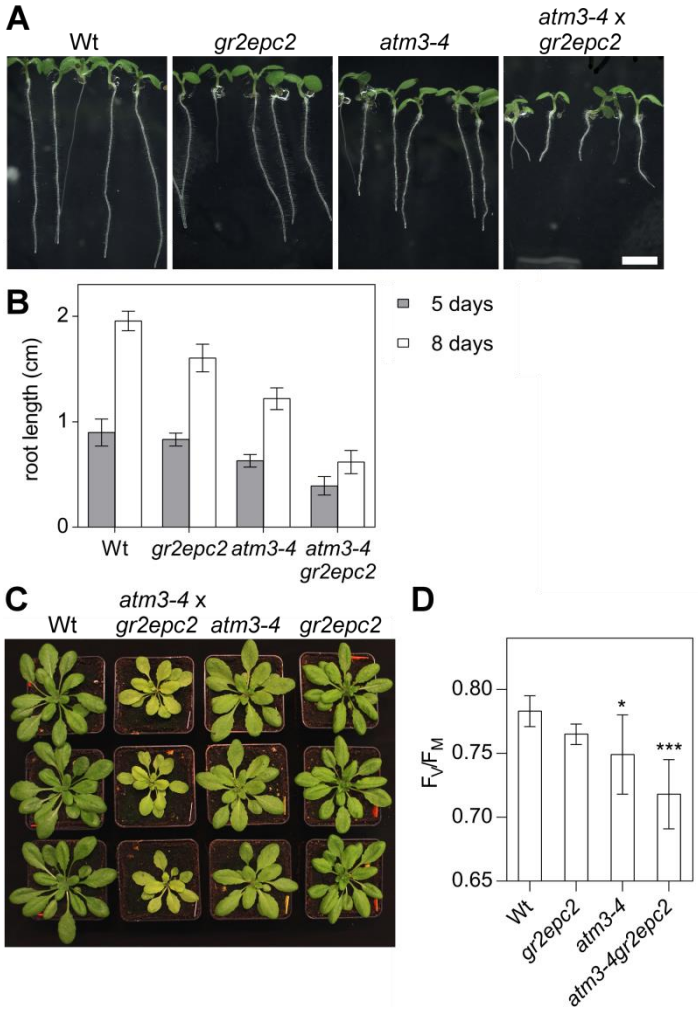

Figure 31: *atm3-4gr2epc2* double mutants show an enhanced dwarfed and chlorotic phenotype.
A: 8-d-old seedlings of the *atm3-4gr2epc2* double mutant compared to wild-type (Wt) and single mutants. Scale bar = 0.5 cm.
B: Root length of the mutants compared to wild-type. Plants were grown on 0.5 MS medium containing 0.5 % (w/v) sucrose and 0.8 % (w/v) phytagel for 5-8 d under long-day conditions after 2 d stratification (n = 5-12 ± SD).
C: Phenotype of individual mutants and the *atm3-4gr2epc2* double mutant of soil grown plants at rosette stage. Plants were grown under long-day conditions for 4 weeks.
D: Pulse-amplitude modulated (PAM) fluorimetry was performed with 4-week-old plants grown on soil under long-day conditions using the JUNIOR-PAM (WALZ) (n = 7 ± SD). The statistical analysis (one way ANOVA with post hoc Holm-Sidak comparisons for wild-type vs. mutant) indicated significant changes; *P ≤ 0.05; ***P ≤ 0.001.

To further support the hypothesis that the increase in matrix GSSG does not affect the activity of GRXS15 but can compete as a putative substrate of ATM3 with the export of the unknown sulfur-compound X-S, root growth of the partially GSH-depleted mutants *rml1* and *zir1* as well as the *atm3-4gr2epc2* mutant was analysed using medium with different nitrogen sources. In contrast to the *grxs15* mutant, whose growth retardation of the roots is more pronounced on

nitrate than on ammonium (Figure 16), the other mutants react similar to the wild-type and develop shorter roots when grown on ammonium (Figure 32). An exception in this case is *rml1*, which does not react at all due to a general block in post-germination development. This of course is not surprising as the root generally does not grow at all. Nevertheless, the relative growth retardation on ammonium was similar for all other mutant lines when compared to the respective wild-type.

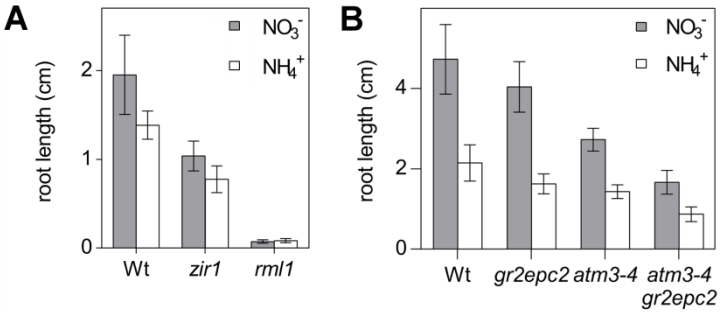

Figure 32: GSH-deficiency and a block in GSSG export do not affect the use of different nitrogen sources.
A: Root length of wild-type and GSH mutants *zir1* and *rml1*. Seedlings were grown for 7 d on medium containing 5 mM KNO_3 or 2.5 mM $(NH_4)_2SO_4$, 0.1 % (w/v) sucrose and 0.8 % (w/v) phytagel under long-day conditions after 2 d stratification (Wt, *zir1*: *n* = 44-49 ± SD; *rml1*: *n* = 8-12 ± SD).
B: Root length of *gr2epc2* and *atm3-4* as well as the double mutant *atm3-4gr2epc2* compared to the wild-type. Seedlings were grown for 11 d on medium containing 5 mM KNO_3 or 2.5 mM $(NH_4)_2SO_4$, 0.5 % (w/v) sucrose and 0.8 % (w/v) phytagel under long-day conditions after 2 d stratification (*n* = 25-33 ± SD).

Continuing the analysis whether the mitochondrial glutathione redox state has any impact on the maturation of cytosolic FeS-proteins, the XDH activity of *gr2epc2* and *atm3-4* as well as the double mutant *atm3 4gr2epc2* and the wild-type was analysed. Here, no differences were revealed via the semiquantitative in-gel method. The decrease in XDH activity of the double mutant *atm3-4gr2epc2* was comparable to the *atm3-4* mutant (Figure 33). No difference was observed between the *gr2epc2* mutant and wild-type. Thus, the underlying biochemical causes of the observed aggravated *atm3-4gr2epc2* phenotype is not based on impaired maturation of cytosolic FeS-proteins and has still to be figured out.

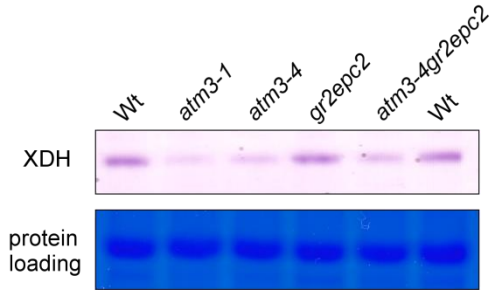

Figure 33: The *atm3-4gr2epc2* double mutant shows no enhanced malfunction in cytosolic FeS-protein maturation. In-gel XDH activity of *gr2epc2* and *atm* mutants as well as the double mutant *atm3-4gr2epc2* compared to the wild-type. Equal amounts of total protein (70 µg) extracted from 11-d-old seedlings were separated on a native gel and stained for XDH activity using hypoxanthine as substrate.

3.3 The oxidoreductase activity of GRXS15

3.3.1 GRXS15 shows a negligible oxidoreductase activity

In eukaryotic cells the redox state of protein thiols is controlled by GRXs or TRXs, respectively. Since GRXS15 is most likely the only Arabidopsis GRX located in mitochondria, we wondered whether GRXS15 can also act as an oxidoreductase. Particularly, because Hoffmann and colleagues showed that mitochondrial GDC is activated by a GRX *in vitro*. This GRX, however, was not GRXS15 (Hoffmann et al., 2013).

GRXs are routinely assayed as catalysts of reactions in which GSH reduces a disulfide, usually HED. In this assay, GRX activity is monitored spectrophotometrically as the oxidation of NADPH in a coupled system with GSH and GR. In order to study the oxidoreductase activity of GRXS15, the sequence without target peptide was cloned into an expression vector and expressed in *E. coli* to produce the recombinant protein without its native targeting peptide ($GRXS15_{38\text{-}169}$). Furthermore, the dithiol glutaredoxin GRXC1 was used as a positive control as recent studies have shown that GRXC1 shows enzyme activity in the HED assay (Riondet et al., 2012).

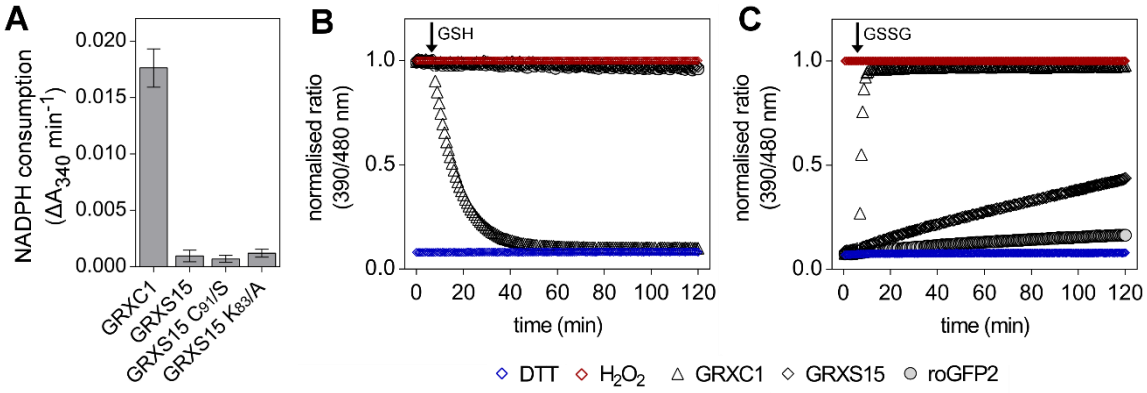

Figure 34: Catalytic activity of GRXS15 in standard assays is negligible.
A: A: NADPH consumption (ΔA_{340} min^{-1}) of GRXS15 mutants and GRXC1 using HED as substrate. GRXs were used at a final concentration of 3 µM. Basal background activities in the absence of GRX were subtracted. (n = 4 ± SD).
B, C: roGFP2-interaction assay with GRXC1 (Δ) and GRXS15 (◊). Oxidised roGFP2 was mixed with or without 3 µM GRXC1 and GRXS15. Negative controls contained roGFP2 without glutaredoxin. 2 mM reduced glutathione (GSH) together with 1 U GR and 100 µM NADPH was used for reduction of the oxidised sensor **(B)**. In contrast, the pre-reduced sensor was oxidised by addition of glutathione disulfide (GSSG) to a final concentration of 40 µM **(C)**. Furthermore, H_2O_2 and DTT were used at a final concentration of 10 mM to define maximum reduction (◊) and oxidation (◊) of roGFP2. Fluorescence was excited at 390 and 480 nm and continuously detected at 520 nm. The fluorescence ratios measured for fully oxidised roGFP2 in the presence of 10 mM H_2O_2 was set to 1 and all data normalised accordingly. The presented curves are means of three technical replicates.

In the HED assay reductive activities of GRXS15 as well as its mutant variants C_{91}/S and K_{83}/A were only just above background and less than 3 % of the activity observed for GRXC1 (Figure 34A). In a second approach GRXS15 was analysed regarding the ability to reduce or oxidise roGFP2. To define maximum oxidation and reduction of roGFP2, the protein was incubated with 10 mM H_2O_2 or DTT, respectively. For GRXC1 a direct reduction of roGFP2 was observed after addition of GSH. In contrast, GRXS15 was not able to reduce roGFP2 in the presence of GSH as reducing agent (Figure 34B). Interestingly, GRXS15 was able to oxidise the reduced sensor, nevertheless, approximately 30 times slower than GRXC1 (Figure 34C).

3.3.2 The GRXS15 K_{83}/A mutant shows an enhanced oxidation of roGFP2

As shown above, GRXS15 just has a slow oxidoreductase activity *in vitro* using roGFP2 as substrate. The reactivity of catalytic cysteines is also influenced by neighbouring residues generating a specific microenvironment. For example, lowering the pK_a of the thiol group with the help of basic amino acids or via ionic interactions with positively charged residues will affect the nucleophilicity of the cysteine (e.g. thiolates are stronger nucleophiles than thiols). As K_{83} is highly conserved among all GRXs and positioned near C_{91} (Figure 12) we were wondering whether the K_{83}/A mutation has any influence on the ability of GRXS15 to catalyse reduction or oxidation roGFP2. Interestingly, no GSH-dependent reduction of roGFP2 by GRXS15 K_{83}/A was observed similar to the native GRXS15 (Figure 35A). However, the K_{83}/A variant showed a strongly enhanced GSSG-dependent oxidation of roGFP2 compared to the native GRXS15. Still, the oxidation of roGFP2 by the K_{83}/A mutant was with less speed compared to GRXC1 (Figure 35B).

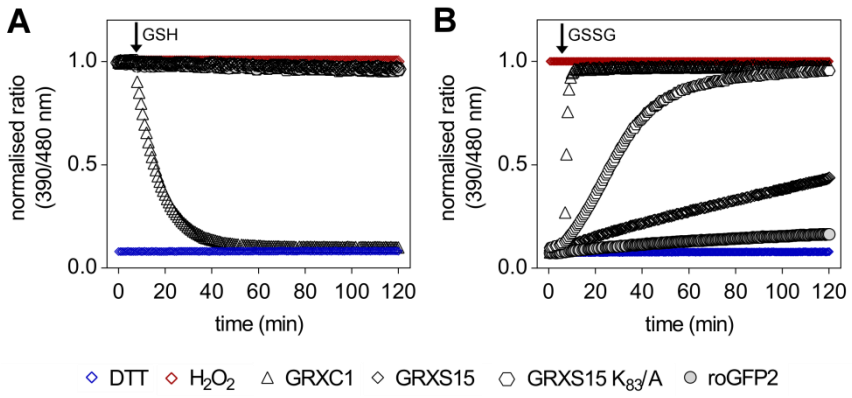

Figure 35: roGFP2 interaction of GRXS15 K_{83}/A.
A: GSH-dependent reduction of roGFP2**.** Oxidised roGFP2 was mixed with or without 3 µM GRXS15 K_{83}/A. GRXC1 and GRXS15 served as controls.
B: GSSG-dependent oxidation of roGFP2. Reduced roGFP2 was mixed with or without 3 µM GRXS15 K_{83}/A. GRXC1 and GRXS15 served as controls.

3.3.3 roGFP2 R_{168}/A – an optimised redox sensor?

The surface of GRXS15 near the catalytic C_{91} is extremely positive because of several lysyl residues (K_{83}, K_{120} and K_{124}). Because correct reaction geometries, together with complementary surfaces for the respective protein and interacting partners, are crucial parameters for the specificity, it was questioned if roGFP2 could be optimised for the analysis of the oxidoreductase activity of GRXs. Therefore, the structure and electrostatic surface of roGFP2 was confronted with a homology model of GRXS15 based on the human GLRX5 as well as poplar GRXC1, a homolog of Arabidopsis GRXC1 but with available crystal structure (Figure 36). On the surface of roGFP2, the residue R_{168} in close proximity to the catalytic C_{147}/C_{204} disulfide engineered into the GFP barrel provides a positive charge that may interfere with the positive charges on the surface of GRXS15 (Figure 36A). The attempt to modify roGFP2 was triggered by the loss of the positive charge and the presence of a positive charge near the disulfide of roGFP2. (Figure 36B). Similar to GRXS15, GRXC1 has a positive electrostatic surface potential. However, two small neutral surface patches near the catalytic C_{31} due to the two tyrosine residues Y_{30} and Y_{33} distinguish between GRXC1 and GRXS15 (Figure 36C).

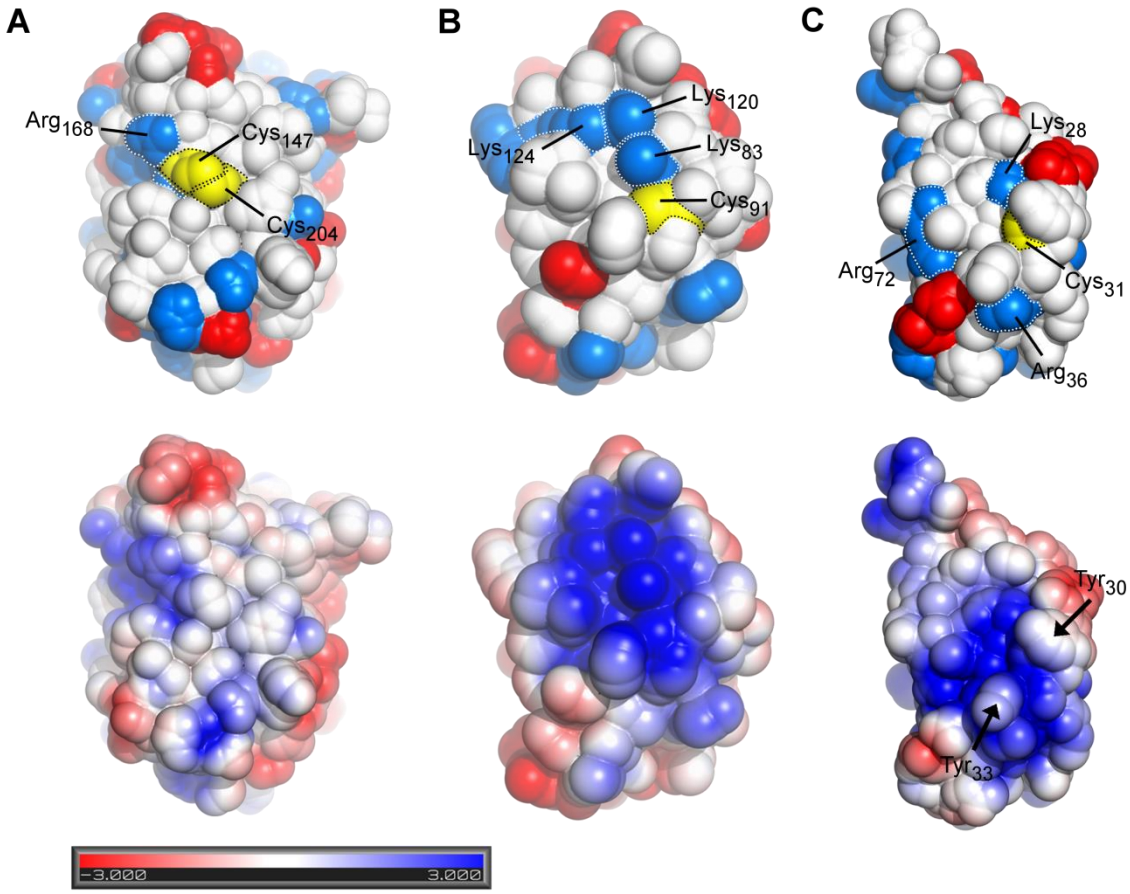

Figure 36: Structure and electrostatic surface of roGFP2, GRXS15 and *Pt*GRXC1.
Upper: Solvent-accessible surfaces of roGFP2 (PDB: 1JC1) (**A**), the homology model of GRXS15 (**B**) and *Pt*GRXC1 (PDB: 1Z7P) (**C**). All positively charged side chains are depicted in blue, all negatively charged side chains in red, redox-active cysteines in yellow. Lower: Solvent-accessible surface potential of the respective proteins calculated with the APBS tool at pH 7 and 25 °C and displayed between -3 and +3 kT/e (Boltzmann constant, k; temperature, T and energy, e). The arrows in **C** depict two neutral surface patches of GRXC1 near the catalytic cysteine due to the two tyrosine residues Y_{30} and Y_{33}.

Thus, assuming that the roGFP2-GRX interaction includes many backbone–backbone interactions, we were wondering if roGFP2 can be optimised for the interaction with GRXs by deleting the positive surface patch near the two surface cysteines of roGFP2 and preventing the repulsion of the two proteins because of the similar charge. Therefore, we substituted the R_{168} residue to alanine (roGFP2 R_{168}/A) and compared first the general spectral properties of the recombinant protein *in vitro*. IPTG-induction of *E. coli* cultures transformed with roGFP2 R_{168}/A already resulted in green cultures suggesting that the introduced mutations did not abolish fluorescence. Furthermore, comparison of absorption and excitation spectra of roGFP2 and the roGFP2 R_{168}/A variant did not show pronounced differences in spectral properties nor in the dual excitation behaviour of the sensor (Figure 37). Oxidation of both proteins using H_2O_2 caused an increase of fluorescence when excited at ~390 nm and a corresponding decrease

when excited at ~480 nm. Conversely, full reduction with DTT led do a decrease in excitation at 390 nm and an increase in excitation at 480 nm. However, the excitation peak at 480 nm of roGFP2 R_{168}/A was in all cases not quite as high as in the native roGFP2.

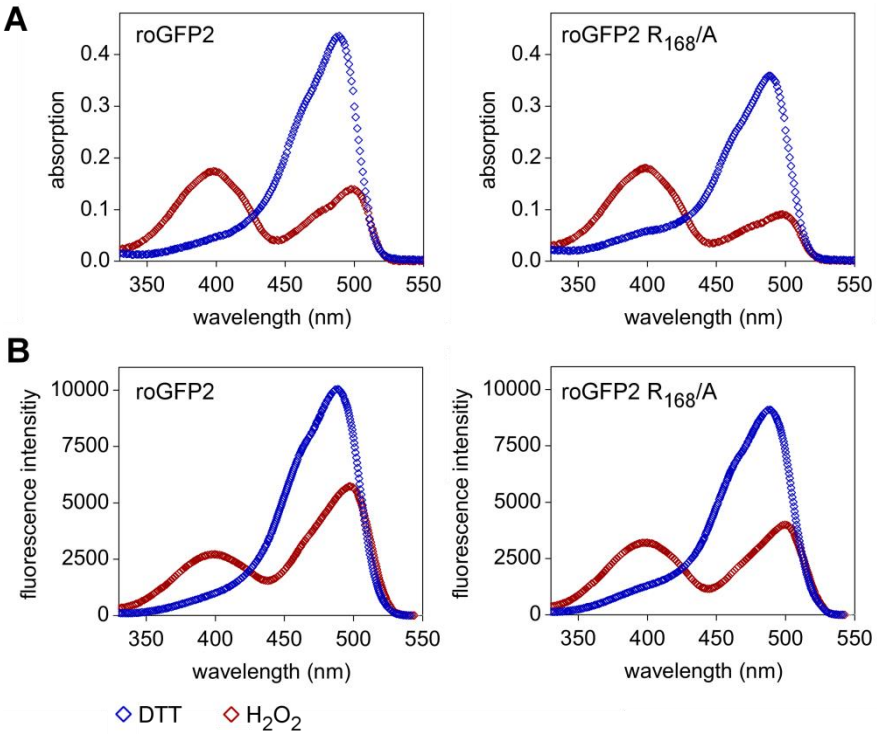

Figure 37: Spectral properties of roGFP2 R_{168}/A.
A: Absorption spectrum of roGFP2 and roGFP2 R_{168}/A in fully oxidised (red) and fully reduced (blue) state. 50 µM protein was incubated in 10 mM DTT or 10 mM H_2O_2 for 20 min.
B: Excitation spectrum of roGFP2 and roGFP2 R_{168}/A in fully oxidised (red) and fully reduced (blue) state. 5 µM protein was incubated in 10 mM DTT or 10 mM H_2O_2 for 20 min. Emission was monitored at 520 nm.

Further equilibration of both sensors in buffers with different pH revealed that the roGFP2 variant is insensitive in the physiological range of pH 7 - 7.8 similar to roGFP2 (Figure 38). However, the fluorescence ratio of the fully oxidised state of roGFP2 R_{168}/A was more sensitive to changes in the direction of a more alkaline pH resulting in a strong decrease of the dynamic range (δ). While roGFP2 R_{168}/A at a pH of 7 had a $\delta_{390/480}$ of 11.7 the $\delta_{390/480}$ at pH 5.8 was found to be 7.6.

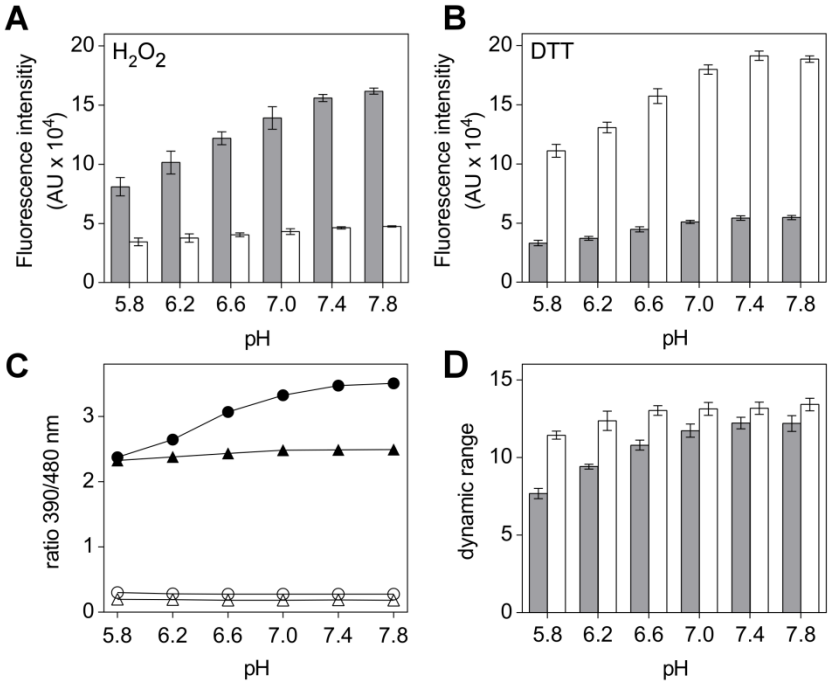

Figure 38: pH-dependence of roGFP2 R_{168}/A fluorescence.
A, B: Recombinant roGFP2 R_{168}/A was incubated in 0.1 M potassium phosphate buffer at different pH values. The changes in roGFP2 R_{168}/A fluorescence intensity of the 390 nm (grey) and 480 nm channel (white) in buffers of different pH values under full oxidation with 10 mM H_2O_2 (**A**) and full reduction by 10 mM DTT (**B**) are shown.
C: The excitation ratios (390/480 nm) in 10 mM H_2O_2 and in 10 mM DTT of roGFP2 (▲ or Δ) and roGFP2 R_{168}/A (● or ○) are plotted against the respective pH solution. (*n* = 3 technical replicates).
D: Dynamic range of roGFP2 (white) and roGFP2 R_{168}/A (grey) calculated from the respective max and min values as depicted in **C**.

To further test whether the amino acid substitution R_{168}/A has any influence on the formation and stability of the disulfide bridge the standard redox potential (*E*°') was determined through titration with DTT. For roGFP2, Dooley and colleagues suggested a consensus midpoint potentials of -280 mV (Dooley et al., 2004). Plotting the degree of oxidation of the sensor and its variant against the redox potential of the ambient DTT_{red}/DTT_{ox} buffer revealed an *E*°' of -289.4 ± 3.5 mV for roGFP2 and a slightly more negative redox potential of -293 ± 1.7 mV for roGFP2 R_{168}/A (Figure 39).

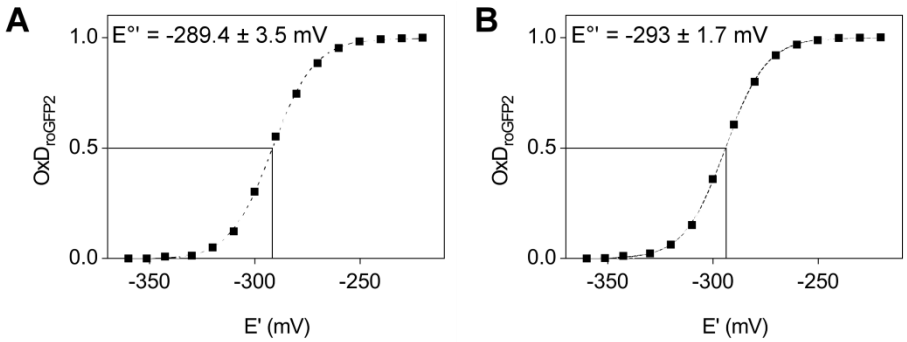

Figure 39: Determination of the redox potential of roGFP2 and roGFP2 R_{168}/A.
For determination of the midpoint potentials *E*°' of roGFP2 **(A)** and roGFP2 R_{168}/A **(B)** OxD_{roGFP2} was plotted against the calculated redox potentials of the respective DTT redox buffers and all data points were fitted to a sigmoidal dose-response curve using GraphPadPrism7. The titration of each protein was carried out 3 times with 3 technical replicates ($E°'_{DTT}$ = -323 mV, Shaked et al. (1980)).

As the deletion of basic amino acids next to cysteines may lead to destabilisation of the thiolate, we were wondering if the roGFP2 R_{168}/A variant shows any changes in the kinetic properties determined through interaction with GRXs. On the one hand, there would be the possibility of an enhancement of the reactivity with GRXs due to the decreased positive electrostatic surface but on the other hand, there might be a decreased reactivity due to destabilisation of the thiolate. Analysis of the ability of GRXC1 to reduce or oxidise roGFP2 or the R_{168}/A variant revealed no enhanced activity in the GSH-dependent reduction of mutant variant. In contrast, GSSG-dependent oxidation of roGFP2 R_{168}/A was even slightly slower compared to roGFP2 (Figure 40).

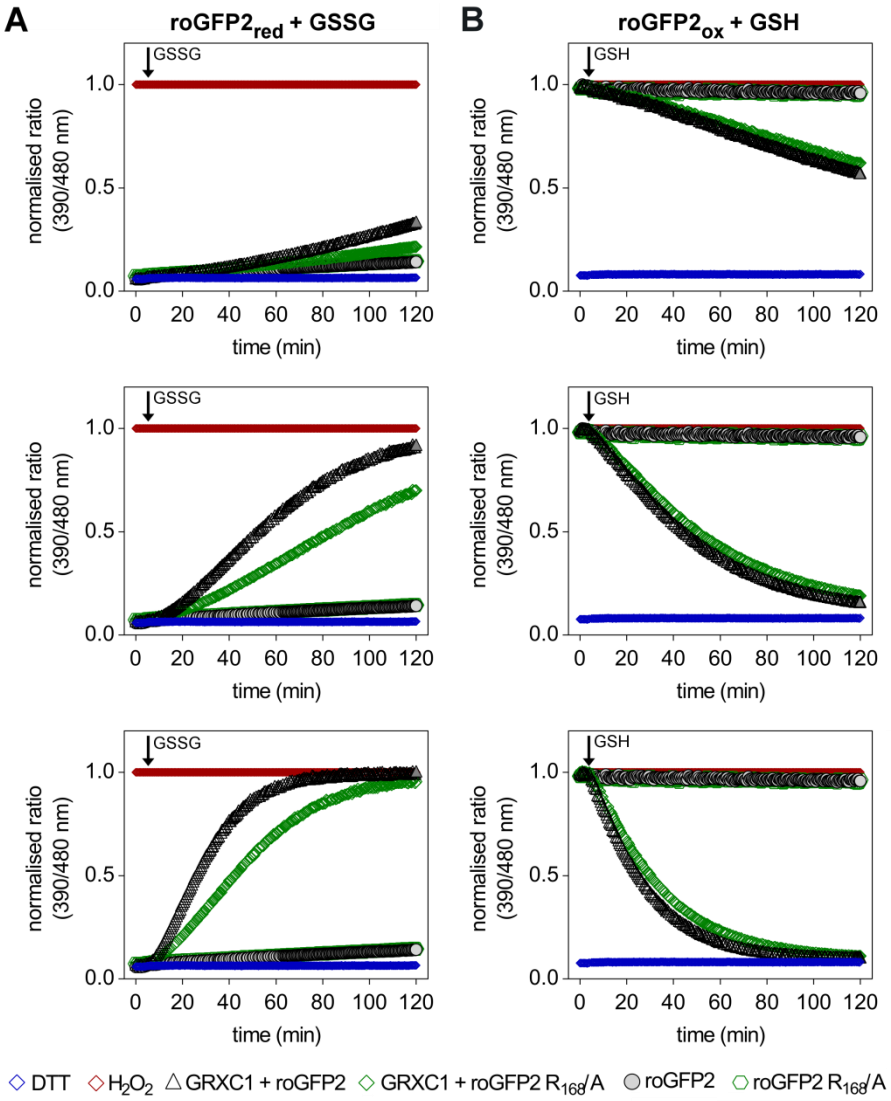

Figure 40: GRXC1 catalysed redox reactions of roGFP2 and roGFP2 R_{168}/A.
A: GSSG-dependent oxidation kinetics of 1 µM reduced roGFP2 in the presence of 0.1 µM (upper), 0.5 µM (middle) and 1 µM (lower) GRXC1.
B: GSH-dependent reduction kinetics of 1 µM oxidised roGFP2 in the presence presence of 0.1 µM (upper), 0.5 µM (middle) and 1 µM (lower) GRXC1. Negative controls contained roGFP2 without GRXC1. Samples with 10 mM DTT or H_2O_2 were used to fully oxidise or reduce roGFP2. Maximal oxidised roGFP2 by 10 mM H_2O_2 was set to 1 for each measured time point. Shown are the means of three technical replicates.

4. Discussion

4.1 Localisation of GRXS15 is fundamental for its function

Mitochondria are the cellular site of respiration, where energy is released from the sugar metabolism and used for the synthesis of ATP. Notably, these organelles are not just creating vital energy but are also involved in several other essential processes as hormone signalling, Ca^{2+} regulation or assembly of iron-sulfur cluster. An unavoidable consequence, however, of the respiration is the production of mitochondrial reactive oxygen species. In plant mitochondria, the redox balance is primarily maintained by ascorbate and glutathione acting together in the ascorbate–glutathione cycle (Chew et al., 2003b). Although GSH is synthesised in plastids and in the cytosol, immunocytochemical staining suggested that mitochondria contain particularly high GSH concentrations (Zechmann et al., 2008). GRXs are generally considered to mediate reactions involving GSH for de-glutathionylation of target proteins or as a cofactor for ISC coordination. In yeast and humans, two GRXs are located in mitochondria and in both organisms one has been described to perform oxidoreductase reactions (Lillig et al., 2005; Pedrajas et al., 2002), whereas the other is involved in the maturation of FeS-proteins (Johansson et al., 2011; Picciocchi et al., 2007; Rodríguez-Manzaneque et al., 2002). Surprisingly, for Arabidopsis just GRXS15 is predicted by bioinformatical algorithms to be a mitochondrial protein. In contrast to the claims by Cheng (2008), who presented a chloroplast localisation in tobacco leaves, we found GRXS15 exclusively localised in mitochondria confirming the results reported elsewhere using mass spectrometry (Klodmann et al., 2011; Salvato et al., 2014). Furthermore, in a report published during this study by Ströher and colleagues (2016), dual-targeting of GRXS15 to the mitochondria and the chloroplasts as well as the presence of other GRXs in Arabidopsis mitochondria was excluded (Ströher et al., 2016). Thus, these results leave Arabidopsis with just only GRXS15 in mitochondria that has, indeed, a vital role as previously unrecognised Arabidopsis null mutants are embryonic lethal. TRXs and GRXs are generally described as the master regulators of the redox state of the thiol groups of the proteome (Berndt et al., 2015). Still, our experiments from different GRX assays, suggest that GRXS15 has no reducing activity and, if at all, only a minor oxidation activity. This effect, however, was approximately 30 times lower than catalysis by GRXC1. The negligible reducing activity was further supported by Ströher et al. (2016), who showed a reducing activity of GRXS15 in the HED and dehydroascorbate assay more than 360 times lower than human GLRX2. The reduced activity is comparable to the mitochondrial monothiol GLRX5, where the relative catalytic activity was approximately 500-fold times lower than GLRX2 (Johansson et al., 2011). Similar, a 20-fold lower activity observed for yeast Grx5p compared with dithiol

Grx1 from *E. coli* with GSH as electron donor has been explained by inefficient reduction of monothiol GRXs by GSH (Tamarit et al., 2003). This result is in line with independent observations showing low or even negligible levels of thiol-disulfide oxidoreductase activity of several other monothiol GRXs (Cheng et al., 2006; Fernandes et al., 2005), suggesting that this function became secondary during evolution. Thus, it remains an open question which enzymes mediate protein deglutathionylation effectively in plant mitochondria.

4.2 GRXS15 is as an essential component of the mitochondrial ISC machinery

Monothiol GRXs are proposed to be involved in the last step of FeS-protein maturation, transferring the ISC to apoproteins or being involved in the protection of FeS-proteins. Indeed, at least one monothiol GRX is located in each subcellular compartment possessing an ISC assembly machinery (Figure 41).

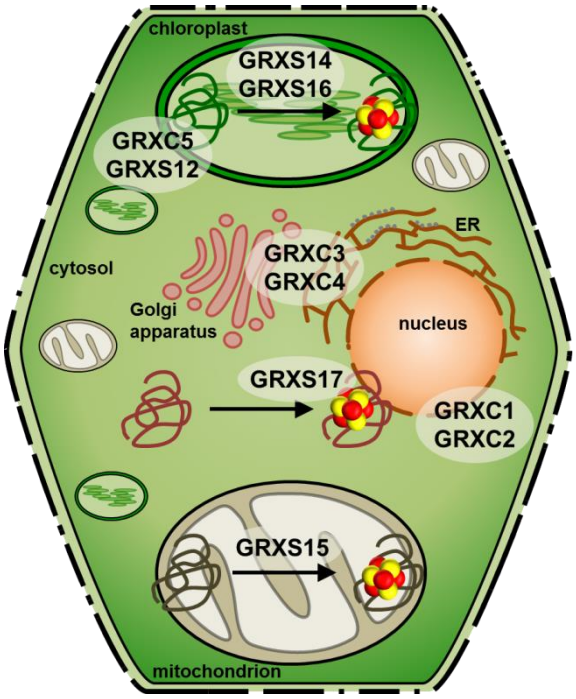

Figure 41: Overview of plant class I & II GRXs and their putative subcellular localisation in plant cells. For the sake of simplicity just the subcellular compartments where GRXs are located are depicted. ER = Endoplasmic reticulum

The assembly and transfer of ISCs, however, is a complex process that has not been completely characterised on a molecular level. Still, the fundamental role of ISCs for building the

machineries that are at the centre of maintaining life is emphasised by the fact that mutants affecting genes of the mitochondrial ISC assembly pathway like frataxin or IBA57 are frequently embryo-lethal (Busi et al., 2006; Waller et al., 2012). Loss of GRXS15 in Arabidopsis causes also embryonic lethality in contrast to *Δgrx5* yeast cells which are still viable. Viability of *Δgrx5* seems to be maintained by the mitochondrial dithiol Grx2p as a backup, as *Δgrx2Δgrx5* mutants are synthetic lethal (Rodríguez-Manzaneque et al., 1999). Surprisingly, overexpression of the dithiol Grx2p and human GLRX2 did not rescue Grx5p deletion phenotype or lethality of *Δgrx2Δgrx5* mutants indicating no overlapping functions of the two classes of GRXs (Molina et al., 2004; Uzarska, 2013). Similar to Arabidopsis, deficiency of Grx5 in zebrafish is lethal between 7 and 10 d after fertilisation (Wingert et al., 2005). These results indicate that the monothiol GRXs are less critical during fertilisation but essential for vegetative growth or development, respectively. Regarding Arabidopsis, this phenomenon may be explained by residual ISC assembled before meiosis or by the fact that energy metabolism in pollen tubes can undergo fast rearrangements shifting from aerobic respiration to ethanol fermentation (Obermeyer et al., 2013). Pollen tube growth has been shown to continue even under anaerobic conditions or on inhibitors of the respiratory electron transport or ATP synthase albeit at lower speed (Obermeyer et al., 2013; Rounds et al., 2010). This effect may explain the slight deviations from Mendelian segregation observed for selfed *grxs15-3* mutants. So far for plants, the involvement of a monothiol GRX in the ISC pathway, such as GRXS15, has only been speculated, mainly as the presence of an ISC could not be shown for poplar GRXS15 (Bandyopadhyay et al., 2008). The data presented here reveals that recombinant GRXS15 in the presence of GSH indeed coordinates an ISC and, moreover, supports the presence of a [2Fe-2S] type cluster or a mixture of $[2Fe\text{-}2S]^{2+}$ and linear $[3Fe\text{-}4S]^{+}$ clusters similar to other class II GRXs. Reconstitution assays confirmed the incorporation of an ISC and the resulting A_{420}/A_{280} ratio of 0.36 was in a similar range as for other monothiol GRXs coordinating ISCs [GRXS14: 0.31 ± 0.04 (Bandyopadhyay et al., 2008) and GRXS17: 0.29 (Knüsting et al., 2015)]. The ability for GRXS15 to coordinate ISCs was also shown by Ströher and colleagues. Furthermore, the capability to transfer the ISC to the mitochondrial ferredoxin MFDX1 *in vitro* (Moseler et al., 2015) as well as the interaction with the transfer protein ISCA (Consortium, 2011) points to a role of GRXS15 in ISC transfer similar to yeast Grx5p. Surprisingly, in contrast to the other CGFS GRXs of Arabidopsis, GRXS15 is the only one that is not able to fully complement the yeast *Δgrx5* phenotype. The reason for only partial complementation is unknown, but one can speculate about differences between yeast and Arabidopsis proteins leading to less stable ISC coordination or partially impaired protein–

protein interactions as a result of the coevolution between the interacting proteins within a given organism. For instance, compared with yeast Grx5p, plant GRXS15 isoforms have a clear N-terminal extension containing many conserved Asp residues, whereas they have a slightly shorter C-terminal part missing charged residues found in Grx5p. Nevertheless, it is still remarkable that the two plastidic GRXS14 and GRXS16 or the cytosolic GRXS17 are able to fully complement the yeast mutant (Cheng et al., 2006; Knüsting et al., 2015; Liu et al., 2013). Considering that the C-terminal part of monothiol GRXs was shown to be responsible for protein–protein interaction (Roret et al., 2014), variations in this protein region might be crucial. Indeed, another important difference is that yeast Grx5p as well as GRXS14, GRXS16 and GRXS17 contain an additional cysteine residue implicated in intramolecular disulfide exchange reactions (Figure 42) (Tamarit et al., 2003).

```
GRX5p      YQNRMYLSTEIRKAIEDAIESAPVVLFMKGTPEFPKCGFSRATIGLLGNQGVDPAKFA  81
GRXS14     RCSASALTPQLKDTLEKLVNSEKVVLFMKGTRDFPMCGFSNTVVQILKNLNVP---FE  115
GRXS15     QKVPPDSTDSLKDIVENDVKDNPVMIYMKGVPESPQCGFSSLAVRVLQQYNVP---IS  109
GRXS16     PGRHVELTVPLEELIDRLVKESKVVAFIKGSRSAPQCGFSQRVVGILESQGVD---YE  237
GRXS17 d1  RAQPVSTADALKSRLEKLTNSHPVMLFMKGIPEEPRCGFSRKVVDILKEVNVD---FG  197
GRXS17 d2  SSGNTGLSETLRARLEGLVNSKPVMLFMKGRPEEPKCGFSGKVVEILNQEKIE---FG  327
GRXS17 d3  ---GITGEQSLEDRLKALINSSEVMLFMKGSPDEPKCGFSSKVVKALRGENVS---FG  434

GRX5p      AYNVLEDPE---LREGIKEFSEWPTIPQLYVNKEFIGGCDVITSMARSGELADLLEEA 138
GRXS14     DVNILENEM---LRQGLKEYSNWPTFPQLYIGGEFFGGCDITLEAFKTGELQEEVEKA 172
GRXS15     SRNILEDQE---LKNAVKSFSHWPTFPQIFIKGEFIGGSDIILNMHKEGELEQKLKDV 166
GRXS16     TVDVLDDEYNHGLRETLKNYSNWPTFPQIFVKGELVGGCDILTSMYENGELANILN-- 293
GRXS17 d1  SFDILSDNE---VREGLKKFSNWPTFPQLYCNGELLGGADIAIAMHESGELKDAFKDL 254
GRXS17 d2  SFDILLDDE---VRQGLKVYSNWSSYPQLYVKGELMGGSDIVLEMQKSGELKKVLTEK 382
GRXS17 d3  SFDILTDEE---VRQGIKNFSNWPTFPQLYYKGELIGGCDIIMELSESGELKATLSE- 488
```

Figure 42: Amino acid alignment of yeast GRX5p and Arabidopsis GRXS14, GRXS15, GRXS16 and GRXS17. An alignment of full length amino acid sequences, which were retrieved from TAIR, was generated with ClustalW and additionally the other two GRX domains of GRXS17 (d2 and d3) were aligned by hand. Shown is a section of the GRX domains and the three GRX domain of GRXS17, respectively. Highly conserved amino acid residues are indicated by grey background. Totally and partially conserved cysteines are indicated by a yellow background. The active site motif CGFS is boxed.

Whereas genetic analyses indicated that this cysteine does not seem essential for ISC biogenesis (Belli et al., 2002), Zhang et al. showed in mutational studies that this cysteine is required for the assembly of Fe_4S_4 cluster and that the Fe_4S_4 cluster-bound form of Grx5p is competent for restoring the activity of recombinant ACO *in vitro* (Zhang et al., 2013). However, supported by the fact that mutations in GRXS15 interfering with the ISC coordination impair the ability to

complement the *Δgrx5* yeast mutant, we can summarise that GRXS15 is as an essential component of the mitochondrial ISC machinery in Arabidopsis.

4.3 The role of GRXS15 in ISC transfer

How is GRXS15 involved in ISC transfer to apoproteins? As the function of GRXS15 in mitochondria is pivotal, the question raises whether GRXS15 plays a central role in the ISC machinery or belongs to a maturation pathway specific for particular target proteins. In this study we showed that complete absence of GRXS15 is embryonic lethal. Nevertheless 5 % of the wild-type protein level is enough for survival, albeit with a smaller growth phenotype, while 20 % of the GRXS15 amount allows wild-type-like growth under normal growth conditions (Ströher et al., 2016). This is probably linked to degrees of efficiency in ISC transfer to specific target proteins and indicates that a certain threshold of GRXS15 is critical. Concomitant with this, the function of GRXS15 is not redundant and cannot be compensated by another component of the ISC pathway. Complementation of the Arabidopsis null mutant with the GRXS15 K_{83}/A variant and the concomitant partial depletion of GRXS15 activity in mitochondria slowed down whole plant development and particularly root growth. Indeed, GRXS15 is especially strongly expressed in roots and in particular, in the maturation and meristematic zone (Belin et al., 2015). In addition to the impaired root growth, root respiration was decreased in comparison to the wild-type. However, the reduced respiration was not present in the knock-down mutant containing ~20 % of the wild-type GRXS15 level indicating that the reduction of GRXS15 has to reach a certain threshold to have a negative effect on mitochondrial respiration (Ströher et al., 2016). In humans, it was observed that a GLRX5-deficient patient has a decrease of complex I activity and also diminished quantities (Ye et al., 2010), whereas in yeast, *Δgrx5* mutants displayed a decreased complex II activity, but contained the same protein amount (Rodríguez-Manzaneque et al., 2002). Interestingly, in the complemented K_{83}/A mutant as well as in the more severe knock-down line the abundance and activity of complex I and II of the respiratory chain were not altered compared to the wild-type.

In both cases, however, GRXS15 was shown to be especially important for lipoic acid-dependent enzymes in mitochondria, highlighting a putative role in the transfer of ISCs in this process (see Figure 24 and Ströher et al. (2016)). Although the activity of the mitochondrial pyruvate dehydrogenase complex (mtPDC) was not significantly decreased in isolated mitochondria of the K_{83}/A mutant line, the amount of lipoylated proteins of GDC H-proteins was immensely reduced. Additionally, pyruvate accumulates highly in the Arabidopsis mutant

pointing to a limited activity of mtPDC *in vivo*. Since mtPDC serves as an entry point for carbon into the TCA cycle it is an important site for metabolic regulation. Moreover, it seems that the TCA cycle flux is somehow perturbed as also the other metabolites like citrate or isocitrate accumulate slightly. Thus, this might lead to an energy-limited condition for the plant resulting in decreased respiration and less production of ATP. Nevertheless, analysing the cytosolic ATP level did not reveal any differences between the K_{83}/A mutant and wild-type. As this experiment was performed under illumination, it might be that the cytosolic ATP pool is fed by the plastids due to photosynthetic ATP generation. Amino acid profiling of the *grxs15* mutant reveals an accumulation of nearly all amino acids indicating the use of amino acids as alternative respiratory substrates during carbohydrate starvation. The pyruvate as well as the amino acid accumulation was also shown for mutants of the mtPDC (Yu et al., 2012). In addition, especially the branched chain amino acids (BCAA) accumulate in the *grxs15* mutant. BCAA degradation generates alternative sources of energy in plants under energy-limited conditions (Araujo et al., 2010; Peng et al., 2015). Therefore, it was unexpected that mainly these amino acids accumulate. However, focussing at the degradation pathway of BCAAs, another enzyme that contains lipoic acid as cofactor is required: the branched-chain α-ketoacid dehydrogenase complex (BCKDC). Similar to plants growing under carbohydrate starvation (Binder, 2010; Fujiki et al., 2001), the BCKDC was highly expressed in GRXS15 knock-down mutants (Ströher et al., 2016). As other mutants like *rml1* that contain also an increased amino acid amount do not specifically accumulate the BCAAs we could assume that in the *grxs15* mutant the BCKDC is less functional because of limited lipoic acid as cofactor. Furthermore, in the *grxs15* mutant but not in *rml1*, the ketoacids of the BCAAs α-ketoisocaproic acid (KIC), α-keto-β-methylvaleric acid (KMV) and α-ketoisovaleric acid (KIV) accumulated highly. Since these ketoacids are the direct substrate of the BCKDC (Figure 25) we can suppose that in the degradation pathway of the BCAAs the turnover of the BCKDC the limiting factor is. In addition, immunoblot analyses showed that the lipoylated amount of H protein of GDC is strongly decreased reflecting limited lipoic acid synthesis, which depends on the ISC containing protein lipoyl synthase. Interestingly, the mitochondrial proteome of the GRXS15 knock-down line showed a greater abundance of mtPDC and BCKDC protein subunits that contain normally lipoic acid as cofactor (Ströher et al., 2016). In this case, however, the lipoic acid is missing indicating that the plant is somehow trying to compensate the lack of lipoic acid by overexpression of the respective subunit. Similar to the Arabidopsis mutants also humans containing mutations in the mitochondrial GLRX5 are deficient in lipoylation of mitochondrial proteins (Baker et al., 2014). Interestingly, the patients also contained other mutations in the

genes of lipoyl synthase as well as BOLA3. Regarding BOLA3, it has been suggested previously to interact with GLRX5 in the maturation of lipoate-containing 2-oxoacid dehydrogenases (Cameron et al., 2011). Similar, also in yeast mitochondrial Bol1p and Bol3p are required for the lipoylation of proteins by forming dimeric complexes with both Grx5p and Nfu1p (Uzarska et al., 2016). Work in human cells revealed also the role of a cytosolic GLRX3-BOLA2 complex as [2Fe-2S] cluster chaperone (Frey et al., 2016). Beside this role, it is also suggested that the GLRX3-BOLA2 complex acts as a reservoir of cytosolic [2Fe-2S] clusters, as the complex increased 6-8-fold in response to increasing iron (Frey et al., 2016).

Indeed, a strong genome co-occurrence exists for these two genes. With a few exceptions all organisms having CGFS GRXs also possess a BolA member and the opposite is true, all organisms lacking CGFS GRX do not possess a BolA member (Couturier et al., 2009; Huynen et al., 2005). Concerning GRXS15, interaction of GRXS15 with the dual-targeted BOLA4 was found in Y2H and BiFC assays in both mitochondria and chloroplasts (Couturier et al., 2014). In this case, the plastidic interaction might be due to the overexpression of GRXS15, which is routed to chloroplasts via the BOLA4 interaction. Summarised, we can assume that GRXS15 is in association with BOLA4 essential for the maturation of mitochondrial lipoyl synthase and related to this lipoylated proteins. This might also explain the high sensitivity of GRXS15 knock-down mutants to arsenite (Ströher et al., 2016) as arsenite inhibits the PDH complex by binding to the lipoic acid moiety (Shen et al., 2013). Since other applications of exogenous stress did not enhance the root phenotype of the GRXS15 knock-down mutants, the addition of arsenite might be the drop in the bucket for the already less amount of lipoylated proteins.

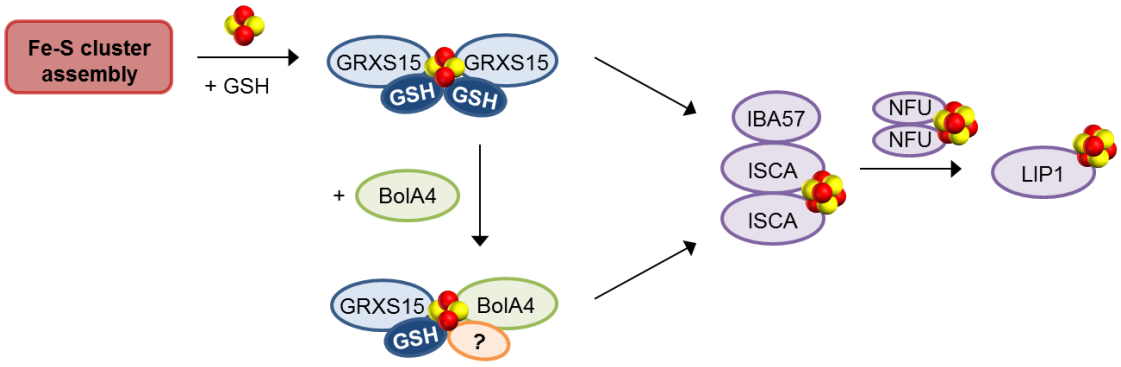

Figure 43: Maturation of the FeS-protein lipoyl synthase.
A [2Fe-2S] cluster is assembled on the scaffold protein ISU. Since the GRXS15-bound, GSH-coordinated bridging [2Fe-2S] cluster is bound in a labile fashion, GRXS15 is potentially a transfer protein that is able to easily donate its cluster to target proteins. BOLA4 possibly functions by interacting with GRXS15 but the identity of the fourth iron ligand is unknown. ISCA and IBA57 as well as NFU are required for the maturation of the radical SAM enzymes like lipoyl synthase (LIP1).

As the biosynthetic pathway for lipoic acid is present in plastids and mitochondria in Arabidopsis (Yasuno and Wada, 2002), the plastidic PDC seems not being effected in the K_{83}/A mutant. Plastidic PDC plays a dominant role in providing acetyl-CoA for fatty acid synthesis. No changes in the total amount as well as composition of fatty acids were observed in the K_{83}/A mutant compared to the wild-type emphasising the independency of the plastidic SUF and mitochondrial ISC machinery. Another conclusion that can be made from the similar fatty acid pattern is that the mitochondrial FeS-protein biotin synthase is not effected by the less functional K_{83}/A variant. Biotin is exported from mitochondria to the cytosol and chloroplasts where it is required for synthesis and elongation of fatty acids by hetero- and homomeric acetyl-CoA carboxylase. Thus, there seems no lack of biotin inhibiting full activity of biotin dependent enzymes.

A FeS-protein that is affected in the K_{83}/A mutant is aconitase. Although the protein amount did not differ, a significant decrease in activity was observed in the *grxs15* mutants. Surprisingly, no reduced activity of aconitase was observed in GRXS15 knock-down mutants. Nevertheless, the reduced aconitase activity as well as the unchanged protein amount also occurs in yeast *Δgrx5* mutants and furthermore, in GLRX5-deficient humans (Rodríguez-Manzaneque et al., 2002; Ye et al., 2010). Thus, it might be that 5 % of GRXS15 is still sufficient for proper ISC transfer and that the mutated protein variant K_{83}/A results in a dysfunction in the ISC transfer to aconitase. Indeed, Liu et al. (2016) demonstrated that mutations of highly conserved amino acid residues in GLRX5 can have different effects on downstream FeS-proteins. Here, a significant reduction of aconitase activity in a GLRX5 K_{59}/E mutant that is the equivalent of K_{83} in Arabidopsis was observed in contrast to an K_{51}/E mutant (Liu et al., 2016). Thus, these data point to a role of GRXS15 in the maturation of aconitase in Arabidopsis.

4.4 The glutathione pool does not affect the function of GRXS15

So far, in this work several key observations were made that allow a better definition of the function of GRXS15 in the mitochondrial ISC assembly pathway although GRXS15 is not able to fully rescue the phenotype of yeast *Δgrx5* mutants. Another broad difference between Arabidopsis and yeast is that no oxidative stress occurs in the mitochondria of *grxs15* mutants excluding that the oxidative stress leads to damages of FeS-proteins like aconitase. In yeast, the release of the ISC from the scaffold protein Isu1p is mediated by the dedicated chaperone system comprising Ssq1p, Jac1p, and Mge1p as well as Grx5p. Depletion of the ISC

components Ssq1p, Jac1p and Grx5p leads to an accumulation of iron probably because of the accumulation of ISCs on Isu1p (Mühlenhoff et al., 2003; Uzarska et al., 2013). Hence, the oxidative stress phenotype of *Δgrx5* cells might be a secondary effect of the impaired ISC machinery. Indeed, in *Δgrx5* cells or other mutants like *Δssq1* an impairment of the mitochondrial superoxide dismutase Sod1p activity was observed (Yang et al., 2006). Additionally, activity of aconitase could be partially restored under anaerobic conditions but still, also under anaerobic conditions there was an ISC accumulation on Isu1p (Uzarska, 2013). Although the decreased activity of mitochondrial FeS-proteins is specific for Grx5p disruption and the consequent impairment in the ISC machinery, the question is if it is also specific for the decreased activity of cytosolic FeS-proteins. Mitochondria contain the highly conserved ABC transporter ATM in the inner membrane that exports an unknown sulfur component in a glutathione-dependent fashion which is essential for the maturation of cytosolic FeS-proteins. In yeast, it is assumed that Grx5p is somehow involved in the transfer of this unknown molecule to the ABC transporter. In contrast, in this study no decreased activity of cytosolic FeS-proteins like AAO or XDH was observed in the complemented *grxs15* mutants nor in the knock-down lines. Thus, on the one hand you can argue that the export mechanism of the unknown sulfur compound differs between yeast and Arabidopsis and that GRXS15 is not involved in the export. On the other hand, regarding yeast Grx5p, however, the mitochondria show an oxidative-stress phenotype that might influence the mitochondrial glutathione pool. The GSH requirement for viability could theoretically be linked to either its thiol-redox function or role in maturation of FeS-proteins, as both these processes are essential. Although it has been shown that depletion of the mitochondrial GSH pool in yeast does not affect the activity of mitochondrial FeS-proteins (Sipos et al., 2002), it strongly influences the maturation of cytosolic FeS-proteins (Ozer et al., 2015). In this study, we could show that the glutathione-depleted Arabidopsis mutants *rml1* and *zir1* do not phenocopied the *grxs15* mutants indicating that in Arabidopsis a GSH-depletion does not affect the downstream targets of GRXS15. Additionally, we showed that a more oxidised mitochondrial glutathione pool is not influencing the maturation of cytosolic FeS-proteins as the XDH activity was the same in the *gr2epc2* mutant compared to the wild-type. Furthermore, no stronger reduction of the XDH activity was observed in the *atm3-4gr2epc2* double mutant compared to the *atm3-4* single mutant. This indicates that the increased matrix GSSG cannot compete as a putative substrate of ATM3 with the export of the unknown sulfur-compound X-S from the matrix. ATM3 transports multiple substrates, including the pterin precursor of Moco (Teschner et al., 2010). In yeast, *Δatm1* mutant show a mitochondrial iron accumulation as well as increased levels of GSSG (Kispal et

al., 1997). Although Arabidopsis *atm3* mutants do not show a mitochondrial iron accumulation, it might be that ATM3 is involved in the export of oxidised GSSG. To test if the aggravated phenotype of *atm3-4gr2epc2* is based on the accumulation of matrix GSSG, the double mutant as well as single mutants were transformed with mitochondrial targeted roGFP2:hGRX1. As the fused hGRX1 mediates the redox equilibration of roGFP2 with the glutathione redox buffer the mitochondrial E_{GSH} of the single mutants *atm3-4* and *gr2epc2* can be compared to the double mutant. Still, it might be possible that there is an alternative reduction of GSSG by TRX in mitochondrial *gr2* null mutants similar to the observed functional redundancy of the cytosolic NTR/TRX system with GR1 (Marty et al., 2009). This might be leading to a slight but not effective accumulation of matrix GSSG.

4.5 The influence of a highly conserved lysine on GRX oxidoreductase activity

The E_{GSH} in living cells varies depending on the subcellular compartment and on environmental conditions imposing stress situations for the plant. In Arabidopsis, the ER maintains E_{GSH} values less negative than -240 mV, while cytosol, peroxisomes, mitochondria and plastids contain a highly reduced glutathione buffer with redox potentials of less than -310 mV (Meyer et al., 2007; Schwarzländer et al., 2008). As mentioned above, one tool to sense the local E_{GSH} is the genetically encoded roGFP2:hGRX1 fusion protein (Meyer et al., 2007). In contrast to GRXS15, hGRX1 is able to reduce and oxidise roGFP2 efficiently in a glutathione-dependent way. GRXS15, however, shows only a negligible activity in the GSSG-dependent oxidation of roGFP2. This difference might be because of the requirement of two distinct glutathione interaction sites for efficient redox catalysis. Begas and colleagues showed that GRXs have one site that interacts with the glutathionylated disulfide substrate whereas the other site interacts with GSH (Begas et al., 2017). Furthermore, they argued that the inefficient reduction of numerous GRXs by GSH results in a decoupling from the GSH pool, which allows the formation of stable complexes, e.g. with ISCs. Thus, probably the ability of CGFS GRXs to reduce target proteins got lost during evolution while the ability to oxidise proteins is still present although not as primary function. Surprisingly, the K_{83}/A variant of GRXS15 was able to oxidise roGFP2 more efficiently than the native GRXS15, but in the absence of any effects on the reduction of roGFP2. Because of the loss of the positive charge in the K_{83}/A variant and the presence of a positive charge near the disulfide of roGFP2, it was questioned if roGFP2 could be optimised for the analysis of the oxidoreductase activity of GRXs. For a faster "real-time" monitoring of acute and rapid stress-induced oxidative events a R_{168}/A substitution was introduced in roGFP2. Similar to roGFP1 variants that correspond with more positive charges near the disulfide to more oxidising midpoint potential (Cannon and Remington, 2006), the roGFP2 R_{168}/A variant showed a slightly more reducing midpoint potential. Additionally, spectroscopic properties were similar to roGFP2. Thus, the sensor is still suitable for analysis of E_{GSH} , e.g. in mitochondria. In contrast to our initial hypothesis, the amino acid substitution R_{168}/A did not enhance the GSH-dependent reduction of roGFP2 with GRXC1 and even reduced the rate of GSSG-dependent oxidation. This is also consistent with roGFP1 variants, in which increasing basic charges near the disulfide leads to increasing rates of disulfide formation (Cannon and Remington, 2006). Thus, the enhanced oxidation of roGFP2 via GRXS15 K_{83}/A is not based on an improvement of the complementary surfaces for the respective protein and interacting partner.

Interestingly, enzymatically active and inactive GRXs, mainly CGFS GRXs, cluster in two clades (Figure 44 and Figure 12C). The K_{83} of GRXS15 is highly conserved in all GRXs or replaced by other positively charged amino acids as in case of *E. coli* Grx1. This lysine, however, in inactive isoforms is separated from the catalytic cysteine residue (C_{91} in case of GRXS15) in the primary sequence by five amino acids forming an additional loop (Figure 44).

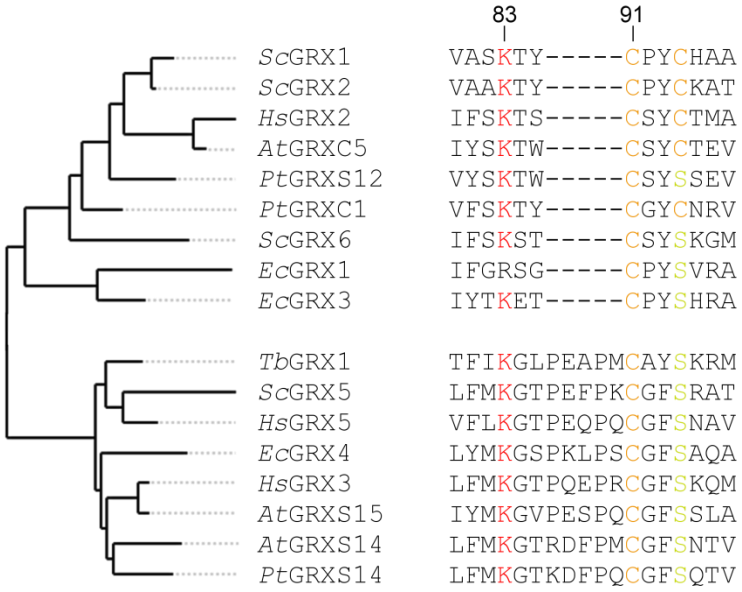

Figure 44: A phylogenetic tree of crystallised GRXs and GRXS15. The tree was calculated at phylogeny.fr (Dereeper et al., 2008). Enumeration of the amino acids is based on GRXS15.

This additional loop in CGFS GRXs might stabilise the incorporation of GSH as cofactor and the coordination of the ISC. In the absence of the cluster, the CGFS GRXs can still be glutathionylated and might slowly transfer the glutathione moiety to the reduced cysteine residue of roGFP2. Concerning the conserved lysine, it is assumed that in enzymatically active GRXs the positively charged lysine residue stabilises the thiolate of the catalytic cysteine resulting in the low pK_a. Lysine mutants of human GLRX1 or yeast Grx7p showed indeed reduced catalytic rates (Begas et al., 2017; Jao et al., 2006). Moreover, yeast Grx8p, which is also lacking the additional loop but has an alanine residue at the lysine position, was shown to have a very low activity in standard assays (Eckers et al., 2009; Tang et al., 2014). In contrast, in *E. coli* Grx3 mutants truncation of the functional group resulted in a more efficient enzyme suggesting an important role of the lysine residue as a gatekeeper to modify the reactivity (Shekhter et al., 2009). Future studies will reveal the necessity of the additional loop and the

conserved lysine, for example, to activate enzymatically inactive GRXs via loop deletion or *vice versa* insertion of the loop in enzymatically active GRXs for inactivation.

5. References

Aller, I., Rouhier, N., and Meyer, A.J. (2013). Development of roGFP2-derived redox probes for measurement of the glutathione redox potential in the cytosol of severely glutathione-deficient *rml1* seedlings. Frontiers in Plant Science *4*, 506.

Araujo, W.L., Ishizaki, K., Nunes-Nesi, A., Larson, T.R., Tohge, T., Krahnert, I., Witt, S., Obata, T., Schauer, N., Graham, I.A., *et al.* (2010). Identification of the 2-hydroxyglutarate and isovaleryl-CoA dehydrogenases as alternative electron donors linking lysine catabolism to the electron transport chain of Arabidopsis mitochondria. The Plant Cell *22*, 1549-1563.

Arnal, N., Alban, C., Quadrado, M., Grandjean, O., and Mireau, H. (2006). The Arabidopsis Bio2 protein requires mitochondrial targeting for activity. Plant Molecular Biology *62*, 471-479.

Arnaud, N., Ravet, K., Borlotti, A., Touraine, B., Boucherez, J., Fizames, C., Briat, J.F., Cellier, F., and Gaymard, F. (2007). The iron-responsive element (IRE)/iron-regulatory protein 1 (IRP1)-cytosolic aconitase iron-regulatory switch does not operate in plants. Biochemical Journal *405*, 523-531.

Baker, I.I.P.R., Friederich, M.W., Swanson, M.A., Shaikh, T., Bhattacharya, K., Scharer, G.H., Aicher, J., Creadon-Swindell, G., Geiger, E., MacLean, K.N., *et al.* (2014). Variant non ketotic hyperglycinemia is caused by mutations in LIAS, BOLA3 and the novel gene GLRX5. Brain *137*, 366-379.

Balk, J., and Lobreaux, S. (2005). Biogenesis of iron-sulfur proteins in plants. Trends in Plant Science *10*, 324-331.

Balk, J., and Pilon, M. (2011). Ancient and essential: the assembly of iron-sulfur clusters in plants. Trends in Plant Science *16*, 218-226.

Balk, J., and Schaedler, T.A. (2014). Iron cofactor assembly in plants. Annual Review of Plant Biology *65*, 125-153.

Bandyopadhyay, S., Gama, F., Molina-Navarro, M.M., Gualberto, J.M., Claxton, R., Naik, S.G., Huynh, B.H., Herrero, E., Jacquot, J.P., Johnson, M.K., *et al.* (2008). Chloroplast monothiol glutaredoxins as scaffold proteins for the assembly and delivery of [2Fe-2S] clusters. The EMBO Journal *27*, 1122-1133.

Begas, P., Liedgens, L., Moseler, A., Meyer, A.J., and Deponte, M. (2017). Glutaredoxin catalysis requires two distinct glutathione interaction sites. Nature Communications *8*.

Begas, P., Staudacher, V., and Deponte, M. (2015). Systematic re-evaluation of the bis(2-hydroxyethyl) disulfide (HEDS) assay reveals an alternative mechanism and activity of glutaredoxins. Chemical Science *6*, 3788-3796.

Beinert, H. (2000). Iron-sulfur proteins: ancient structures, still full of surprises. Journal of Biological Inorganic Chemistry *5*, 2-15.

Beinert, H., Holm, R.H., and Münck, E. (1997). Iron-sulfur clusters: nature's modular, multipurpose structures. Science *277*, 653-659.

Belin, C., Bashandy, T., Cela, J., Delorme-Hinoux, V., Riondet, C., and Reichheld, J.P. (2015). A comprehensive study of thiol reduction gene expression under stress conditions in *Arabidopsis thaliana*. Plant, Cell & Environment *38*, 299-314.

Belli, G., Polaina, J., Tamarit, J., de la Torre, M.A., Rodríguez-Manzaneque, M.T., Ros, J., and Herrero, E. (2002). Structure-function analysis of yeast Grx5 monothiol glutaredoxin defines essential amino acids for the function of the protein. Journal of Biological Chemistry *277*, 37590-37596.

Bender, K.W., Wang, X., Cheng, G.B., Kim, H.S., Zielinski, R.E., and Huber, S.C. (2015). Glutaredoxin *At*GRXC2 catalyses inhibitory glutathionylation of Arabidopsis BRI1-associated receptor-like kinase 1 (BAK1) *in vitro*. Biochemical Journal *467*, 399-413.

Bernard, D.G., Cheng, Y., Zhao, Y., and Balk, J. (2009). An allelic mutant series of ATM3 reveals its key role in the biogenesis of cytosolic iron-sulfur proteins in Arabidopsis. Plant Physiology *151*, 590-602.

Berndt, C., Hudemann, C., Hanschmann, E., Axelsson, R., Holmgren, A., and Lillig, C. (2007). How does iron-sulfur cluster coordination regulate the activity of human glutaredoxin 2? Antioxidants & Redox Signaling *9*, 151-157.

Berndt, C., Schwenn, J.D., and Lillig, C.H. (2015). The specificity of thioredoxins and glutaredoxins is determined by electrostatic and geometric complementarity and not by redox potential. The FEBS Journal *282*, 110-110.

Binder, S. (2010). Branched-chain amino acid metabolism in *Arabidopsis thaliana*. Arabidopsis Book *8*, e0137.

Bittner, F. (2014). Molybdenum metabolism in plants and crosstalk to iron. Frontiers in Plant Science *5*, 28.

Björkman, O., and Demmig, B. (1987). Photon yield of O_2 evolution and chlorophyll fluorescence characteristics at 77 K among vascular plants of diverse origins. Planta *170*, 489-504.

Blanc, B., Gerez, C., and Ollagnier de Choudens, S. (2015). Assembly of Fe/S proteins in bacterial systems: Biochemistry of the bacterial ISC system. Biochimica et Biophysica Acta *6*, 13.

Booker, S.J., Cicchillo, R.M., and Grove, T.L. (2007). Self-sacrifice in radical S-adenosylmethionine proteins. Current Opinion in Chemical Biology *11*, 543-552.

Boyd, E.S., Thomas, K.M., Dai, Y.Y., Boyd, J.M., and Outten, F.W. (2014). Interplay between oxygen and Fe-S cluster biogenesis: Insights from the suf pathway. Biochemistry *53*, 5834-5847.

Brach, T., Soyk, S., Müller, C., Hinz, G., Hell, R., Brandizzi, F., and Meyer, A.J. (2009). Non-invasive topology analysis of membrane proteins in the secretory pathway. The Plant Journal *57*, 534-541.

Bradford, M.M. (1976). A rapid and sensitive method for the quantitation of microgram quantities of protein utilizing the principle of protein-dye binding. Analytical Biochemistry *72*, 248-254.

Browse, J., McCourt, P.J., and Somerville, C.R. (1986). Fatty acid composition of leaf lipids determined after combined digestion and fatty acid methyl ester formation from fresh tissue. Analytical Biochemistry *152*, 141-145.

Bushweller, J.H., Aslund, F., Wuthrich, K., and Holmgren, A. (1992). Structural and functional-characterization of the mutant *Escherichia coli* glutaredoxin (C14-]S) and its mixed disulfide with glutathione. Biochemistry *31*, 9288-9293.

Busi, M., Maliandi, M., Valdez, H., Clemente, M., Zabaleta, E., Araya, A., and Gomez-Casati, D. (2006). Deficiency of *Arabidopsis thaliana* frataxin alters activity of mitochondrial Fe-S proteins and induces oxidative stress. The Plant Journal *48*, 873-882.

Bych, K., Kerscher, S., Netz, D., Pierik, A., Zwicker, K., Huynen, M., Lill, R., Brandt, U., and Balk, J. (2008). The iron-sulphur protein Ind1 is required for effective complex I assembly. The EMBO Journal *27*, 1736-1746.

Cairns, N.G., Pasternak, M., Wachter, A., Cobbett, C.S., and Meyer, A.J. (2006). Maturation of Arabidopsis seeds is dependent on glutathione biosynthesis within the embryo. Plant Physiology *141*, 446-455.

Camaschella, C., Campanella, A., De Falco, L., Boschetto, L., Merlini, R., Silvestri, L., Levi, S., and Iolascon, A. (2007). The human counterpart of zebrafish shiraz shows sideroblastic-like microcytic anemia and iron overload. Blood *110*, 1353-1358.

Cameron, J.M., Janer, A., Levandovskiy, V., MacKay, N., Rouault, T.A., Tong, W.H., Ogilvie, I., Shoubridge, E.A., and Robinson, B.H. (2011). Mutations in iron-sulfur cluster scaffold genes NFU1 and BOLA3 cause a fatal deficiency of multiple respiratory chain and 2-oxoacid dehydrogenase enzymes. American Journal of Human Genetics *89*, 486-495.

Cannon, M.B., and Remington, S.J. (2006). Re-engineering redox-sensitive green fluorescent protein for improved response rate. Protein Science *15*, 45-57.

Chen, O.S., Crisp, R.J., Valachovic, M., Bard, M., Winge, D.R., and Kaplan, J. (2004). Transcription of the yeast iron regulon does not respond directly to iron but rather to iron-sulfur cluster biosynthesis. Journal of Biological Chemistry *279*, 29513-29518.

Cheng, N.-H., Liu, J.-Z., Brock, A., Nelson, R.S., and Hirschi, K.D. (2006). *At*GRXcp, an Arabidopsis chloroplastic glutaredoxin, is critical for protection against protein oxidative damage. Journal of Biological Chemistry *281*, 26280-26288.

Cheng, N.-H., Liu, J.-Z., Liu, X., Wu, Q., Thompson, S.M., Lin, J., Chang, J., Whitham, S.A., Park, S., Cohen, J.D., *et al.* (2011). Arabidopsis monothiol glutaredoxin, *At*GRXS17, is critical for temperature-dependent postembryonic growth and development via modulating auxin response. Journal of Biological Chemistry *286*, 20398-20406.

Cheng, N. (2008). *At*GRX4, an Arabidopsis chloroplastic monothiol glutaredoxin, is able to suppress yeast *grx5* mutant phenotypes and respond to oxidative stress. FEBS Letters *582*, 848-854.

Chew, O., Rudhe, C., Glaser, E., and Whelan, J. (2003a). Characterization of the targeting signal of dual-targeted pea glutathione reductase. Plant Molecular Biology *53*, 341-356.

Chew, O., Whelan, J., and Millar, A.H. (2003b). Molecular definition of the ascorbate-glutathione cycle in Arabidopsis mitochondria reveals dual targeting of antioxidant defenses in plants. Journal of Biological Chemistry *278*, 46869-46877.

Clough, S.J., and Bent, A.F. (1998). Floral dip: a simplified method for Agrobacterium-mediated transformation of *Arabidopsis thaliana*. The Plant Journal *16*, 735-743.

Consortium, A.I.M. (2011). Evidence for network evolution in an Arabidopsis interactome map. Science *333*, 601-607.

Cook, J., Kondapalli, K., Rawat, S., Childs, W., Murugesan, Y., Dancis, A., and Stemmler, T. (2010). Molecular details of the yeast frataxin-Isu1 interaction during mitochondrial Fe-S cluster assembly. Biochemistry *49*, 8756-8765.

Couturier, J., Jacquot, J., and Rouhier, N. (2009). Evolution and diversity of glutaredoxins in photosynthetic organisms. Cellular and Molecular Life Sciences *66*, 2539-2557.

Couturier, J., Jacquot, J.P., and Rouhier, N. (2013). Toward a refined classification of class I dithiol glutaredoxins from poplar: biochemical basis for the definition of two subclasses. Frontiers in Plant Science *4*.

Couturier, J., Ströher, E., Albetel, A.-N., Roret, T., Muthuramalingam, M., Tarrago, L., Seidel, T., Tsan, P., Jacquot, J.-P., Johnson, M.K., *et al.* (2011). Arabidopsis chloroplastic glutaredoxin C5 as a model to explore molecular determinants for iron-sulfur cluster binding into glutaredoxins. Journal of Biological Chemistry *286*, 27515-27527.

Couturier, J., Wu, H.C., Dhalleine, T., Pegeot, H., Sudre, D., Gualberto, J.M., Jacquot, J.P., Gaymard, F., Vignols, F., and Rouhier, N. (2014). Monothiol glutaredoxin BolA interactions: redox control of *Arabidopsis thaliana* BolA2 and SufE1. Molecular Plant *7*, 187-205.

Crack, J.C., Green, J., Thomson, A.J., and Le Brun, N.E. (2014). Iron-sulfur clusters as biological sensors: the chemistry of reactions with molecular oxygen and nitric oxide. Accounts of Chemical Research *47*, 3196-3205.

Curtis, M.D., and Grossniklaus, U. (2003). A Gateway cloning vector set for high-throughput functional analysis of genes *in planta*. Plant Physiology *133*, 462-469.

De Col, V., Fuchs, P., Nietzel, T., Elsässer, M., Voon, C.P., Candeo, A., Seeliger, I., Fricker, M., Grefen, C., Møller, I.M., *et al.* (2017). ATP sensing in living plant cells reveals tissue gradients and stress dynamics of energy physiology. bioRxiv.

Deponte, M. (2013). Glutathione catalysis and the reaction mechanisms of glutathione-dependent enzymes. Biochimica et Biophysica Acta *1830*, 3217-3266.

Deponte, M., and Lillig, C.H. (2015). Enzymatic control of cysteinyl thiol switches in proteins. Biological Chemistry *396*, 401-413.

Dereeper, A., Guignon, V., Blanc, G., Audic, S., Buffet, S., Chevenet, F., Dufayard, J.F., Guindon, S., Lefort, V., Lescot, M., *et al.* (2008). Phylogeny.fr: robust phylogenetic analysis for the non-specialist. Nucleic Acids Research *36*, 19.

Dooley, C.T., Dore, T.M., Hanson, G.T., Jackson, W.C., Remington, S.J., and Tsien, R.Y. (2004). Imaging dynamic redox changes in mammalian cells with green fluorescent protein indicators. Journal of Biological Chemistry *279*, 22284-22293.

Eckers, E., Bien, M., Stroobant, V., Herrmann, J.M., and Deponte, M. (2009). Biochemical characterization of dithiol glutaredoxin 8 from Saccharomyces cerevisiae: the catalytic redox mechanism redux. Biochemistry *48*, 1410-1423.

Edgar, R.C. (2004). MUSCLE: multiple sequence alignment with high accuracy and high throughput. Nucleic Acids Research *32*, 1792-1797.

Edwards, K., Johnstone, C., and Thompson, C. (1991). A simple and rapid method for the preparation of plant genomic DNA for PCR analysis. Nucleic Acids Research *19*, 1349.

Eklund, H., Ingelman, M., Soderberg, B.O., Uhlin, T., Nordlund, P., Nikkola, M., Sonnerstam, U., Joelson, T., and Petratos, K. (1992). Structure of oxidized bacteriophage-T4 Glutaredoxin (Thioredoxin) - refinement of native and mutant proteins. Journal of Molecular Biology *228*, 596-618.

Emanuelsson, O., Nielsen, H., Brunak, S., and von Heijne, G. (2000). Predicting subcellular localization of proteins based on their N-terminal amino acid sequence. Journal of Molecular Biology *300*, 1005-1016.

Escobar, M.A., Geisler, D.A., and Rasmusson, A.G. (2006). Reorganization of the alternative pathways of the Arabidopsis respiratory chain by nitrogen supply: opposing effects of ammonium and nitrate. The Plant Journal *45*, 775-788.

Fenton, H.J.H. (1894). LXXIII.-Oxidation of tartaric acid in presence of iron. Journal of the Chemical Society, Transactions *65*, 899-910.

Fernandes, A.P., Fladvad, M., Berndt, C., Andresen, C., Lillig, C.H., Neubauer, P., Sunnerhagen, M., Holmgren, A., and Vlamis-Gardikas, A. (2005). A novel monothiol glutaredoxin (Grx4) from *Escherichia coli* can serve as a substrate for thioredoxin reductase. Journal of Biological Chemistry *280*, 24544-24552.

Frazzon, A.P., Ramirez, M.V., Warek, U., Balk, J., Frazzon, J., Dean, D.R., and Winkel, B.S. (2007). Functional analysis of Arabidopsis genes involved in mitochondrial iron-sulfur cluster assembly. Plant Molecular Biology *64*, 225-240.

Frey, A.G., Palenchar, D.J., Wildemann, J.D., and Philpott, C.C. (2016). A Glutaredoxin-BolA complex serves as an iron-sulfur cluster chaperone for the cytosolic cluster assembly machinery. Journal of Biological Chemistry *12*, 744946.

Fujiki, Y., Ito, M., Nishida, I., and Watanabe, A. (2001). Leucine and its keto acid enhance the coordinated expression of genes for branched-chain amino acid catabolism in Arabidopsis under sugar starvation. FEBS Letters *499*, 161-165.

Gan, Z.R., Polokoff, M.A., Jacobs, J.W., and Sardana, M.K. (1990). Complete amino acid sequence of yeast thioltransferase (glutaredoxin). Biochemical and Biophysical Research Communications *168*, 944-951.

Gelling, C., Dawes, I.W., Richhardt, N., Lill, R., and Mühlenhoff, U. (2008). Mitochondrial Iba57p is required for Fe/S cluster formation on aconitase and activation of radical SAM enzymes. Molecular and Cellular Biology *28*, 1851-1861.

Gerber, J., Mühlenhoff, U., and Lill, R. (2003). An interaction between frataxin and Isu1/Nfs1 that is crucial for Fe/S cluster synthesis on Isu1. EMBO Reports *4*, 906-911.

Gietz, R.D., and Schiestl, R.H. (2007). High-efficiency yeast transformation using the LiAc/SS carrier DNA/PEG method. Nature Protocols *2*, 31-34.

Giles, N.M., Watts, A.B., Giles, G.I., Fry, F.H., Littlechild, J.A., and Jacob, C. (2003). Metal and redox modulation of cysteine protein function. Chemistry & Biology *10*, 677-693.

Guo, Y., Huang, C., Xie, Y., Song, F., and Zhou, X. (2010). A tomato glutaredoxin gene SlGRX1 regulates plant responses to oxidative, drought and salt stresses. Planta *232*, 1499-1509.

Gupta, R., and Luan, S. (2003). Redox control of protein tyrosine phosphatases and mitogen-activated protein kinases in plants. Plant Physiology *132*, 1149-1152.

Gutsche, N., Thurow, C., Zachgo, S., and Gatz, C. (2015). Plant-specific CC-type glutaredoxins: functions in developmental processes and stress responses. Biological Chemistry *396*, 495-509.

Gutscher, M., Pauleau, A., Marty, L., Brach, T., Wabnitz, G., Samstag, Y., Meyer, A.J., and Dick, T. (2008). Real-time imaging of the intracellular glutathione redox potential. Nature Methods *5*, 553-559.

Hagen, K.S., Reynolds, J.G., and Holm, R.H. (1981). Definition of reaction sequences resulting in self-assembly of $[Fe_4S_4(SR)_4]^{2-}$ clusters from simple reactants. Journal of the American Chemical Society *103*, 4054-4063.

Hanschmann, E.M., Godoy, J.R., Berndt, C., Hudemann, C., and Lillig, C.H. (2013). Thioredoxins, glutaredoxins, and peroxiredoxins-molecular mechanisms and health significance: from cofactors to antioxidants to redox signaling. Antioxidants & Redox Signaling *19*, 1539-1605.

Hanson, G.T., Aggeler, R., Oglesbee, D., Cannon, M., Capaldi, R.A., Tsien, R.Y., and Remington, S.J. (2004). Investigating mitochondrial redox potential with redox-sensitive green fluorescent protein indicators. Journal of Biological Chemistry *279*, 13044-13053.

Hänzelmann, P., Hernandez, H.L., Menzel, C., Garcia-Serres, R., Huynh, B.H., Johnson, M.K., Mendel, R.R., and Schindelin, H. (2004). Characterization of MOCS1A, an oxygen-sensitive iron-sulfur protein involved in human molybdenum cofactor biosynthesis. Journal of Biological Chemistry *279*, 34721-34732.

Haunhorst, P., Berndt, C., Eitner, S., Godoy, J.R., and Lillig, C.H. (2010). Characterization of the human monothiol glutaredoxin 3 (PICOT) as iron-sulfur protein. Biochemical and Biophysical Research Communications *394*, 372-376.

Heazlewood, J.L., Howell, K.A., and Millar, A.H. (2003). Mitochondrial complex I from Arabidopsis and rice: orthologs of mammalian and fungal components coupled with plant-specific subunits. Biochimica et Biophysica Acta *10*, 159-169.

Heazlewood, J.L., Verboom, R.E., Tonti-Filippini, J., Small, I., and Millar, A.H. (2007). SUBA: the Arabidopsis Subcellular Database. Nucleic Acids Research *35*, D213-218.

Heineke, D., Bykova, N., Gardestrom, P., and Bauwe, H. (2001). Metabolic response of potato plants to an antisense reduction of the P-protein of glycine decarboxylase. Planta *212*, 880-887.

Hesberg, C., Hansch, R., Mendel, R.R., and Bittner, F. (2004). Tandem orientation of duplicated xanthine dehydrogenase genes from *Arabidopsis thaliana*: differential gene expression and enzyme activities. Journal of Biological Chemistry *279*, 13547-13554.

Hinks, J.A., Evans, M.C., De Miguel, Y., Sartori, A.A., Jiricny, J., and Pearl, L.H. (2002). An iron-sulfur cluster in the family 4 uracil-DNA glycosylases. Journal of Biological Chemistry *277*, 16936-16940.

Hoffmann, C., Plocharski, B., Haferkamp, I., Leroch, M., Ewald, R., Bauwe, H., Riemer, J., Herrmann, J.M., and Neuhaus, H.E. (2013). From endoplasmic reticulum to mitochondria: absence of the Arabidopsis ATP Antiporter Endoplasmic Reticulum Adenylate Transporter1 perturbs photorespiration. The Plant Cell *25*, 2647-2660.

Holmgren, A. (1976). Hydrogen donor system for *Escherichia coli* ribonucleoside-diphosphate reductase dependent upon glutathione. Proceedings of the National Academy of Sciences of the United States of America *73*, 2275-2279.

Holmgren, A. (1979). Glutathione-dependent synthesis of deoxyribonucleotides - purification and characterization of glutaredoxin from *Escherichia coli*. Journal of Biological Chemistry *254*, 3664-3671.

Holmgren, A. (1989). Thioredoxin and glutaredoxin systems. Journal of Biological Chemistry *264*, 13963-13966.

Hooks, M.A., Allwood, J.W., Harrison, J.K.D., Kopka, J., Erban, A., Goodacre, R., and Balk, J. (2014). Selective induction and subcellular distribution of ACONITASE 3 reveal the importance of cytosolic citrate metabolism during lipid mobilization in Arabidopsis. Biochemical Journal *463*, 309-317.

Hopper, S., Johnson, R.S., Vath, J.E., and Biemann, K. (1989). Glutaredoxin from rabbit bone marrow. Purification, characterization, and amino acid sequence determined by tandem mass spectrometry. Journal of Biological Chemistry *264*, 20438-20447.

Huang, M.S., Friso, G., Nishimura, K., Qu, X., Olinares, P.D.B., Majeran, W., Sun, Q., and van Wijk, K.J. (2013). Construction of plastid reference proteomes for maize and Arabidopsis and evaluation of their orthologous relationships; The concept of orthoproteomics. Journal of Proteome Research *12*, 491-504.

Huang, S., Van Aken, O., Schwarzländer, M., Belt, K., and Millar, A.H. (2016). The roles of mitochondrial reactive oxygen species in cellular signaling and stress response in plants. Plant Physiology *171*, 1551-1559.

Hung, Y., Albeck, J., Tantama, M., and Yellen, G. (2011). Imaging cytosolic NADH-NAD^+ redox state with a genetically encoded fluorescent biosensor. Cell Metabolism *14*, 545-554.

Huynen, M.A., Spronk, C.A., Gabaldon, T., and Snel, B. (2005). Combining data from genomes, Y2H and 3D structure indicates that BolA is a reductase interacting with a glutaredoxin. FEBS Letters *579*, 591-596.

Igamberdiev, A.U., Bykova, N.V., Lea, P.J., and Gardeström, P. (2001). The role of photorespiration in redox and energy balance of photosynthetic plant cells: A study with a barley mutant deficient in glycine decarboxylase. Physiologia Plantarum *111*, 427-438.

Imamura, H., Huynh Nhat, K.P., Togawa, H., Saito, K., Iino, R., Kato-Yamada, Y., Nagai, T., and Noji, H. (2009). Visualization of ATP levels inside single living cells with fluorescence resonance energy transfer-based genetically encoded indicators. Proceedings of the National Academy of Sciences of the United States of America *106*, 15651-15656.

Imsande, J. (1999). Iron-sulfur clusters: Formation, perturbation, and physiological functions. Plant Physiology and Biochemistry *37*, 87-97.

Inigo, S., Nagels Durand, A., Ritter, A., Le Gall, S., Termathe, M., Klassen, R., Tohge, T., De Coninck, B., Van Leene, J., De Clercq, R., *et al.* (2016). Glutaredoxin GRXS17 associates with the cytosolic iron-sulfur cluster assembly pathway. Plant Physiology *172*, 858-873.

Isakov, N., Witte, S., and Altman, A. (2000). PICOT-HD: a highly conserved protein domain that is often associated with thioredoxin and glutaredoxin modules. Trends in Biochemical Sciences *25*, 537-539.

Iwema, T., Picciocchi, A., Traore, D.A.K., Ferrer, J.L., Chauvat, F., and Jacquamet, L. (2009). Structural basis for delivery of the intact [Fe2S2] cluster by monothiol glutaredoxin. Biochemistry *48*, 6041-6043.

Jacobson, M.R., Brigle, K.E., Bennett, L.T., Setterquist, R.A., Wilson, M.S., Cash, V.L., Beynon, J., Newton, W.E., and Dean, D.R. (1989). Physical and genetic map of the major nif gene cluster from *Azotobacter vinelandii*. Journal of Bacteriology *171*, 1017-1027.

Jao, S., English Ospina, S., Berdis, A., Starke, D., Post, C., and Mieyal, J. (2006). Computational and mutational analysis of human glutaredoxin (thioltransferase): probing the molecular basis of the low pK_a of cysteine 22 and its role in catalysis. Biochemistry *45*, 4785-4796.

Johansson, C., Kavanagh, K.L., Gileadi, O., and Oppermann, U. (2007). Reversible sequestration of active site cysteines in a 2Fe-2S-bridged dimer provides a mechanism for glutaredoxin 2 regulation in human mitochondria. Journal of Biological Chemistry *282*, 3077-3082.

Johansson, C., Roos, A.K., Montano, S.J., Sengupta, R., Filippakopoulos, P., Guo, K., von Delft, F., Holmgren, A., Oppermann, U., and Kavanagh, K.L. (2011). The crystal structure of human GLRX5: iron-sulfur cluster co-ordination, tetrameric assembly and monomer activity. Biochemical Journal *433*, 303-311.

Johnson, D.C., Dean, D.R., Smith, A.D., and Johnson, M.K. (2005). Structure, function, and formation of biological iron-sulfur clusters. Annual Review of Biochemistry *74*, 247-281.

Journet, E.-P., Neuburger, M., and Douce, R. (1981). Role of glutamate-oxaloacetate transaminase and malate dehydrogenase in the regeneration of NAD^+ for glycine oxidation by spinach leaf mitochondria. Plant Physiology *67*, 467-469.

Karimi, M., Inze, D., and Depicker, A. (2002). GATEWAY vectors for Agrobacterium-mediated plant transformation. Trends in Plant Sciences *7*, 193-195.

Kasimova, M.R., Grigiene, J., Krab, K., Hagedorn, P.H., Flyvbjerg, H., Andersen, P.E., and Møller, I.M. (2006). The free NADH concentration is kept constant in plant mitochondria under different metabolic conditions. The Plant Cell *18*, 688-698.

Kataya, A.R., and Reumann, S. (2010). Arabidopsis glutathione reductase 1 is dually targeted to peroxisomes and the cytosol. Plant Signaling & Behavior *5*, 171-175.

Kelley, L.A., Mezulis, S., Yates, C.M., Wass, M.N., and Sternberg, M.J.E. (2015). The Phyre2 web portal for protein modeling, prediction and analysis. Nature Protocols *10*, 845-858.

Kelliher, T., and Walbot, V. (2012). Hypoxia triggers meiotic fate acquisition in maize. Science *337*, 345-348.

Kennedy, M.C., Emptage, M.H., Dreyer, J.L., and Beinert, H. (1983). The role of iron in the activation-inactivation of aconitase. Journal of Biological Chemistry *258*, 1098-1105.

Kispal, G., Csere, P., Guiard, B., and Lill, R. (1997). The ABC transporter Atm1p is required for mitochondrial iron homeostasis. FEBS Letters *418*, 346-350.

Klodmann, J., Senkler, M., Rode, C., and Braun, H.-P. (2011). Defining the protein complex proteome of plant mitochondria. Plant Physiology *157*, 587-598.

Knüsting, J., Riondet, C., Maria, C., Kruse, I., Becuwe, N., König, N., Berndt, C., Tourrette, S., Guilleminot-Montoya, J., Herrero, E., *et al.* (2015). Arabidopsis glutaredoxin S17 and its partner NF-YC11/NC2α contribute to maintenance of the shoot apical meristem under long-day photoperiod. Plant Physiology *167*, 1643-1658.

Koshiba, T., Saito, E., Ono, N., Yamamoto, N., and Sato, M. (1996). Purification and properties of flavin- and molybdenum-containing aldehyde oxidase from coleoptiles of maize. Plant Physiology *110*, 781-789.

Krebs, M., Beyhl, D., Gorlich, E., Al-Rasheid, K.A.S., Marten, I., Stierhof, Y.D., Hedrich, R., and Schumacher, K. (2010). Arabidopsis V-ATPase activity at the tonoplast is required for efficient nutrient storage but not for sodium accumulation. Proceedings of the National Academy of Sciences of the United States of America *107*, 3251-3256.

Krömer, S. (1995). Respiration during photosynthesis. Annual Review of Plant Biology *46*, 45-70.

Krömer, S., and Heldt, H.W. (1991). Respiration of pea leaf mitochondria and redox transfer between the mitochondrial and extramitochondrial compartment. Biochimica et Biophysica Acta - Bioenergetics *1057*, 42-50.

La Camera, S., L'Haridon, F., Astier, J., Zander, M., Abou-Mansour, E., Page, G., Thurow, C., Wendehenne, D., Gatz, C., Metraux, J.P., *et al.* (2011). The glutaredoxin ATGRXS13 is required to facilitate *Botrytis cinerea* infection of *Arabidopsis thaliana* plants. The Plant Journal *68*, 507-519.

Laemmli, U.K. (1970). Cleavage of structural proteins during the assembly of the head of bacteriophage T4. Nature *227*, 680-685.

Lamesch, P., Berardini, T.Z., Li, D., Swarbreck, D., Wilks, C., Sasidharan, R., Muller, R., Dreher, K., Alexander, D.L., Garcia-Hernandez, M., *et al.* (2012). The Arabidopsis Information Resource (TAIR): improved gene annotation and new tools. Nucleic Acids Research *40*, D1202-D1210.

Lee, C.P., Eubel, H., and Millar, A.H. (2010). Diurnal changes in mitochondrial function reveal daily optimization of light and dark respiratory metabolism in Arabidopsis. Molecular & Cellular Proteomics *9*, 2125-2139.

Lemaire, S.D. (2004). The glutaredoxin family in oxygenic photosynthetic organisms. Photosynthesis Research *79*, 305-318.

Leon, S., Touraine, B., Briat, J.F., and Lobreaux, S. (2005). Mitochondrial localization of *Arabidopsis thaliana* Isu Fe-S scaffold proteins. FEBS Letters *579*, 1930-1934.

Leon, S., Touraine, B., Ribot, C., Briat, J.F., and Lobreaux, S. (2003). Iron-sulphur cluster assembly in plants: distinct NFU proteins in mitochondria and plastids from *Arabidopsis thaliana*. Biochemical Journal *371*, 823-830.

Li, H., Mapolelo, D.T., Dingra, N.N., Naik, S.G., Lees, N.S., Hoffman, B.M., Riggs-Gelasco, P.J., Huynh, B.H., Johnson, M.K., and Outten, C.E. (2009a). The yeast iron regulatory proteins Grx3/4 and Fra2 form heterodimeric complexes containing a [2Fe-2S] cluster with cysteinyl and histidyl ligation. Biochemistry *48*, 9569-9581.

Li, S., Lauri, A., Ziemann, M., Busch, A., Bhave, M., and Zachgo, S. (2009b). Nuclear activity of ROXY1, a glutaredoxin interacting with TGA factors, is required for petal development in *Arabidopsis thaliana*. The Plant Cell *21*, 429-441.

Li, W.F., Yu, J., Ma, X.X., Teng, Y.B., Luo, M., Tang, Y.J., and Zhou, C.Z. (2010). Structural basis for the different activities of yeast Grx1 and Grx2. Biochimica Et Biophysica Acta-Proteins and Proteomics *1804*, 1542-1547.

Lill, R., Hoffmann, B., Molik, S., Pierik, A., Rietzschel, N., Stehling, O., Uzarska, M., Webert, H., Wilbrecht, C., and Mühlenhoff, U. (2012). The role of mitochondria in cellular iron-sulfur protein biogenesis and iron metabolism. Biochimica et Biophysica Acta *1823*, 1491-1508.

Lill, R., and Kispal, G. (2000). Maturation of cellular Fe-S proteins: an essential function of mitochondria. Trends in Biochemical Sciences *25*, 352-356.

Lill, R., Srinivasan, V., and Mühlenhoff, U. (2014). The role of mitochondria in cytosolic-nuclear iron-sulfur protein biogenesis and in cellular iron regulation. Current Opinion in Microbiology *22C*, 111-119.

Lillig, C.H., Berndt, C., Vergnolle, O., Lonn, M.E., Hudemann, C., Bill, E., and Holmgren, A. (2005). Characterization of human glutaredoxin 2 as iron-sulfur protein: a possible role as redox sensor. Proceedings of the National Academy of Sciences of the United States of America *102*, 8168-8173.

Liu, G., Wang, Y., Anderson, G.J., Camaschella, C., Chang, Y., and Nie, G. (2016). Functional analysis of *GLRX5* mutants reveals distinct functionalities of GLRX5 protein. Journal of Cellular Biochemistry *117*, 207-217.

Liu, X., Liu, S., Feng, Y., Liu, J.-Z., Chen, Y., Pham, K., Deng, H., Hirschi, K.D., Wang, X., and Cheng, N. (2013). Structural insights into the N-terminal GIY-YIG endonuclease activity of Arabidopsis glutaredoxin *At*GRXS16 in chloroplasts. Proceedings of the National Academy of Sciences of the United States of America *110*, 9565-9570.

Lundberg, M., Johansson, C., Chandra, J., Enoksson, M., Jacobsson, G., Ljung, J., Johansson, M., and Holmgren, A. (2001). Cloning and expression of a novel human glutaredoxin (Grx2) with mitochondrial and nuclear isoforms. Journal of Biological Chemistry *276*, 26269-26275.

Lyons, T.W., Reinhard, C.T., and Planavsky, N.J. (2014). The rise of oxygen in Earth's early ocean and atmosphere. Nature *506*, 307-315.

Marty, L., Siala, W., Schwarzländer, M., Fricker, M.D., Wirtz, M., Sweetlove, L.J., Meyer, Y., Meyer, A.J., Reichheld, J.-P., and Hell, R. (2009). The NADPH-dependent thioredoxin system constitutes a functional backup for cytosolic glutathione reductase in Arabidopsis. Proceedings of the National Academy of Sciences of the United States of America *106*, 9109-9114.

Meinhard, M., and Grill, E. (2001). Hydrogen peroxide is a regulator of ABI1, a protein phosphatase 2C from Arabidopsis. FEBS Letters *508*, 443-446.

Mesecke, N., Spang, A., Deponte, M., and Herrmann, J.M. (2008). A novel group of glutaredoxins in the cis-Golgi critical for oxidative stress resistance. Molecular Biology of the Cell *19*, 2673-2680.

Meyer, A.J., Brach, T., Marty, L., Kreye, S., Rouhier, N., Jacquot, J.-P., and Hell, R. (2007). Redox-sensitive GFP in *Arabidopsis thaliana* is a quantitative biosensor for the redox potential of the cellular glutathione redox buffer. The Plant Journal *52*, 973-986.

Meyer, Y., Belin, C., Delorme-Hinoux, V., Reichheld, J.P., and Riondet, C. (2012). Thioredoxin and glutaredoxin systems in plants: molecular mechanisms, crosstalks, and functional significance. Antioxidants & Redox Signaling *17*, 1124-1160.

Miseta, A., and Csutora, P. (2000). Relationship between the occurrence of cysteine in proteins and the complexity of organisms. Molecular Biology and Evolution *17*, 1232-1239.

Mittler, R., Vanderauwera, S., Gollery, M., and Van Breusegem, F. (2004). Reactive oxygen gene network of plants. Trends in Plant Science *9*, 490-498.

Molina, M.M., Belli, G., de la Torre, M.A., Rodriguez-Manzaneque, M.T., and Herrero, E. (2004). Nuclear monothiol glutaredoxins of *Saccharomyces cerevisiae* can function as mitochondrial glutaredoxins. Journal of Biological Chemistry *279*, 51923-51930.

Møller, I.M. (2001). Plant mitochondria and oxidative stress: electron transport, NADPH turnover, and metabolism of reactive oxygen species. Annual Review of Plant Physiology and Plant Molecular Biology *52*, 561-591.

Møller, I.M., Jensen, P.E., and Hansson, A. (2007). Oxidative modifications to cellular components in plants. Annual Review of Plant Biology *58*, 459-481.

Moseler, A., Aller, I., Wagner, S., Nietzel, T., Przybyla-Toscano, J., Mühlenhoff, U., Lill, R., Berndt, C., Rouhier, N., Schwarzländer, M., *et al.* (2015). The mitochondrial monothiol glutaredoxin S15 is essential for iron-sulfur protein maturation in *Arabidopsis thaliana*. Proceedings of the National Academy of Sciences of the United States of America *112*, 13735-13740.

Moulis, J.M., Davasse, V., Golinelli, M.P., Meyer, J., and Quinkal, I. (1996). The coordination sphere of iron-sulfur clusters: lessons from site-directed mutagenesis experiments. Journal of Biological Inorganic Chemistry *1*, 2-14.

Mühlenhoff, U., Gerber, J., Richhardt, N., and Lill, R. (2003). Components involved in assembly and dislocation of iron-sulfur clusters on the scaffold protein Isu1p. The EMBO Journal *22*, 4815-4825.

Mühlenhoff, U., Molik, S., Godoy, J., Uzarska, M., Richter, N., Seubert, A., Zhang, Y., Stubbe, J., Pierrel, F., Herrero, E., *et al.* (2010). Cytosolic monothiol glutaredoxins function in intracellular iron sensing and trafficking via their bound iron-sulfur cluster. Cell Metabolism *12*, 373-385.

Mühlenhoff, U., Richter, N., Pines, O., Pierik, A.J., and Lill, R. (2011). Specialized function of yeast Isa1 and Isa2 proteins in the maturation of mitochondrial [4Fe-4S] proteins. Journal of Biological Chemistry *286*, 41205-41216.

Nachin, L., Loiseau, L., Expert, D., and Barras, F. (2003). SufC: an unorthodox cytoplasmic ABC/ATPase required for [Fe-S] biogenesis under oxidative stress. The EMBO Journal *22*, 427-437.

Navarre, D.A., Wendehenne, D., Durner, J., Noad, R., and Klessig, D.F. (2000). Nitric oxide modulates the activity of tobacco aconitase. Plant Physiology *122*, 573-582.

Navarro-Sastre, A., Tort, F., Stehling, O., Uzarska, M., Arranz, J., Del Toro, M., Labayru, M., Landa, J., Font, A., Garcia-Villoria, J., *et al.* (2011). A fatal mitochondrial disease is associated with defective NFU1 function in the maturation of a subset of mitochondrial Fe-S proteins. American Journal of Human Genetics *89*, 656-667.

Navrot, N., Gelhaye, E., Jacquot, J., and Rouhier, N. (2006). Identification of a new family of plant proteins loosely related to glutaredoxins with four CxxC motives. Photosynthesis Research *89*, 71-79.

Ndamukong, I., Abdallat, A., Thurow, C., Fode, B., Zander, M., Weigel, R., and Gatz, C. (2007). SA-inducible Arabidopsis glutaredoxin interacts with TGA factors and suppresses JA-responsive PDF1.2 transcription. The Plant Journal *50*, 128-139.

Noctor, G., and Foyer, C.H. (1998). Ascorbate and glutathione: keeping active oxygen under control. Annual Review of Plant Physiology and Plant Molecular Biology *49*, 249-279.

Noctor, G., Mhamdi, A., Chaouch, S., Han, Y., Neukermans, J., Marquez-Garcia, B., Queval, G., and Foyer, C. (2011). Glutathione in plants: an integrated overview. Plant, Cell & Environment *35*, 454–484.

Obermeyer, G., Fragner, L., Lang, V., and Weckwerth, W. (2013). Dynamic adaption of metabolic pathways during germination and growth of lily pollen tubes after inhibition of the electron transport chain. Plant Physiology *162*, 1822-1833.

Ojeda, L., Keller, G., Mühlenhoff, U., Rutherford, J.C., Lill, R., and Winge, D.R. (2006). Role of glutaredoxin-3 and glutaredoxin-4 in the iron regulation of the Aft1 transcriptional activator in *Saccharomyces cerevisiae*. Journal of Biological Chemistry *281*, 17661-17669.

Ollagnier-De Choudens, S., Sanakis, Y., Hewitson, K.S., Roach, P., Baldwin, J.E., Munck, E., and Fontecave, M. (2000). Iron-sulfur center of biotin synthase and lipoate synthase. Biochemistry *39*, 4165-4173.

Outten, F.W., Djaman, O., and Storz, G. (2004). A *suf* operon requirement for Fe-S cluster assembly during iron starvation in *Escherichia coli*. Molecular Microbiology *52*, 861-872.

Ozer, H.K., Dlouhy, A.C., Thornton, J.D., Hu, J., Liu, Y., Barycki, J.J., Balk, J., and Outten, C.E. (2015). Cytosolic Fe-S cluster protein maturation and iron regulation are independent of the mitochondrial Erv1/Mia40 import system. Journal of Biological Chemistry *290*, 27829-27840.

Padilla, C.A., Martinezgalisteo, E., Barcena, J.A., Spyrou, G., and Holmgren, A. (1995). Purification from placenta, amino-acid-sequence, structure comparisons and cDNA cloning of human glutaredoxin. European Journal of Biochemistry *227*, 27-34.

Pasternak, M., Lim, B., Wirtz, M., Hell, R., Cobbett, C.S., and Meyer, A.J. (2008). Restricting glutathione biosynthesis to the cytosol is sufficient for normal plant development. The Plant Journal *53*, 999-1012.

Patton, D.A., Schetter, A.L., Franzmann, L.H., Nelson, K., Ward, E.R., and Meinke, D.W. (1998). An embryo-defective mutant of arabidopsis disrupted in the final step of biotin synthesis. Plant Physiology *116*, 935-946.

Pedrajas, J.R., Porras, P., Martinez-Galisteo, E., Padilla, C.A., Miranda-Vizuete, A., and Barcena, J.A. (2002). Two isoforms of *Saccharomyces cerevisiae* glutaredoxin 2 are expressed *in vivo* and localize to different subcellular compartments. Biochemical Journal *364*, 617-623.

Peng, C., Uygun, S., Shiu, S.H., and Last, R.L. (2015). The impact of the branched-chain ketoacid dehydrogenase complex on amino acid homeostasis in Arabidopsis. Plant Physiology *169*, 1807-1820.

Peyret, P., Perez, P., and Alric, M. (1995). Structure, genomic organization, and expression of the *Arabidopsis thaliana* aconitase gene. Plant aconitase show significant homology with mammalian iron-responsive element-binding protein. Journal of Biological Chemistry *270*, 8131-8137.

Picciocchi, A., Saguez, C., Boussac, A., Cassier-Chauvat, C., and Chauvat, F. (2007). CGFS-type monothiol glutaredoxins from the cyanobacterium Synechocystis PCC6803 and other evolutionary distant model organisms possess a glutathione-ligated [2Fe-2S] cluster. Biochemistry *46*, 15018-15026.

Pujol-Carrion, N., Belli, G., Herrero, E., Nogues, A., and de la Torre-Ruiz, M.A. (2006). Glutaredoxins Grx3 and Grx4 regulate nuclear localisation of Aft1 and the oxidative stress response in *Saccharomyces cerevisiae*. Journal of Cell Science *119*, 4554-4564.

Riondet, C., Desouris, J., Montoya, J., Chartier, Y., Meyer, Y., and Reichheld, J. (2012). A dicotyledon-specific glutaredoxin GRXC1 family with dimer-dependent redox regulation is functionally redundant with GRXC2. Plant, Cell & Environment *35*, 360-373.

Robinson, A.C., Dean, D.R., and Burgess, B.K. (1987). Iron-molybdenum cofactor biosynthesis in *Azotobacter vinelandii* requires the iron protein of nitrogenase. Journal of Biological Chemistry *262*, 14327-14332.

Rodríguez-Manzaneque, M.T., Ros, J., Cabiscol, E., Sorribas, A., and Herrero, E. (1999). Grx5 glutaredoxin plays a central role in protection against protein oxidative damage in *Saccharomyces cerevisiae*. Molecular and Cellular Biology *19*, 8180-8190.

Rodríguez-Manzaneque, M.T., Tamarit, J., Belli, G., Ros, J., and Herrero, E. (2002). Grx5 is a mitochondrial glutaredoxin required for the activity of iron/sulfur enzymes. Molecular Biology of the Cell *13*, 1109-1121.

Roret, T., Tsan, P., Couturier, J., Zhang, B., Johnson, M.K., Rouhier, N., and Didierjean, C. (2014). Structural and spectroscopic insights into BolA-glutaredoxin complexes. Journal of Biological Chemistry *289*, 24588-24598.

Rouault, T.A. (2006). The role of iron regulatory proteins in mammalian iron homeostasis and disease. Nature Chemical Biology *2*, 406-414.

Rouhier, N., Couturier, J., and Jacquot, J.P. (2006). Genome-wide analysis of plant glutaredoxin systems. Journal of Experimental Botany *57*, 1685-1696.

Rouhier, N., Gelhaye, E., and Jacquot, J. (2004). Plant glutaredoxins: still mysterious reducing systems. Cellular and Molecular Life Sciences *61*, 1266-1277.

Rouhier, N., Lemaire, S.D., and Jacquot, J.-P. (2008). The role of glutathione in photosynthetic organisms: emerging functions for glutaredoxins and glutathionylation. Annual Review of Plant Biology *59*, 143.

Rounds, C.M., Hepler, P.K., Fuller, S.J., and Winship, L.J. (2010). Oscillatory growth in lily pollen tubes does not require aerobic energy metabolism. Plant Physiology *152*, 736-746.

Rutherford, J.C., Ojeda, L., Balk, J., Mühlenhoff, U., Lill, R., and Winge, D.R. (2005). Activation of the iron regulon by the yeast Aft1/Aft2 transcription factors depends on mitochondrial but not cytosolic iron-sulfur protein biogenesis. Journal of Biological Chemistry *280*, 10135-10140.

Salvato, F., Havelund, J.F., Chen, M.J., Rao, R.S.P., Rogowska-Wrzesinska, A., Jensen, O.N., Gang, D.R., Thelen, J.J., and Møller, I.M. (2014). The potato tuber mitochondrial proteome. Plant Physiology *164*, 637-653.

Schaedler, T.A., Thornton, J.D., Kruse, I., Schwarzländer, M., Meyer, A.J., van Veen, H.W., and Balk, J. (2014). A conserved mitochondrial ATP-binding cassette transporter exports glutathione polysulfide for cytosolic metal cofactor assembly. Journal of Biological Chemistry *289*, 23264-23274.

Scheible, W.-R., Lauerer, M., Schulze, E.-D., Caboche, M., and Stitt, M. (1997). Accumulation of nitrate in the shoot acts as a signal to regulate shoot-root allocation in tobacco. The Plant Journal *11*, 671-691.

Schneider, T., Dinkins, R., Robinson, K., Shellhammer, J., and Meinke, D.W. (1989). An embryo-lethal mutant of *Arabidopsis thaliana* is a biotin auxotroph. Developmental Biology *131*, 161-167.

Schwarzländer, M., and Finkemeier, I. (2013). Mitochondrial energy and redox signaling in plants. Antioxidants & Redox Signaling *18*, 2122-2144.

Schwarzländer, M., Fricker, M., Müller, C., Marty, L., Brach, T., Novak, T., Sweetlove, L., Hell, R., and Meyer, A.J. (2008). Confocal imaging of glutathione redox potential in living plant cells. Journal of Microscopy *231*, 299-316.

Sha, S., Minakuchi, K., Higaki, N., Sato, K., Ohtsuki, K., Kurata, A., Yoshikawa, H., Kotaru, M., Masumura, T., Ichihara, K.i., *et al.* (1997). Purification and characterization of glutaredoxin (Thioltransferase) from rice (*Oryza sativa* L.). Journal of Biochemistry *121*, 842-848.

Shaked, Z., Szajewski, R.P., and Whitesides, G.M. (1980). Rates of thiol-disulfide interchange reactions involving proteins and kinetic measurements of thiol pK_a values. Biochemistry *19*, 4156-4166.

Shanmugam, V., Tsednee, M., and Yeh, K. (2012). *Zinc tolerance induced by iron 1* reveals the importance of glutathione in the cross-homeostasis between zinc and iron in *Arabidopsis thaliana*. The Plant Journal *69*, 1006-1017.

Shekhter, T., Metanis, N., Dawson, P.E., and Keinan, E. (2009). A residue outside the active site CXXC motif regulates the catalytic efficiency of Glutaredoxin 3. Molecular Biosystems *6*, 241-248.

Shen, S.W., Li, X.F., Cullen, W.R., Weinfeld, M., and Le, X.C. (2013). Arsenic binding to proteins. Chemical Reviews *113*, 7769-7792.

Shenton, D., Perrone, G., Quinn, K.A., Dawes, I.W., and Grant, C.M. (2002). Regulation of protein S-thiolation by glutaredoxin 5 in the yeast *Saccharomyces cerevisiae*. Journal of Biological Chemistry *277*, 16853-16859.

Sipos, K., Lange, H., Fekete, Z., Ullmann, P., Lill, R., and Kispal, G. (2002). Maturation of cytosolic iron-sulfur proteins requires glutathione. Journal of Biological Chemistry *277*, 26944-26949.

Somerville, C., and Ogren, W. (1982). Isolation of photorespiration mutants in *Arabidopsis thaliana*. Methods in chloroplast molecular biology/M Edelman, RB Hallick, and NH Chua, editors.

Srinivasan, V., Pierik, A.J., and Lill, R. (2014). Crystal structures of nucleotide-free and glutathione-bound mitochondrial ABC transporter Atm1. Science *343*, 1137-1140.

Ströher, E., Grassl, J., Carrie, C., Fenske, R., Whelan, J., and Millar, A.H. (2016). Glutaredoxin S15 is involved in Fe-S cluster transfer in mitochondria influencing lipoic acid-dependent enzymes, plant growth and arsenic tolerance in Arabidopsis. Plant Physiology *170*, 1284-1299.

Ströher, E., and Millar, A. (2012). The biological roles of glutaredoxins. Biochemical Journal *446*, 333-348.

Takahashi, Y., and Tokumoto, U. (2002). A third bacterial system for the assembly of iron-sulfur clusters with homologs in archaea and plastids. Journal of Biological Chemistry *277*, 28380-28383.

Tamarit, J., Belli, G., Cabiscol, E., Herrero, E., and Ros, J. (2003). Biochemical characterization of yeast mitochondrial Grx5 monothiol glutaredoxin. Journal of Biological Chemistry *278*, 25745-25751.

Tamura, K., Stecher, G., Peterson, D., Filipski, A., and Kumar, S. (2013). MEGA6: molecular evolutionary genetics analysis version 6.0. Molecular Biology and Evolution *30*, 2725-2729.

Tang, Y., Zhang, J., Yu, J., Xu, L., Wu, J., Zhou, C.-Z., and Shi, Y. (2014). Structure-guided activity enhancement and catalytic mechanism of yeast Grx8. Biochemistry *53*, 2185-2196.

Taylor, N.L., Heazlewood, J.L., Day, D.A., and Millar, A.H. (2004). Lipoic acid-dependent oxidative catabolism of α-keto acids in mitochondria provides evidence for branched-chain amino acid catabolism in Arabidopsis. Plant Physiology *134*, 838-848.

Teschner, J., Lachmann, N., Schulze, J., Geisler, M., Selbach, K., Santamaria-Araujo, J., Balk, J., Mendel, R.R., and Bittner, F. (2010). A novel role for Arabidopsis mitochondrial ABC transporter ATM3 in molybdenum cofactor biosynthesis. The Plant Cell *22*, 468-480.

Thannickal, V.J. (2009). Oxygen in the evolution of complex life and the price we pay. American Journal of Respiratory Cell and Molecular Biology *40*, 507-510.

Thordal-Christensen, H., Zhang, Z., Wei, Y., and Collinge, D.B. (1997). Subcellular localization of H_2O_2 in plants. H_2O_2 accumulation in papillae and hypersensitive response during the barley-powdery mildew interaction. The Plant Journal *11*, 1187-1194.

Tse Sum Bui, B., Florentin, D., Fournier, F., Ploux, O., Méjean, A., and Marquet, A. (1998). Biotin synthase mechanism: on the origin of sulphur. FEBS Letters *440*, 226-230.

Turowski, V.R., Busi, M.V., and Gomez-Casati, D.F. (2012). Structural and functional studies of the mitochondrial cysteine desulfurase from *Arabidopsis thaliana*. Molecular Plant *5*, 1001-1010.

Uzarska, M.A. (2013). Mechanistic characterization of the late steps of mitochondrial iron-sulfur cluster protein maturation, Dissertation. Philipps-Universität Marburg.

Uzarska, M.A., Dutkiewicz, R., Freibert, S.-A., Lill, R., and Mühlenhoff, U. (2013). The mitochondrial Hsp70 chaperone Ssq1 facilitates Fe/S cluster transfer from Isu1 to Grx5 by complex formation. Molecular Biology of the Cell *24*, 1830-1841.

Uzarska, M.A., Nasta, V., Weiler, B.D., Spantgar, F., Ciofi-Baffoni, S., Saviello, M.R., Gonnelli, L., Mühlenhoff, U., Banci, L., and Lill, R. (2016). Mitochondrial Bol1 and Bol3 function as assembly factors for specific iron-sulfur proteins. eLife *5*, e16673.

Verniquet, F., Gaillard, J., Neuburger, M., and Douce, R. (1991). Rapid inactivation of plant aconitase by hydrogen peroxide. Biochemical Journal *276*, 643-648.

Vernoux, T., Wilson, R.C., Seeley, K.A., Reichheld, J.P., Muroy, S., Brown, S., Maughan, S.C., Cobbett, C.S., Van Montagu, M., Inze, D., *et al.* (2000). The ROOT MERISTEMLESS1/CADMIUM SENSITIVE2 gene defines a glutathione-dependent pathway involved in initiation and maintenance of cell division during postembryonic root development. The Plant Cell *12*, 97-110.

Wächtershäuser, G. (1992). Groundworks for an evolutionary biochemistry - the iron sulfur world. Progress in Biophysics & Molecular Biology *58*, 85-201.

Wagner, S., Behera, S., De Bortoli, S., Logan, D.C., Fuchs, P., Carraretto, L., Teardo, E., Cendron, L., Nietzel, T., Fussl, M., *et al.* (2015). The EF-hand Ca^{2+} binding protein MICU choreographs mitochondrial Ca^{2+} dynamics in Arabidopsis. The Plant Cell *27*, 3190-3212.

Walden, W.E., Selezneva, A.I., Dupuy, J., Volbeda, A., Fontecilla-Camps, J.C., Theil, E.C., and Volz, K. (2006). Structure of dual function iron regulatory protein 1 complexed with ferritin IRE-RNA. Science *314*, 1903-1908.

Waldron, K., Rutherford, J., Ford, D., and Robinson, N. (2009). Metalloproteins and metal sensing. Nature *460*, 823-830.

Waller, J.C., Ellens, K.W., Alvarez, S., Loizeau, K., Ravanel, S., and Hanson, A.D. (2012). Mitochondrial and plastidial COG0354 proteins have folate-dependent functions in iron-sulphur cluster metabolism. Journal of Experimental Botany *63*, 403-411.

Webert, H., Freibert, S.A., Gallo, A., Heidenreich, T., Linne, U., Amlacher, S., Hurt, E., Mühlenhoff, U., Banci, L., and Lill, R. (2014). Functional reconstitution of mitochondrial Fe/S cluster synthesis on Isu1 reveals the involvement of ferredoxin. Nature Communications *5*.

White, M.F. (2009). Structure, function and evolution of the XPD family of iron-sulfur-containing 5'-->3' DNA helicases. Biochemical Society Transactions *37*, 547-551.

Wilkinson, J.Q., and Crawford, N.M. (1993). Identification and characterization of a chlorate-resistant mutant of *Arabidopsis thaliana* with mutations in both nitrate reductase structural genes Nia1 and Nia2. Molecular & General Genetics *239*, 289-297.

Wingert, R.A., Galloway, J.L., Barut, B., Foott, H., Fraenkel, P., Axe, J.L., Weber, G.J., Dooley, K., Davidson, A.J., Schmid, B., *et al.* (2005). Deficiency of glutaredoxin 5 reveals Fe-S clusters are required for vertebrate haem synthesis. Nature *437*, 920-920.

Wu, Q., Lin, J., Liu, J., Wang, X., Lim, W., Oh, M., Park, J., Rajashekar, C., Whitham, S., Cheng, N., *et al.* (2012). Ectopic expression of Arabidopsis glutaredoxin *At*GRXS17 enhances thermotolerance in tomato. Plant Biotechnology Journal *10*, 945-955.

Wydro, M.M., Sharma, P., Foster, J.M., Bych, K., Meyer, E.H., and Balk, J. (2013). The evolutionarily conserved iron-sulfur protein INDH is required for complex I assembly and mitochondrial translation in Arabidopsis. The Plant Cell *25*, 4014-4027.

Xia, T., Bushweller, J., Sodano, P., Billeter, M., Bjornberg, O., Holmgren, A., and Wuthrich, K. (1992). NMR structure of oxidized *Escherichia coli* glutaredoxin: comparison with reduced *E. coli* glutaredoxin and functionally related proteins. Protein Science *1*, 310-321.

Xing, S., Lauri, A., and Zachgo, S. (2006). Redox regulation and flower development: a novel function for glutaredoxins. Plant Biology *8*, 547-555.

Xing, S., Rosso, M.G., and Zachgo, S. (2005). ROXY1, a member of the plant glutaredoxin family, is required for petal development in *Arabidopsis thaliana*. Development *132*, 1555-1565.

Xing, S., and Zachgo, S. (2008). ROXY1 and ROXY2, two Arabidopsis glutaredoxin genes, are required for anther development. The Plant Journal *53*, 790-801.

Xu, X.M., Adams, S., Chua, N.H., and Møller, S.G. (2005). *At*NAP1 represents an atypical SufB protein in Arabidopsis plastids. Journal of Biological Chemistry *280*, 6648-6654.

Xu, X.M., Lin, H., Latijnhouwers, M., and Møller, S.G. (2009). Dual localized *At*HscB involved in iron sulfur protein biogenesis in Arabidopsis. PLOS ONE *4*.

Xu, X.M., and Møller, S.G. (2006). *At*SufE is an essential activator of plastidic and mitochondrial desulfurases in Arabidopsis. The EMBO Journal *25*, 900-909.

Yamaguchi-Iwai, Y., Stearman, R., Dancis, A., and Klausner, R.D. (1996). Iron-regulated DNA binding by the AFT1 protein controls the iron regulon in yeast. The EMBO Journal *15*, 3377-3384.

Yang, M., Cobine, P.A., Molik, S., Naranuntarat, A., Lill, R., Winge, D.R., and Culotta, V.C. (2006). The effects of mitochondrial iron homeostasis on cofactor specificity of superoxide dismutase 2. The EMBO Journal *25*, 1775-1783.

Yasuno, R., and Wada, H. (2002). The biosynthetic pathway for lipoic acid is present in plastids and mitochondria in *Arabidopsis thaliana*. FEBS Letters *517*, 110-114.

Ye, H., Abdel-Ghany, S.E., Anderson, T.D., Pilon-Smits, E.A., and Pilon, M. (2006). CpSufE activates the cysteine desulfurase CpNifS for chloroplastic Fe-S cluster formation. Journal of Biological Chemistry *281*, 8958-8969.

Ye, H., Jeong, S.Y., Ghosh, M.C., Kovtunovych, G., Silvestri, L., Ortillo, D., Uchida, N., Tisdale, J., Camaschella, C., and Rouault, T.A. (2010). Glutaredoxin 5 deficiency causes sideroblastic anemia by specifically impairing heme biosynthesis and depleting cytosolic iron in human erythroblasts. Journal of Clinical Investigation *120*, 1749-1761.

Yu, H., Du, X., Zhang, F., Hu, Y., Liu, S., Jiang, X., Wang, G., and Liu, D. (2012). A mutation in the E2 subunit of the mitochondrial pyruvate dehydrogenase complex in Arabidopsis reduces plant organ size and enhances the accumulation of amino acids and intermediate products of the TCA cycle. Planta *236*, 387-399.

Yu, H., Yang, J., Shi, Y., Donelson, J., Thompson, S.M., Sprague, S., Roshan, T., Wang, D.-L., Liu, J., Park, S., *et al.* (2017). Arabidopsis glutaredoxin S17 contributes to vegetative growth, mineral accumulation, and redox balance during iron deficiency. Frontiers in Plant Science *8*.

Zander, M., Chen, S.X., Imkampe, J., Thurow, C., and Gatz, C. (2012). Repression of the *Arabidopsis thaliana* jasmonic acid/ethylene-induced defense pathway by TGA-interacting glutaredoxins depends on their C-terminal ALWL motif. Molecular Plant *5*, 831-840.

Zechmann, B., Mauch, F., Sticher, L., and Müller, M. (2008). Subcellular immunocytochemical analysis detects the highest concentrations of glutathione in mitochondria and not in plastids. Journal of Experimental Botany *59*, 4017-4027.

Zhang, B., Bandyopadhyay, S., Shakamuri, P., Naik, S.G., Huynh, B.H., Couturier, J., Rouhier, N., and Johnson, M.K. (2013). Monothiol glutaredoxins can bind linear $[Fe_3S_4]^+$ and $[Fe_4S_4]^{2+}$ clusters in addition to $[Fe_2S_2]^{2+}$ clusters: spectroscopic characterization and functional implications. Journal of the American Chemical Society *135*, 15153-15164.

Zhang, B., Crack, J.C., Subramanian, S., Green, J., Thomson, A.J., Le Brun, N.E., and Johnson, M.K. (2012). Reversible cycling between cysteine persulfide-ligated [2Fe-2S] and cysteine-ligated [4Fe-4S] clusters in the FNR regulatory protein. Proceedings of the National Academy of Sciences of the United States of America *109*, 15734-15739.

Zheng, L.M., White, R.H., Cash, V.L., Jack, R.F., and Dean, D.R. (1993). Cysteine desulfurase activity indicates a role for NIFS in metallocluster biosynthesis. Proceedings of the National Academy of Sciences of the United States of America *90*, 2754-2758.

Supplementary Tables

Supplementary Table 1: Components of the mitochondrial ISC assembly machinery in Arabidopsis and their homologues in yeast and bacteria (modified after Balk and Pilon (2011)).

protein name	locus	yeast[12]	bacteria
ISU1/2/3	At4g22220 At3g01020 At4g04080	ISU1/ISU2 (YPL135W/ YOR226C)	IscU
NFS1	At5g65720	NFS1 (YCL017C)	IscS
ISD11	At5g61220	ISD11 (YER048W-A)	
FH	At4g03240	YFH1 (YDL120W)	Cyay
ADX/mFDX	At4g21090 At4g05450	YAH1 (YPL252C)	Fdx
ADXR/mFDR	At4g32360	ARH1 (YDR376W)	FNR
HSCA1/2	At4g37910 At5g09590	SSQ1 (YLR369W)	HscA
HSCB	At5g06410	JAC1 (YGL018C)	HscB
MGE1	At5g55200 At4g26780	MGE1 (YOR232W)	-
GRXS15	At3g15660	GRX5 (YPL059W)	Grx4
ISCA	At2g16710 At2g36260 At5g03905	ISA1/ISA2 (YLL027W/ YPR067W)	IscA
IBA57	At4g12130	IBA57 (YJR122W)	YgfZ
NFU4/5	At3g20970 At1g51390	NFU1 (YKL040C)	NfuA
INDL	At4g19540	IND1 (absent in *S. cerevisiae)*	Mrp
ATM3	At5g58270	ATM1 (YMR301C)	-

[12] yeast systematic names based on "Saccharomyces genome database" (www.yeastgenome.org)

Supplementary Table 2: Table of standard amino acid abbreviations.

amino acid	3-letter code	1-letter code
alanine	Ala	A
arginine	Arg	R
asparagine	Asn	N
aspartic acid	Asp	D
cysteine	Cys	C
glutamic acid	Glu	E
glutamine	Gln	Q
glycine	Gly	G
histidine	His	H
isoleucine	Ile	I
leucine	Leu	L
lysine	Lys	K
methionine	Met	M
phenylalanine	Phe	F
proline	Pro	P
serine	Ser	S
threonine	Thr	T
tryptophan	Trp	W
tyrosine	Tyr	Y
valine	Val	V

Supplementary Table 3: Enzymes referred to in this study and respective EC numbers.

name	EC number[13]
NADH:ubiquinone oxidoreductase (Complex I)	1.6.5.3
succinate dehydrogenase (Complex II)	1.3.5.1
cytochrome c reductase (Complex III)	1.10.2.2
biotin synthase (BIO2)	2.8.1.6
methylcrotonoyl-CoA carboxylase (MCCase)	6.4.1.4
acetyl-CoA carboxylase (ACCase)	6.4.1.2
aconitase (ACO)	4.2.1.3
cofactor of nitrate reductase and xanthine dehydrogenase 2 (CNX2)	4.1.99.18
nitrate reductase (NR)	1.7.1.1
abscisic aldehyde oxidase (AAO)	1.2.3.14
xanthine dehydrogenase (XDH)	1.17.1.4
sulfite oxidase (SO)	1.8.3.1
lipoyl synthase (LIP1)	2.8.1.8
pyruvate dehydrogenase complex (PDC)	1.2.4.1
α-ketoglutarate dehydrogenase (OGDHC)	1.2.4.2
glycine decarboxylase complex (GDC)	1.4.4.2
branched-chain ketoacid dehydrogenase (BCKDC)	1.2.4.4
branched-chain aminotransferase (BCAT)	2.6.1.42
isovaleryl-CoA dehydrogenase (IVD)	1.3.8.4

[13] EC numbers are based on BRENDA (www.brenda-enzymes.org)

Supplementary Table 4: Oligonucleotides used in this study.

#	**5' → 3'**
oligonucleotides used for sequencing	
689	TCGCGTTAACGCTAGCATGGATCTC
690	GTAACATCAGAGATTTTGAGACAC
oligonucleotides used for RT-PCR	
2455	CCATATTGCAAGAAGTTTGCGCGTCTG
2456	GCAAGTCATCGGGATGGAGAGACG
3218	TGGCGGCTTCTTTATCGAGC
3219	TCCTTCACATCATTCTCAACGATA
oligonucleotides used for genotyping	
328	GCTACCCTTTCAGGACTTCCAGACC
329	CACAATGTTCTCCTGCAAACATGC
641	GCCAATGCTCTCACCCTAAA
642	GGCAATGGTTAGTCAAAATCG
321	TAGCATCTGAATTTCATAACCAATCTCGATACAC
432	CCCATTTGGACGTGAATGTAGACAC
1401	ATTTTGCCGATTTCGGAAC
2708	TGAAGCATACTTTTGGGATGG
2709	ATTCAAAACCATACGCTCACG
2710	GGAGATTCAGGGACACCTTTC
2711	ATGGTCCACTTCGTATGTTGG
2747	CACAGAGCCTAACGCCAATAG
2748	CGGACGTATACTTTGGTGACC
3523	ATTGCTACACTTGCGGGAGATGC
3524	GATGGTGAGTTATCTGAGAGG
oligonucleotides used for mutagenesis	
2753	GCTAAACCCAGACTGAGGAGA
2754	TCTCCTCAGTCTGGGTTTAGC
2839	ATCTACATGGAAGGTGTCCCT
2840	AGGGACACCTTCCATGTAGAT
2841	ATCTACATGGCTGGTGTCCCT
2842	AGGGACACCAGCCATGTAGAT
2843	GGCGGCTCAAGAATCATCCTT
2844	AAGGATGATTCTTGAGCCGCC
2845	GGCGGCTCAGCTATCATCCTT
2846	AAGGATGATAGCTGAGCCGCC
2847	CAAGAGTTGGAAAACGCTGTG
2848	CACAGCGTTTTCCAACTCTTG
2849	CAAGAGTTGGCTAACGCTGTG
2850	CACAGCGTTAGCCAACTCTTG
2851	AACGCTGTGGAATCCTTCAGC
2852	GCTGAAGGATTCCACAGCGTT
2853	AACGCTGTGGCTTCCTTCAGC
2854	GCTGAAGGAAGCCACAGCGTT
3650	TAGAAACATTGCTGAAGACCAAGAGTTGAAAAACG

3651	GAACTGATAGGAACATTATATTG
3652	TAGAAACATTGATGAAGACCAAGAGTTGAAAAAC
3653	TAGAAACATTTTTGAAGACCAAGAGTTG
3654	GATCTACATGGCTGGTGTCCCTGAATC
3655	ATAACAGGATTATCCTTCACATC
oligonucleotides used for Gateway® Cloning[14]	
2592	*GGGGACAAGTTTGTACAAAAAAGCAGGCTTT*ATGGCGGCTTCTTTATCGAGC
2593	*GGGGACCACTTTGTACAAGAAAGCTGGGTC*TCAATCTTGGTTTCCGGAGAC
2594	*GGGGACCACTTTGTACAAGAAAGCTGGGTC*ATCTTGGTTTCCGGAGACGTC
2626	*GGGGACAAGTTTGTACAAAAAAGCAGGCTTT*TCAACAGTGCCAAGTGATTCAG
2659	*GGGGACCACTTTGTACAAGAAAGCTGGGTC*TTACTTGTACAGCTCGTCCATG

Supplementary Table 5: amino acid content of wild-type and *grxs15-3 UBQ10:GRXS15 K_{83}/A* line #3 and #4 ordered after most increased amino acid accumulation in line #4.

amino acid	amount of amino acid (pmol mg^{-1} FW^{-1}); mean ± SEM		
	Wt	**#3**	**#4**
Ala	96,66 ± 6,2	206,49 ± 15,25	237,99 ± 21,35
Leu	6,48 ± 0,53	13,32 ± 1,36	15,55 ± 1,3
Gly	36,79 ± 4,84	67,70 ± 12,19	82,26 ± 2,38
Ser	111,74 ± 9,6	163,90 ± 9,11	234,56 ± 50,21
Val	16,48 ± 0,72	25,45 ± 2,63	33,03 ± 1,64
Ile	5,45 ± 0,29	7,89 ± 1,1	10,70 ± 0,7
Arg	9,96 ± 1,07	12,22 ± 2,56	17,94 ± 1,72
Asn	76,35 ± 9,27	72,38 ± 5,36	125,24 ± 33,73
Lys	6,61 ± 0,65	8,85 ± 0,36	10,49 ± 0,9
Gln	213,64 ± 17,12	262,03 ± 13,91	317,91 ± 52,1
Phe	6,32 ± 0,18	7,49 ± 0,8	9,26 ± 0,36
Tyr	1,50 ± 0,09	1,87 ± 0,08	2,09 ± 0,14
Pro	31,51 ± 3,24	33,73 ± 1,87	42,39 ± 5,11
Thr	58,94 ± 3,66	68,05 ± 4,03	77,90 ± 9,11
Glu	652,08 ± 32,85	730,33 ± 22,23	805,71 ± 90,0
Asp	199,61 ± 15,02	200,89 ± 1,35	243,28 ± 37,33
Met	1,48 ± 0,07	1,44 ± 0,12	1,72 ± 0,12
His	13,46 ± 2,15	12,67 ± 1,24	13,32 ± 0,91

[14] Gateway®sites in italic

Supplementary Figures

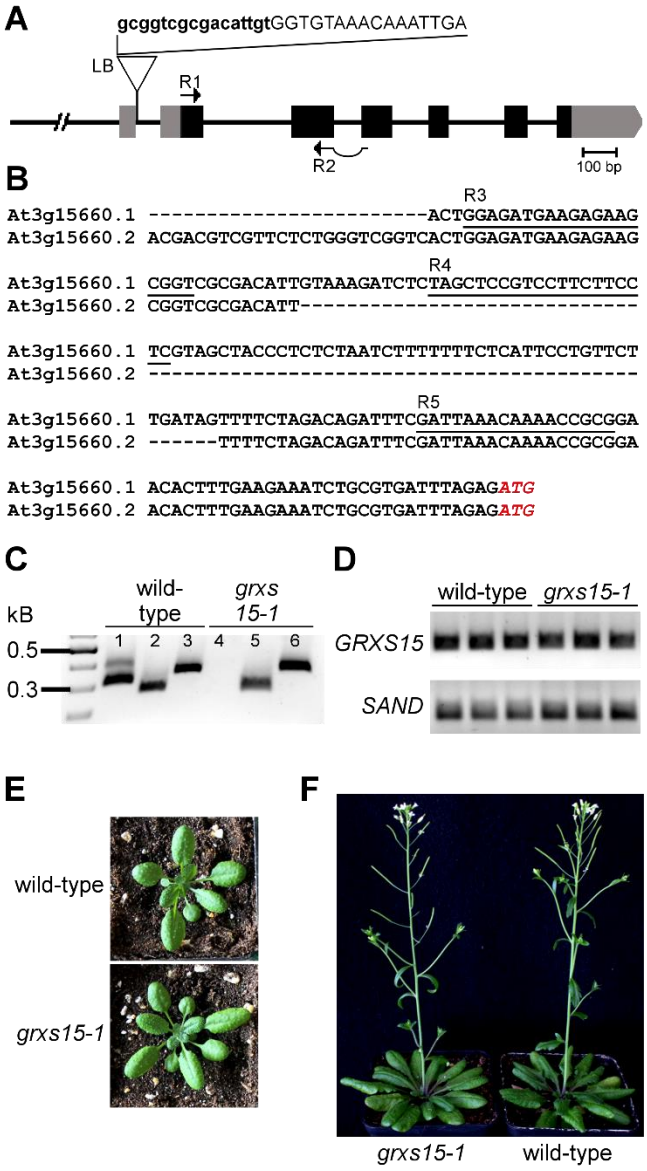

Supplemental Figure 1: Characterisation of *grxs15-1*.

A: Analysis of the T-DNA insertion in *grxs15-1*. The T-DNA is inserted 141 bp upstream of the start codon and localised in an intron of the 5′ UTR of At3g15660.2. Numbered arrows depict the primers used for RT-PCR in D.

B: Sequence alignment of the 5′ UTR of the transcripts At3g15660.1 and At3g15660.2. The start codon is indicated by a red ATG. Forward primers used for PCR are underlined. The sequence alignment was performed with MUSCLE.

C: Analysis of the 5′ UTR of both isoforms in wild-type and *grxs15-1*. cDNA of wild-type and *grxs15-1* was used as a template for a PCR with the primers shown in B and an exon-exon spanning reverse primer (R2) annealing to exon two and exon three in the coding region of GRXS15 depicted in A. Using primer R3 annealing upstream of the intron leads to the amplification of two fragments (395 bp and 318 bp) in wild-type (lane 1), but not in *grxs15-1* (lane 4), whereas primer R4 and R5 annealing downstream of the T-DNA insertion in both cases generates a PCR fragment of 279 or 356 bp irrespective of whether the primer anneals in the second exon (lanes 2+5) or the intron (lanes 3+6) of the 5′ UTR.

D: Semiquantitative analysis of *GRXS15* expression in *grxs15-1*. For RT-PCR, a forward primer (R1) annealing to the start of the coding region and exon-exon spanning reverse primer (R2) annealing to exon two and exon three in the coding region of *GRXS15* were used. PCR was carried out over 34 cycles on cDNA of 3-week-old wild-type and homozygous *grxs15-1* plants with *GRXS15* and *SAND* (At2g28390) specific primers.

E + F: Phenotypic comparison of 4-week-old plants (D) and 7-week-old plants (E) grown on soil under long-day conditions.

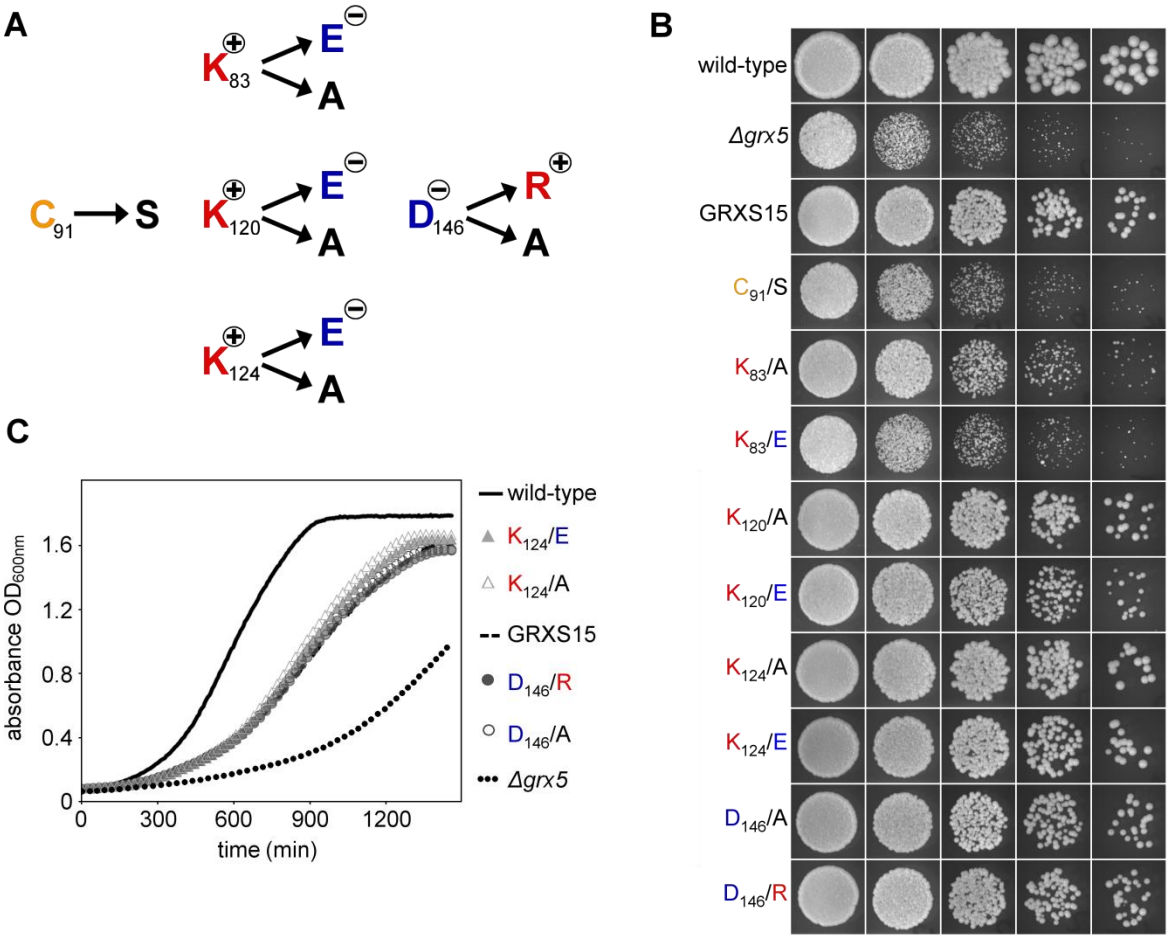

Supplemental Figure 2: Substitutions in GRXS15 and rescue of the yeast *Δgrx5* mutant defects by mutated GRXS15.

A: Performed substitutions in GRXS15 to influence the ability of coordinating the ISC or to bind GSH by hydrogen bonds.

B: Growth of the yeast *Δgrx5* mutant complemented with different versions of mutated GRXS15. Exponentially grown cultures were spotted onto solid drop-out medium containing glucose in fivefold serial dilutions. Colonies were visualized after incubating plates for 2 d at 30 °C. One representative experiment from three independently performed experiments is shown.

C: Growth of the yeast *Δgrx5* mutant complemented with GRXS15 substituted in K_{124} or D_{146} in liquid drop-out medium at 28 °C. The absorbance at 600 nm was followed over time.

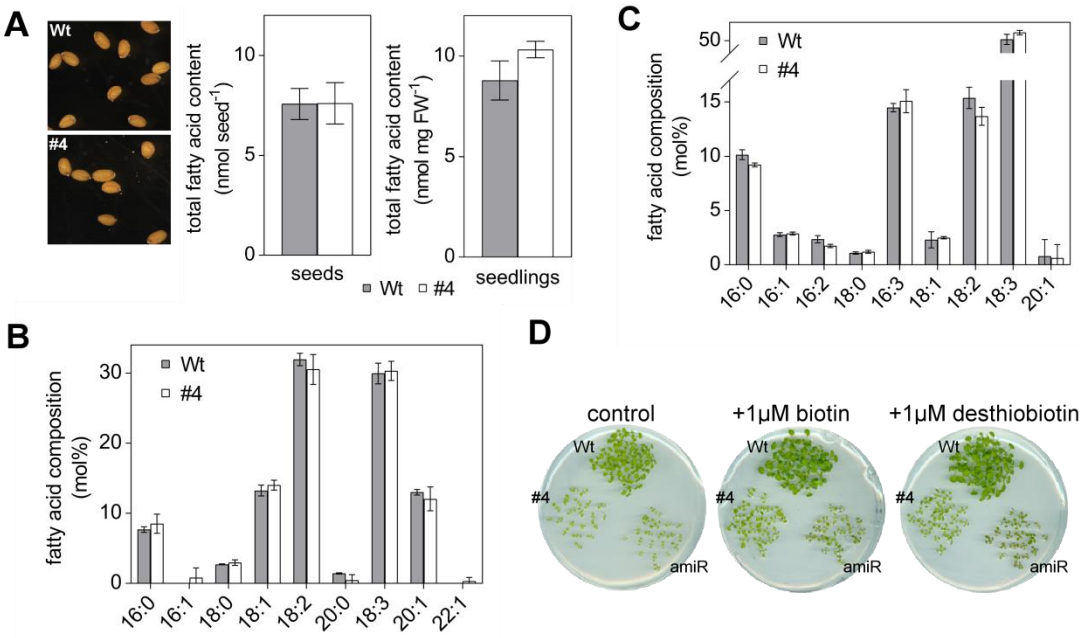

Supplemental Figure 3: The GRXS15 K_{83}/A phenotype is not based on biotin deficiency.
A: Seeds of of GRXS15 K_{83}/A line #4 compared with wild-type and the respective total amount of fatty acids in seeds and 8-d-old seedlings. (n = 3-4 ± SD).
B+C: Fatty acid composition of seeds and 8-d-old seedlings of GRXS15 K_{83}/A line #4 compared with wild-type. Results are expressed in mol % of a given fatty acid compared with the sum of total fatty acids. (n = 3-4 ± SD).
D: GRXS15 K_{83}/A line #4, a knockdown line (amiR) and wild-type plants were grown on agar plates containing no (control) or 1 µM biotin or 1 µM desthiobiotin. Data were provided by Inga Kruse and Janneke Balk.

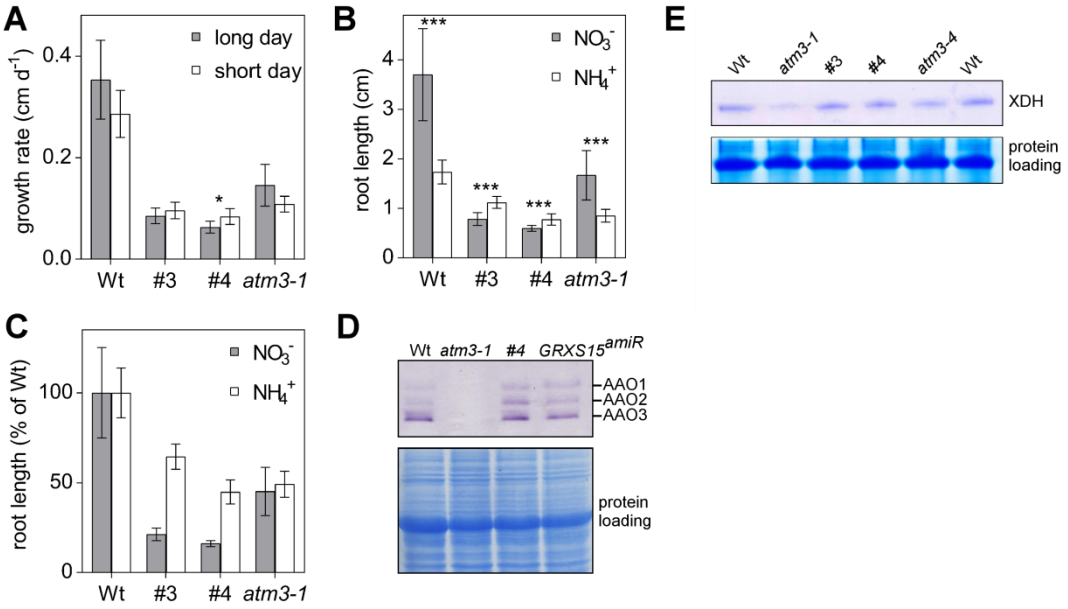

Supplemental Figure 4: Influence of light period and nitrogen source on root growth

A: Growth rate calculations from root length measurements at day 5 and day 8 under short-day (8 h light/16 h dark) and long-day (16 h light/8 h dark) conditions (n = 20-30 ± SD). Student's t-Test analysis showed one significant difference between long-day and short-day treatment (*P ≤0.05).

B: Primary root length of GRXS15 K_{83}/A line #3 and #4 as well as *atm3-1* mutant seedlings compared to wild-type (Wt) grown on vertical agar plates for 9 d under long-day conditions containing 5 mM KNO_3 or 5 mM NH_4Cl as N-source (n = 35 ± SD). Student's t-Test analysis showed significant differences between nitrate and ammonium treatment (***P ≤0.001).

C: Relative root length compared to the wild-type of GRXS15 K_{83}/A mutants and *atm3-1* as depicted in B. Wild-type was set to 100 % in both growing conditions.

D: In-gel activities of AAO in wild-type (Wt) and *atm3-1* as well as *grxs15* mutants. Equal amounts of protein were separated on nondenaturing PA gels and stained for AAO activity using synthetic aldehydes (1-naphthaldehyde and indole-3-carboxyaldehyde) as substrates. As a protein-loading control the gel was stained afterwards with Coomassie. Data were provided by Inga Kruse and Janneke Balk.

E: In-gel activity of XDH in wild-type (Wt) and *atm3* as well as *grxs15* mutants. Equal amounts of protein (35 µg) extracted from 8-d-old seedlings were separated on nondenaturing PA gel and stained for XDH activity using hypoxanthine as substrate.

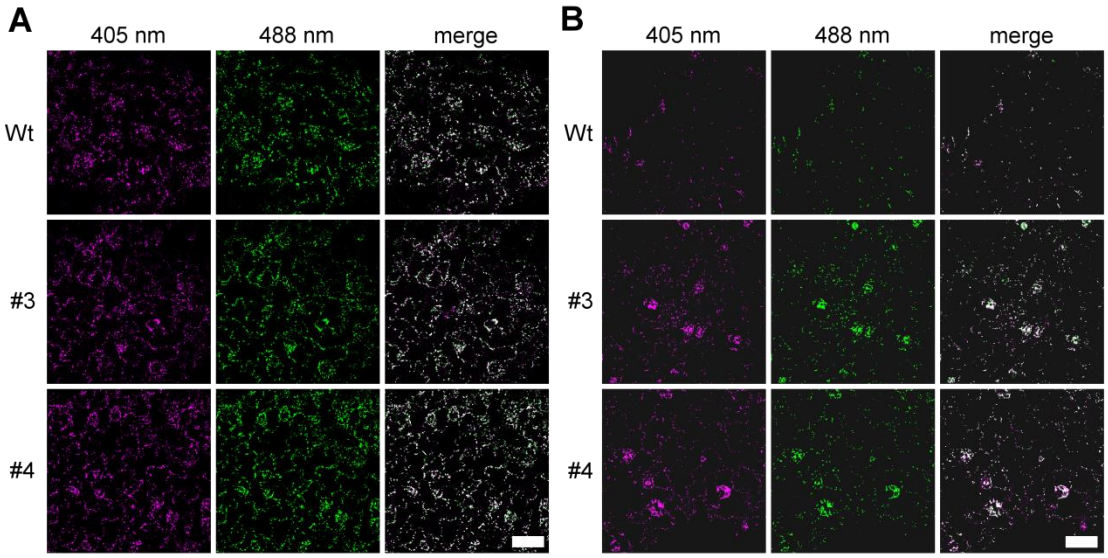

Supplemental Figure 5: Subcellular localisation of roGFP2-sensors.
Genetically encoded sensors roGFP2:Orp1 (**A**) and roGFP2:hGRX1 (**B**) were expressed in the mitochondrial matrix of both wild-type and mutant plants. Scale bar = 40 µm.

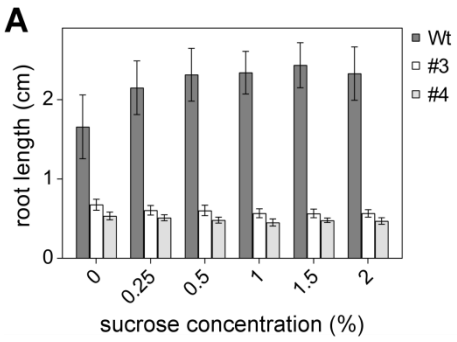

Supplemental Figure 6: Addition of sucrose has no effect on root growth of *grxs15* mutants.
A: Relative root growth of *grxs15-3 UBQ10:GRXS15 K_{83}/A* line #3 and #4 compared to wild-type seedlings. Seedlings were grown on vertical agar plates containing Arabidopsis medium with different sucrose concentrations for 8 d (n = 50-55 ± SD).

List of Abbreviations

ACO	Aconitase
APS	Ammonium persulfate
BSA	Bovine serum albumin
BSO	L-buthionine-(S, R)-sulfoximine
CLSM	Confocal laser scanning microscopy
DAB	3, 3-diaminobenzidine
δ	dynamic range
dNTP	Deoxynucleotide solution mix
DTT	1,4-dithiothreitol
EtOH	Ethanol
GR	Glutathione reductase
GRX	Glutaredoxin
GSH	reduced glutathione
GSSG	oxidised glutathione, glutathione disulfide
IPTG	Isopropyl-D-1-thiogalactopyranoside
ISC	Iron-sulfur cluster
KCN	Potassium cyanide
MDH	Malatedehydrogenase
MeOH	Methanol
MOPS	3-(N-morpholino)propanesulfonic acid
NADH	β-nicotinamide adenine dinucleotide, reduced
NADPH	β-nicotinamide adenine dinucleotide phosphate, reduced
NBT	Nitro blue tetrazolium
NR	Nitrate reductase
OD	Optical density
PCR	Polymerase chain reaction
pGal	Propyl gallate
roGFP	Redox-sensitive green fluorescent protein
ROS	Reactive oxygen species
T-DNA	Transfer deoxyribonucleic acid
TP	Target peptide
Tris-HCl	Tris(hydroxymethyl)aminomethane hydrochloride
TRX	Thioredoxin
UTR	Untranslated region
v/v	volume per volume
w/v	weight per volume

Publications

Parts of this thesis have been published in the following publications:

The mitochondrial monothiol glutaredoxin S15 is essential for iron-sulfur protein maturation in *Arabidopsis thaliana*
Moseler, A., Aller, I., Wagner, S., Nietzel, T., Przybyla-Toscano, J., Mühlenhoff, U., Lill, R., Berndt, C., Rouhier, N., Schwarzländer, M., and Meyer, A. J. (2015).
Proceedings of the National Academy of Sciences 112, 13735-40

During the doctoral studies following publications were published:

Glutathione peroxidase-like enzymes cover five distinct cell compartments and membrane-surfaces in *Arabidopsis thaliana*
Attacha, S., Solbach, D., Bela, K., Moseler, A., Wagner, S., Schwarzländer, M., Aller, I., Müller, S.J., and Meyer, A.J. (2017).
Plant Cell and Environment 19, 12919

Glutaredoxin catalysis requires two distinct glutathione interaction sites.
Begas, P., Liedgens, L., Moseler, A., Meyer, A.J., and Deponte, M. (2017).
Nature Communications 8, 14835

Publications in preparation:

Diminished ISC coordinaton in glutaredoxin S15 causes defects in mitochondrial enzymes dependent on lipoic acid as a cofactor.
Moseler A., Kruse I., Wagner S., Schrader K., Schwarz G., Poschet G., Wirtz M., Hell R., Schwarzländer M., Balk J., Meyer A. J.

The catalytic activity of monothiol glutaredoxins is inhibited by the loop-insertion preceding the active site.
Trnka D., Moseler A., Engelke A., Gellert M., Berndt C., Meyer A. J., Lillig C. H.

General Statement

I declare that I am the sole author of this submitted dissertation and that I did not make use of any sources or help apart from those specifically referred to. Experimental data or material collected from or produced by other persons is made easily identifiable. I also declare that I did not apply for permission to enter the examination procedure at another institution and that the dissertation is neither presented to any other faculty, nor used in its current or any other form in another examination.

…….. ……

Place, Date Anna Moseler

Acknowledgement

Mein besonderer und herzlichster Dank geht an Andreas Meyer für die Möglichkeit meine Promotion in seiner Arbeitsgruppe durchzuführen, aber auch für die viele Unterstützung, Diskussionen und konstruktive Kritik. Außerdem möchte ich mich sehr herzlich bei Markus Schwarzländer bedanken, der durch seine enthusiastische Art und sein kritisches Denken mich sehr unterstützt und motiviert hat.

Des Weiteren geht ein ganz großer Dank an Isabel und Stephan, die mir nicht nur im Labor eine große Hilfe waren, sondern auch menschlich eine wahre Bereicherung sind.

Für eine wunderbare und angenehme Arbeitsatmosphäre möchte ich auch allen Mitgliedern der AG Meyer, Schwarzländer und Hochholdinger (dazu zählen natürlich auch Anja und Marine) danken. Grillabende, Kurztrips oder einfach nur gemeinsames Trinken haben die Arbeitsjahre sehr bereichert und die Entscheidung hier zu promovieren mich nicht bedauern lassen.

Nicht unwesentlich war auch die Unterstützung außerhalb des Labors. Hier möchte ich insbesondere Franzi, Laura und Kerstin danken, die während aber auch nach dem Studium mir in allen Lebenslagen eine Bereicherung waren und es immer noch sind. Außerdem möchte ich der „ökologischen Nische“ Alex, Hannah, Dominik und Regina für ein gemeinsames Biologendasein ab der ersten Minute danken. Des Weiteren möchte ich auch Thierry meinen Dank bekunden für unzählige lustige Abende und Konzerte, durch die ich auch einige wunderbare Menschen kennengelernt habe und nicht mehr missen möchte (der Sophie-loves-Pizza-Fanclub darf sich nun angesprochen fühlen). Auch danke ich Sandra und Aline für ein tolles WG-Leben während der Promotion, wobei insbesondere Trash-TV Abende inklusive Gin Tonic eine willkommene Ablenkung waren. Fast am Ende nun, möchte ich noch ganz lieb Melanie danken, aber auch Vanessa, Christina, Jessy und Lara für viele gemeinsame Wein-, Pferde- und sonstige Feste in der Vergangenheit aber auch sicherlich in der Zukunft.

Aus tiefstem Herzen möchte ich zu guter Letzt meinen Eltern, meinem Bruder Johannes sowie Constanze und Paul danken ohne die das alles sicherlich nicht möglich gewesen wäre. Nicht nur die große finanzielle Unterstützung hat mein Studium erleichtert, sondern der bedingungslose Rückhalt und das große Vertrauen haben maßgeblich zu dem Hier und Jetzt geführt. Tausend Dank!